Rheology of Supramolecular Polymers

Shabbir, Aamir

Publication date:
2016

Document Version
Publisher's PDF, also known as Version of record

Ph.D. Thesis
Doctor of Philosophy

DTU Chemical Engineering
Department of Chemical and Biochemical Engineering

Rheology of Supramolecular Polymers

Aamir Shabbir

September 2016

DTU Chemical Engineering
Department of Chemical and Biochemical Engineering
Technical University of Denmark

Danish Polymer Centre
Building 227
2800 Kongens Lyngby, Denmark
Phone +45 45882161
www.dpc.kt.dtu.dk

Preface

First and foremost I thank God Almighty for giving me the strength and opportunities to accomplish this milestone.

This thesis presents the results of my Ph.D project carried out at the Danish Polymer Centre (DPC), Department of Chemical and Biochemical Engineering, Technical University of Denmark (DTU). The work was performed during the period from Oct. 2013 to Sept. 2016, under the supervision of Professor Ole Hassager and Associate Professor Anne Ladegaard Skov at DTU Chemical Engineering. This Ph.D project was funded under the Marie Curie Initial Training Network SUPOLEN (Supramolecular assembly of polymeric structures: a novel route to enhance soft materials properties) in the European Union Seventh Framework (Grant Agreement No.: 607937).

I would like to express my greatest gratitude to my supervisor Prof. Ole Hassager under whose supervision i have learned a lot. I also thank Prof. Ole Hassager for introducing me to the fracture of polymer melts. Likewise for Asst. Prof. Nicolas J. Alvarez whose guidance has given me strong experimental problem solving skills. I would like to thank Prof. Anne L. Skov for inspiring discussions. I thank Dr. Qian Huang who has always been there to guide me specially when things didn't work out. I also thank Dr. Irakli Javakhishvili for useful scientific discussions and collaboration on one of the project. I would also like to thank Kim Chi Szabo for all the technical support regarding SEC and DSC.

Special thanks to Hanne Pohl and Vibeke H. Christiansen for providing keen assistance regarding administrative matters. I also thank all colleagues at the Danish polymer center for being around specially Sara L. Wingstrand, Ludovica Hengeller and Dr. Martin Van Drongelen. Also, i would like to thank the workshop crew for their technical support on the FSR. Ivan H. Pedersen, Lars Møller and specially Søren V. Madsen for their support on all technical aspects.

I would like to thank my SUPOLEN colleagues for providing an amazing company during the three years. Some of the collaborations in particular with Dr. Hadi Goldansaz, Dr. Guilhem P. Baeza, Srishti Arora and Salvatore Costanzo have been very fruitful and have given me the opportunity to learn about materials outside the scope of my PhD. I would also like to thank Victor Boudara, Jeremy Brassinne and Jan Hendricks for useful discussions. I thank Dr. James Wilson and Dr. Arnaud Cadix for the industrial secondment at Solvay, Paris which lasted two months.

I would also like to thank Prof. Ralph H. Colby (Penn State University), Prof. Evelyne Van Ruymbeke (UCL Louvain-la-Neuve), Prof. Dimitris Vlassopoulos (IESL-FORTH), Prof. Silvina Cerveny (MPC San Sebastian), Prof. Søren Hvilsted (DTU), Dr.

Quan Chen (Chinese Academy of Sciences) and all the other authors for the pleasant collaboration of our joint papers.

The days would have passed far more slowly without the support of my friends. Finally, I thank my parents for their love and support. Without their prayers and wishes I would never have reached this milestone. I also thank my two younger brothers for their love and support.

Aamir Shabbir

Abstract

Supramolecular polymers are a broad class of materials that include all polymers capable of associating via secondary interactions. These materials represent an emerging class of systems with superior versatility compared to classical polymers with applications in food stuff, coatings, cost efficient processes or biomedical areas.

Design and development of supramolecular polymers using ionic, hydrogen bonding or transition metal complexes with tailored properties requires deep understanding of dynamics both in linear and non-linear deformations. While linear rheology is important to understand the dynamics under equilibrium conditions, extensional rheology is relevant during the processing or in the usage of polymers utilizing supramolecular associations for example, acrylic based pressure sensitive adhesives are subjected to extensional deformations during the peeling where strain hardening is often desirable. Such data is also needed to develop sophisticated multi-scale models that can later be used for predicting the flow behavior and molecular dynamics of supramolecular networks.

This thesis focuses on the experimental rheological study of two class of supramolecular polymers namely: (a) hydrogen bonding polymers, and (b) ionic bonding polymers (hereafter termed as ionomers). We study linear and non-linear rheology for a model system of entangled pure poly(*n*-butyl acrylate), PnBA, homopolymer and four poly(acrylic acid), PnBA-PAA, copolymers with varying AA side groups synthesized via hydrolysis of pure PnBA homopolymer. Second, we investigate the linear viscoelastic response of unentangled 2-ureido-4[1*H*]-pyrimidones (UPy) based supramolecular networks. Third, we investigate the rheological response of ionomers synthesized via condenstation of suflonated pthalates with poly(tetramethylene glycol) PTMO, both in non-linear shear and extensional flows. Finally, we study brittle fracture of the above ionomers in extensional flow.

Dansk Resumé

Supramolekylære materialer er en bred klasse af materialer, som inkluderer polymerer som selvorganiserer via intermolekylære eller intramolekylære kræfter. Materialerne besidder en række egenskaber som gør dem til attraktive alternativer til klassiske polymerer f.eks. til emballage til overfladebehandling eller til medicinske anvendelser.

For at designe og udvikle supramolekylære polymerer med ion-bindinger, hydrogenbindinger eller metal-komplex-bindinger med ønskede egenskaber kræves en god forståelse for reologien i både lineære såvel som ikke-lineære deformationer. Medens lineær reologi er væsentlig for at forstå dynamik tæt på ligevægt, er forlængelsesreologi typisk mere vigtig i industrielle processer. Således er det vigtigt at forstå strain-hardening af acryl-baserede trykfølsomme klæbere og for at kunne udvikle multi-skala modeller og molekylær dynamik.

Denne afhandling omhandler reologi af to klasser af supramolekylære polymerer, nemlig (a) hydrogenbindende polymerer og (b) ion-bindende polymerer (herefter kaldet ionomerer). Mere specifikt omhandler den et system med kædeindviklet ren poly(*n*-butyl acrylate), PnBA, homopolymer og fire poly(acrylic acid), PnBA-PAA, copolymerer med varierende AA side grupper syntetiserede via hydrolyse af ren PnBA homopolymer. Dernæst undersøges lineær viskoelasticitet af ikke-kædeindviklet 2-ureido-4[1*H*]-pyrimidones (UPy) baseret supramolecular netværk. For det tredje undersøges rheologien af ionomerer syntetiseret via kondensation af suflonerede pthalater med poly(tetramethylene glycol) PTMO, både i ikke-lineær forskydning og forlængelse. Endelig præsenteres resultater for brudmekanik af udvalgte systemer i forlængelse.

Contents

CHAPTER 1

Introduction

1.1 Supramolecular polymers

Supramolecular polymers are relatively new class of polymers with attractive groups that offer reversible interactions and thus the possibility of tuning the properties on will. These associative polymers present superior versatility compared to their covalent polymeric counterparts. They include charged polymers (ionomers, polyelectrolytes, metal-ligands) [Rossow and Seiffert (2014); Mugemana et al. (2010); Eisenberg and Kim (1998); Zhang et al. (2014); Chen et al. (2013)] and polymers with hydrogen bonding [Lewis et al. (2014); Feldman et al. (2009); Nair et al. (2008)]. A very well known naturally occurring supramolecular system is DNA. Cooperative non-covalent interactions, such as multiple hydrogen bonding and hydrophobic interactions, give rise to its unique architecture. Other example from nature is spider silk whose remarkable strength arises from presence of micro-crystalline domains, formed by secondary interactions, and embedded in a flexible matrix [Hirschberg (2001)]. Amongst the man-made materials, Nylon is a good example in which hydrogen bonding between the polymer chains gives rise to exceptional material properties.

Hydrogen bonding is the most employed non-covalent reversible interaction to create supramolcular poymeric assemblies [Nair et al. (2008)]. The dynamics of hydrogen bonded transient networks can be significantly altered by changing the exchange rate between two hydrogen bonding motifs via external stimuli such as temperature. At high temperatures molecular chains can release stress at a fast rate because of decrease of hydrogen bond life time which can lead to low viscosity melts. This remarkable property thus allows easy processing of such materials for various applications [Yan et al. (2012)]. Alternatively, at low temperatures the hydrogen bond life can be significantly larger than the experimental time scales leading to transient networks. Hydrogen bond strength and density of side groups are two important control variables that can be used to design tailored supramolecular networks. Weak hydrogen bonding motifs including carboxylic acids and amide groups can increase melt viscosity and introduce hierarchical structures in polymer melts [Lewis et al. (2014)]. For much stronger supramolecular networks multiple hydrogen bonding arrays can be exploited [Bosman et al. (2004); Sijbesma et al. (1997)]. One such famous building block unit is 2-ureido-4-pyrimidones (UPy) developed by Beijer et al. (1998) which can dimerize strongly in a self-complementary array of quadruple hydrogen bonds. Another remarkable property of hydrogen bonding supramolecular polymers is the ability to self-heal upon contact. The use of hydrogen bonding has large potential in coatings, pressure sensitive adhesives and as elastomeric materials

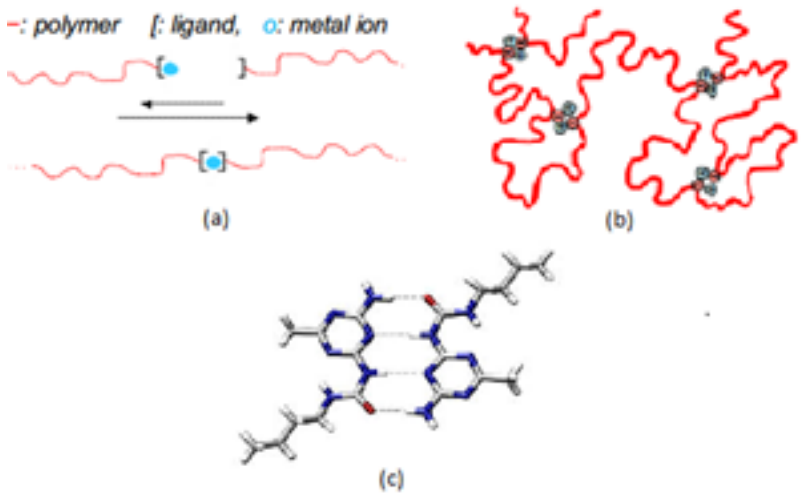

Figure 1.1: (a) Metal-ligand interactions, (b) Ionic bonding interactions, (c) Hydrogen bonding interactions.

[Bosman et al. (2004); Cordier et al. (2008); Creton (2011)].

Ionomers represent another class of associative polymers where ionic groups are covalently attached to the polymer backbone. The key feature of ionomers is that a relatively modest concentration of ionic groups attached to a low dielectric constant polymer can provide significant changes in physical, mechanical and dynamic properties of a polymer. Ionomers are nano-structured materials, similar to nanocomposites and block polymers. Ionomers have applications in polymer blends, film and packaging, coatings and adhesives [Zhang et al. (2014)].

Supramolecular assemblies utlizing metal-ligand coordination are highly directional and of great strength which have been widely used to build stimuli-responsive polymers. The tunable coordination binding strength, as well as fascinating electrochemical, magnetic properties and photo-physical properties of the metal ions and ligands would benefit the application of metallo-supramolecular polymers in material science [Yan et al. (2012)].

1.2 Supramolecular polymer rheology

The linear rheology of supramolecular polymers is very rich and offers opportunities for property manipulation. Understanding the rich dynamics of such associative polymers is thus interesting from both fundamental and applied standpoints. The rheological response of unentangled suprmolecular polymers is well described using the modified Rouse model called the sticky Rouse model [Chen et al. (2013)]. According to this theory, reversible associations act as a secondary source of friction

for the polymer chains thus delaying the terminal relaxation [Leibler et al. (1991)]. The dynamics of entangled supramolecular polymers is even more complex where both the topological constraints and association/dissociation dynamics play a role. Since these two mechanisms are governed by two different microscopic time scales (internal clocks), a thermorheologically complex behaviour is expected [Shabbir et al. (2015); van Ruymbeke et al. (2010); Stadler et al. (2009)]. Phase separation and aggregation or crystallization of supramolecular motifs can add additional complexities in understanding multi-scale dynamics of supramolecular polymeric assemblies. Based on the multi-scale nature of these materials, combination of different techniques, such as dielectric spectroscopy (DRS), rheology and nuclear magnetic relaxometry (NMR) are required to gain complete insight of the dynamics involved. For example, the association lifetime can be independently quantified by DRS and compared with rheology [Chen et al. (2013); Shabbir et al. (2016b); Goldansaz et al. (2016)].

The role of supramolecular building block architecture also plays a significant role on the rheology of these materials. For linear polymers, two categories can be distinguished. In the first category, a suprmolecular moiety is connected to each end of the linear polymer chains (also called telechelic polymers). When the end groups associate through non-directional interactions like the Coulomb forces in telechelic ionomers, and hydrophobic interactions in hydrophobic endcapped urethanes (HEUR), clusters containing end group associations are formed [Hirschberg (2001)]. This results in the formation of reversible networks capable of flowing at long time scales. When the end groups associate through directional interactions like the hydrogen bonding, the hydrogen bonds may aggregrate in cooperative fashion to form ordered clusters resulting in thermoplastic elastomers (TPE). However, polymers in which end groups exclusively form dimers, but do not aggregate, form long chains by concatenation of molecules [Hirschberg (2001)]. In the second category, the supramolecular moiety is grafted on the side of polymer backbone. The formation of a supramolecular network depends on the association bond strength and density of side groups. Figure 1.2 a, shows Small amplitude oscillatory shear (SAOS) rheology for unentangled copolymers of poly(*n*-butyl acrylate), PnBA, and 2-ureido-4[1*H*]-pyrimidones (UPy) synthesized using free radical polymerization [Lewis et al. (2014)]. An extended rubbery plateau is noticed similar to well entangled linear polymer melts. Notice, the almost parallel slopes in the terminal regime suggesting the presence of hydrogen bonding even at long time scales. On long time scales flow is possible but it is impaired by the interchain sticking [Seiffert (2016)]. Similarly, if the side groups associate through non-directional interactions, clusters may be formed for example nanodomains comprising of ionic clusters have been reported by Chen et al. (2014); Ling et al. (2012). SAOS rheology of ionomers synthesized via condenstation of suflonated pthalates with poly(tetramethylene glycol) PTMO is shown in Figure 1.2 b where a rubbery plateau spanning several decades is noticed [Chen et al. (2013)].

While the non-linear rheology of supramolecular polymers has been investigated in shear [Xu et al. (2010); Bossard et al. (2004); Hyun et al. (2006); Suzuki et al. (2012); Qiao and Weiss (2013)], literature on extensional rheology remains less understood

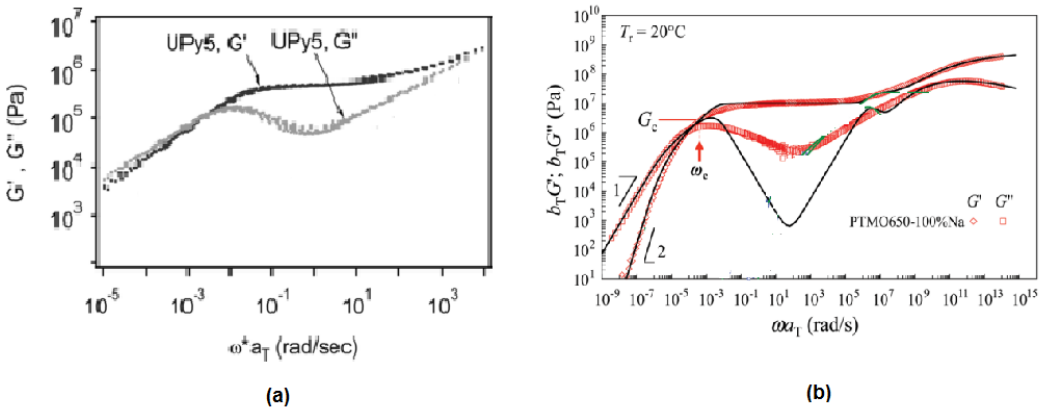

Figure 1.2: Dynamic moduli as a function of frequency for (a) PnBA-UPy 5% copolymer at 25 °C, (b) PTMO-Na ionomer at 20 °C

partly because of the difficulty in attaining stable large extensional deformations. The few available data suggests that they are very promising for tailoring the appearance of strain hardening [Stadler et al. (2010); Ling et al. (2012)]. Non-linear studies have also revealed fracture in associative polymers. For example in the case of ionomers, although strong transient networks can be obtained, they fracture in a brittle manner in extension [Shabbir et al. (2016a); Stadler et al. (2010); Ling et al. (2012)].

1.3 Shear and Extensional Rheology

There are two fundamental flow deformation fields used in rheological studies: 1) simple shear, and 2) uniaxial extension. The simplicity of flow allows for the analytical determination of material functions in rheology such as the viscosity, modulus, relaxation times etc. One fundamental difference between simple shear and uniaxial extension is that shear flow is a rotational flow and for a given shear rate the fluid elements are separated linearly in time (see Figure 1.3),

$$\frac{dx}{dt} = v_x(y) = v_x(0) + \frac{\partial v_x}{\partial y} y = 0 + \dot{\gamma}.y \tag{1.1}$$

if $\dot{\gamma}$ is constant:

$$x(t) = \dot{\gamma}.y.t \tag{1.2}$$

On the other hand, in extensional flow the fluid elements separate exponentially in time (see Figure 1.3). This implies that polymer chains are subject to much larger deformations as compared to in shear flow leading to orientation and stretching.

if the distance between two points x is small:

$$\frac{dx}{dt} = v(x) = v(0) + \frac{\partial v}{\partial x}x = v_0 + \dot{\epsilon}x \tag{1.3}$$

if $\dot{\epsilon}_u$ is constant and $v_0 = 0$:

$$x(t) = x_0.exp(\dot{\epsilon}.t) \tag{1.4}$$

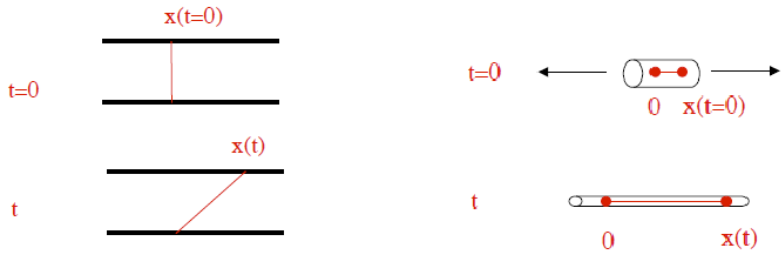

Figure 1.3: Weak flow vs. strong flow: (left) simple shear flow, (right) extensional flow [Bailly (2012)]

At low strain rates (linear viscoelasticity), the transient extensional viscosity is three times the transient shear viscosity. The corresponding curves are called the stress growth curves. At high extension rates compared to terminal relaxation time, some polymers show an increase of the viscosity above the linear viscoelasticity curve. This departure from the linear viscoelasticity is termed as strain hardening. This is due to the orientation and stretching of chains. On the contrary, transient shear viscosity will always be below the linear viscoelasticity curve at rates larger than the terminal relaxation time. This is termed as shear softening [Bailly (2012)]. This is because orientation dominates in shear flows.

1.4 DTU- Filament Stretch Rheometer and VADER 1000

The DTU- filament stretch rheometer (DTU-FSR) was initially designed by Bach et al. (2003). It represents the state of the art in the field of extensional rheology. The FSR is equipped with an oven capable of temperature from 15 °C to 350 °C. In the DTU-FSR the sample is placed between two circular plates (see Figure 1.5), the plates are then separated in a way such that the mid-plane diameter, D decreases exponentially in time. The strain rate $\dot{\epsilon}$ is defined as,

$$\dot{\epsilon} = -\frac{2}{R}\frac{dR}{dt} \tag{1.5}$$

is constant in time. This ensures fluid element at the mid-plane of filament is subjected to ideal uniaxial extension. An online control scheme recently updated by Román Marín et al. (2013) is employed to ensure accurate constant strain strain rate

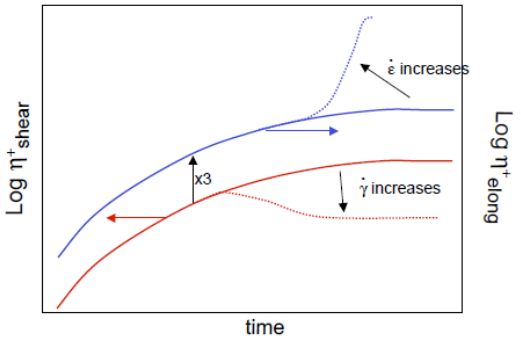

Figure 1.4: Stress growth curves in constant rate shear and extension. The solid lines represent linear viscoelasticity curve (LVE) where the extensional viscosity is three times the transient shear viscosity. Dotted lines represent non-linear shear (resulting in shear softening) and extension flow (resulting in strain hardening) [Bailly (2012)].

and this is one particular feature which makes the DTU-FSR unique. The Hencky strain, ϵ, is defined as,

$$\epsilon(t) = -2 \ln \frac{R(t)}{R_0} \tag{1.6}$$

$R(t)$ and R_0 are the radii at time t and $t = 0$, respectively. The transient stress growth coefficient, η_E^+, as a function of time for fixed Hencky strain rate is given as,

$$\eta_E^+ = \frac{\langle \sigma_{zz} - \sigma_{rr} \rangle}{\dot{\epsilon}} = \frac{F(t)/\pi R(t)^2}{\dot{\epsilon}} \tag{1.7}$$

Recently, a commercial version of DTU-FSR called VADER 1000 (Versatile Accurate Deformation Extensional Rheometer) has been developed by Rheo filament ApS [Alvarez (2015)]. This bench-top filament stretch rheometer has reduced dimensions giving it better temperature control and ability to quench the filament by quick oven release.

1.5 Thesis Outline

This Ph.D is a part of Marie Curie Initial Training Network SUPOLEN (Supramolecular assembly of polymeric structures: a novel route to enhance soft materials properties) in the European Union Seventh Framework. The project is highly interdisciplinary and inter-sectorial, the groups involved are world-leaders in their fields, and the tasks and partners are strategically linked. The SUPOLEN project involves nine universities and three industrial partners across Europe. The objective of SUPOLEN is to understand and tailor the structure and dynamics of supramolecular polymers based on well-defined building blocks, mainly linear and star-like polymers. As

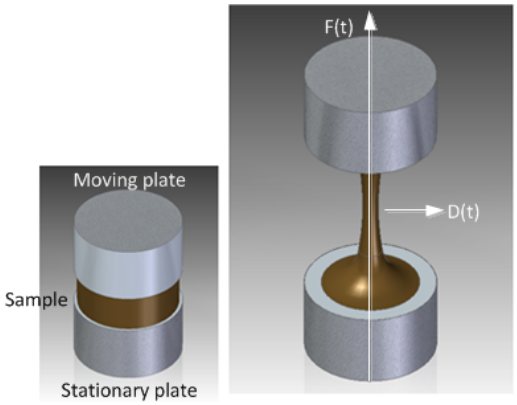

Figure 1.5: (a) Sample between two plates before experiment, (b) stretched filament during experiment where force is measured by weight cell attached to the bottom plate and the diameter is recorded at the mid-plane diameter as a function of time.

part of SUPOLEN, this Ph.D project focuses on the extensional rheology of linear supramolecular polymers.

Three categories of supramolecular polymers have been investigated throughout the thesis as shown in Table 1.1. Extensional rheology measurements have been performed using the DTU-FSR and VADER 1000 in constant strain rate mode.

Table 1.1: Types of supramolecular polymer materials investigated

	Unentangled	Entangled
Hydrogen bonding	P(MEA-co-UPy MA)	P(*n*BA-co-AA)
Ionic bonding	PTMO-Na	-

Chapter 2 and 3 focus on hydrogen bonding systems. **Chapter 2** deals with hydrolysed poly(*n*-butyl acrylate)-poly(acrylic acid), P(*n*BA-AA), copolymers having the same backbone length. We show that using the theoretical dependence of modulus and reptation time on the packing length, we can account for the changes in linear viscoelasticity due to the transformation of nBA side groups to AA along the backbone. Hydrogen bonding affects linear viscoelasticity at frequencies below the reptation time causing shallowing of the storage modulus and loss moduli to a power law scaling of 0.5. Significant strain hardening is noticed in constant strain rate extensional rheological measurements. **Chapter 3** focuses on unentangled 2-ureido-4[1*H*]-pyrimidones (UPy) based supramolecular networks. Using a modified sticky Rouse model, we show that the response of associating polymers does not depend on the chemistry of association, but rather on the polymer molecular weight (MW) and MW distribution, the number of stickers per chain and the distribution of

stickers along the backbone. **Chapter 4** focus on study of unentangled amorphous polyester ionomers based on polyethers and sulphonated phthlates with sodium/ lithium counterions in non-linear shear and extension. The measurements were performed on an updated filament stretch rheometer and on a strain controlled shear rheometer equipped with a cone-partitioned-plate (CPP) setup. The presence of high solvating poly (ethylene oxide) (PEO) along the backbone in the coionomer with PTMO, increases the maximum Hencky strain at fracture thus adding ductility to the brittle PTMO-Na ionomer. As a result, the coionomer deforms much more compared to PTMO-Na but both fracture eventually. On the other hand, whereas PTMO-Na cannot be sheared due to slip at the wall, the coionomer deforms in shear and eventually suffers from edge fracture instabilities. Lastly in **Chapter 5**, fracture of PTMO-Na ionomers is investigated in detail by combining extensional rheology and high speed imaging. When these ionomers are elongated at a rate higher than the inverse relaxation time of physical crosslinks, an edge fracture occurs at a critical stress. Parabolic fracture profiles provide evidence that the phenomenon is purely elastic and bulk dissipation has little impact on the crack profile. Experimental results are interpreted within the Griffiths theory for linear elastic materials and the de Gennes theory for viscoelastic materials.

1.6 Bibliography

Alvarez, N. J. (2015). `http://www.rheofilament.com/filament_stretching_rheometer.html`.

Bach, A., Rasmussen, H. K., and Hassager, O. (2003). Extensional viscosity for polymer melts measured in the filament stretching rheometer. *J. Rheol.*, 47(2).

Bailly, C. (2012). Lecture notes on constitutive modelling (european masters in engineering rheology).

Beijer, F. H., Sijbesma, R. P., Kooijman, H., Spek, A. L., and Meijer, E. W. (1998). Strong dimerization of ureidopyrimidones via quadruple hydrogen bonding. *J. Am. Chem. Soc.*, 120(27):6761–6769.

Bosman, A. W., Sijbesma, R. P., and Meijer, E. W. (2004). Supramolecular polymers at work. *Mater. Today*, 7(4):34–39.

Bossard, F., Sfika, V., and Tsitsilianis, C. (2004). Rheological properties of physical gel formed by triblock polyampholyte in salt-free aqueous solutions. *Macromolecules*, 37(10):3899–3904.

Chen, Q., Masser, H., Shiau, H.-S., Liang, S., Runt, J., Painter, P. C., and Colby, R. H. (2014). Linear Viscoelasticity and Fourier Transform Infrared Spectroscopy of PolyetherEsterSulfonate Copolymer Ionomers. *Macromolecules*, 47(11):3635–3644.

Chen, Q., Tudryn, G., and Colby, R. (2013). Ionomer dynamics and the sticky Rouse model. *J. Rheol.*, 16802(August):1441–1462.

Cordier, P., Tournilhac, F., Souli-Ziakovic, C., and Leibler, L. (2008). Self-healing and thermoreversible rubber from supramolecular assembly. *Nature*, 451:977–980.

Creton, C. (2011). Pressure-sensitive adhesives: An introductory course. *MRS Bulletin*, 28(6):434–439.

Eisenberg, A. and Kim, J. (1998). *Introduction to Ionomers*. Wiley.

Feldman, K. E., Kade, M. J., Meijer, E. W., Hawker, C. J., and Kramer, E. J. (2009). Model Transient Networks from Strongly Hydrogen-Bonded Polymers. *Macromolecules*, 42(22):9072–9081.

Goldansaz, H., Fustin, C.-A., Wbbenhorst, M., and van Ruymbeke, E. (2016). How supramolecular assemblies control dynamics of associative polymers: Toward a general picture. *Macromolecules*, 49(5):1890–1902.

Hirschberg, K. H. E. K. (2001). *Supramolecular polymers*. PhD thesis, Technical University Eindhoven.

Hyun, K., Nam, J. G., Wilhellm, M., Ahn, K. H., and Lee, S. J. (2006). Large amplitude oscillatory shear behavior of peo-ppo-peo triblock copolymer solutions. *Rheol. Acta*, 45(3):239–249.

Leibler, L., Rubinstein, M., and Colby, R. H. (1991). Dynamics of Reversible Networks. *Macromolecules*, 24:4701–4707.

Lewis, C., Stewart, K., and Anthamatten, M. (2014). The Influence of Hydrogen Bonding Side-Groups on Viscoelastic Behavior of Linear and Network Polymers. *Macromolecules*, 47:729–740.

Ling, G. H., Wang, Y., and Weiss, R. A. (2012). Linear Viscoelastic and Uniaxial Extensional Rheology of Alkali Metal Neutralized Sulfonated Oligostyrene Ionomer Melts. *Macromolecules*, 45:481–490.

Mugemana, C., Guillet, P., Hoeppener, S., Schubert, U. S., Fustin, C.-A., and Gohy, J.-F. (2010). Metallo-supramolecular diblock copolymers based on heteroleptic cobalt(III) and nickel(II) bis-terpyridine complexes. *Chem. Commun.*, 46(8):1296–8.

Nair, K. P., Breedveld, V., and Weck, M. (2008). Complementary Hydrogen-Bonded Thermoreversible Polymer Networks with Tunable Properties. *Macromolecules*, 41(10):3429–3438.

Qiao, X. and Weiss, R. A. (2013). Nonlinear Rheology of Lightly Sulfonated Polystyrene Ionomers. *Macromolecules*, 46:2417–2424.

Román Marín, J. M., Huusom, J. K. b., Alvarez, N. J., Huang, Q., Rasmussen, H. K., Bach, A., Skov, A. L., and Hassager, O. (2013). A control scheme for filament stretching rheometers with application to polymer melts. *J. Non-Newtonian Fluid Mech.*, 194:14–22.

Rossow, T. and Seiffert, S. (2014). Supramolecular polymer gels with potential model-network structure. *Polym. Chem.*, 5(8):3018.

Seiffert, S. (2016). Effect of supramolecular interchain sticking on the low-frequency relaxation of transient polymer networks. *Macromol. Rapid Commun.*, 37(3):257–264.

Shabbir, A., Goldansaz, H., Hassager, O., van Ruymbeke, E., and Alvarez, N. J. (2015). Effect of hydrogen bonding on linear and nonlinear rheology of entangled polymer melts. *Macromolecules*, 48(16):5988–5996.

Shabbir, A., Huang, Q., Chen, Q., Colby, R. H., Alvarez, N. J., and Hassager, O. (2016a). Brittle fracture in associative polymers: the case of ionomer melts. *Soft Matter*, 12:7606–7612.

Shabbir, A., Javakhishvili, I., Cerveny, S., Hvilsted, S., Skov, A. L., Hassager, O., and Alvarez, N. J. (2016b). Linear viscoelastic and dielectric relaxation response of unentangled upy-based supramolecular networks. *Macromolecules*, 49(10):3899–3910.

Sijbesma, R. P., Beijer, F. H., Brunsveld, L., Folmer, B. J. B., and Hirschberg, J. H. K. K. (1997). Reversible Polymers Formed from Self-Complementary Monomers Using Quadruple Hydrogen Bonding. *Science*, 278:1601–1604.

Stadler, F. J., Pyckhout-Hintzen, W., Schumers, J.-M., Fustin, C.-A., Gohy, J.-F., and Bailly, C. (2009). Linear Viscoelastic Rheology of Moderately Entangled Telechelic Polybutadiene Temporary Networks. *Macromolecules*, 42(16):6181–6192.

Stadler, F. J., Still, T., Fytas, G., and Bailly, C. (2010). Elongational Rheology and Brillouin Light Scattering of Entangled Telechelic Polybutadiene Based Temporary Networks. *Macromolecules*, 43(18):7771–7778.

Suzuki, S., Uneyama, T., Inoue, T., and Watanabe, H. (2012). Nonlinear rheology of telechelic associative polymer networks: Shear thickening and thinning behavior of hydrophobically modified ethoxylated urethane (heur) in aqueous solution. *Macromolecules*, 45(2):888–898.

van Ruymbeke, E., Vlassopoulos, D., Mierzwa, M., Pakula, T., Charalabidis, D., Pitsikalis, M., and Hadjichristidis, N. (2010). Rheology and structure of entangled telechelic linear and star polyisoprene melts. *Macromolecules*, 43(9):4401–4411.

Xu, D., Hawk, J. L., Loveless, D. M., Jeon, S. L., and Craig, S. L. (2010). Mechanism of shear thickening in reversibly cross-linked supramolecular polymer networks. *Macromolecules*, 43(7):3556–3565.

Yan, X., Wang, F., Zheng, B., and Huang, F. (2012). Stimuli-responsive supramolecular polymeric materials. *Chem. Soc. Rev.*, 41(18):6042–65.

Zhang, L., Brostowitz, N. R., Cavicchi, K. a., and Weiss, R. A. (2014). Perspective: Ionomer Research and Applications. *Macromol. React. Eng.*, 8(2):81–99.

CHAPTER 2

The Effect of Hydrogen Bonding on Linear and Nonlinear Rheology of Entangled Polymer Melts

2.1 Introduction

Supramolecular polymers represent an emerging class of polymers that offer superior material properties compared to their non-associating counterparts. Supramolecular polymers are a broad category of materials that include all polymers whose monomeric units can associate via secondary interactions. These secondary interactions can be due to hydrogen bonding [Lewis et al. (2014); Lange et al. (1999); Nair et al. (2008, 2011); Feldman et al. (2009); Montarnal et al. (2009); Sivakova et al. (2005)] , metal-ligand bonding [Rossow and Seiffert (2014); Mugemana et al. (2010)], and/or ionic bonding [Eisenberg and Kim (1998); Chen et al. (2013); Zhang et al. (2014); Weiss and Yu (2007)]. Hydrogen bonding is the most common non-covalent reversible interaction employed to create supramolecular polymeric assemblies [Nair et al. (2008)]. Although hydrogen bonds form one of the weakest noncovalent interactions, their ability to form highly directional and versatile associations make them very useful [Sijbesma and Meijer (1999)]. For example, cooperative hydrogen bonding is responsible for the material properties of nylons.

The association strength of a single hydrogen bond in a polymer melt (no solvent effects) depends on the nature of donor and acceptor. The association strength of multiple hydrogen bonding units depends on the same, but also the number and arrangement of the hydrogen bonds [Brunsveld et al. (2001); Corbin and Zimmerman (1998)]. One particularly useful trait of hydrogen bonds is that the association strength and dynamics can be significantly altered via external stimuli, e.g. temperature. At high temperatures, the association strength of a hydrogen bond is significantly reduced and thus the presence of hydrogen bonds has little to no effect on material properties. At low temperatures, the association strength of the hydrogen bond is

large and the lifetime is such that the bonds act like weak crosslinks between chains [Lewis et al. (2014)]. This ability to thermally tune association strengths allows for easy processing of such materials for various applications [Yan et al. (2012)].

Although a large body of work on H-bonding supramolecular polymer synthesis exists in the literature, very few studies have examined the mechanical properties of these polymers in the melt state [Brunsveld et al. (2001); Lewis et al. (2014); Feldman et al. (2009); Stadler and de Lucca Freitas (1988)]. Lewis and coworkers in 2014 reported the influence of density, molecular structure, and association strength considering four different hydrogen bonding groups on linear viscoelasticity. The authors determine that the presence of hydrogen bonds (i) elevates the material's glass transition termperature, (ii) copolymers with weakly associating hydrogen bonds (acrylic acid (AA), carboxyethylacrylate (CEA), acrylamidopyridine (AP)) show no evidence of network formation, and finally (iii) conclude that side-group dimerization alone is not sufficient to form a mechanically relevant network [Lewis et al. (2014)]. Almost two decades prior, Stadler and coworkers examined the linear viscoelastic properties of 1,2,4-triazoline-3,5-dione (TAD) modified polybutadiene following a procedure by Stadler and Freitas (1986); Leong and Butler (1980). From this work, the LVE properties of the modified polybutadiene shows three characteristics as a function of the number of hydrogen bonding groups (i) increase in plateau modulus, (ii) decrease in the low frequency crossover ω_L, and (iii) a transition in power law scaling of G' and G'' from 2 and 1, respectively to $\approx$0.5 in the LVE terminal regime. It is not clear from this data since the addition of TAD highly modifies the backbone chemistry by eliminating double bonds, whether all three effects are due to either hydrogen bonding, change in chemistry, or a combination of both. We agree with the comment by Lewis et al. that comparative studies involving a single backbone are necessary to elucidate a clear structure-property relationship in hydrogen bonding polymers [Lewis et al. (2014)].

In this work, we use a model entangled monodisperse linear PnBA polymer, which is selectively hydrolyzed to convert nBA side groups to AA side groups, in order to isolate the effect of hydrogen bonding on linear viscoelasticity of entangled polymer melts. More specifically, we examine four PnBA-PAA copolymers with increasing number of acrylic acid groups: pure PnBA, 6% AA, 13% AA, and 38% AA. The percentage of AA is determined post-hydrolysis using NMR spectroscopy. Since all polymers are synthesized from the same starting PnBA and hydrolysis does not change the chemistry of the backbone, the four polymers have the same backbone chemistry and length. Using a simple model that takes into account changes in packing length, we convincingly show that the contribution of hydrogen bonding to linear viscelasticity is restricted to the viscous terminal regime. In other words, hydrogen bonding only hinders reptation of the entangled chains and at a critical number of AA side groups forms a weak gel at low frequencies. Using this understanding, we probe the nonlinear mechanical properties of the four systems using a filament stretching rheometer. We show that the hydrogen bonds give rise to extreme strain hardening behavior when the strain rates are significantly below the inverse reptation time. Both the linear and nonlinear results are put into the context of the state of the art.

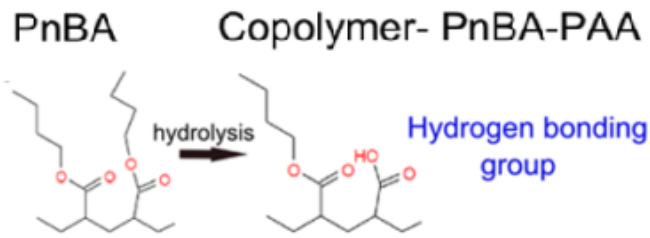

Figure 2.1: Hydrolysis of PnBA into copolymer-PnBA-PAA

2.2 Experimental Details

Materials

Poly(n-butyl acrylate) (PnBA) was used as received from Polymer Source Inc. (Product No. P1111-nBUA lot 18124). The PnBA is reported by supplier to have a Mn=193k, Mw=210k, and PDI=1.085. The Molecular weight was remeasured in-house via a size exclusion chromatography using a Viscotek TriSEC Model 302 triple detector array and a Knauer K-2501 UV detector using two PLgel mixed-D columns from Polymer Laboratories (PL). The samples were run in THF at 30°C. The columns were calibrated using PS standards. The PnBA was measured to have Mn=121k, Mw=166k, and a PDI=1.375. Using the entanglement molecular weight specified by Jullian and coworkers, $M_e = 32$ kg/mol [Jullian et al. (2010)], then the number of entanglements for the pure PnBA is $Z \approx 5$. Three partially hydrolyzed samples of PnBA were produced by dissolving as received PnBA in distilled THF. The polymer solution was then mixed with a solution of water and potassium hydroxide, KOH. The hydrolysis reaction proceeded under reflux conditions at 70°C. After a desired time, the reaction mixtures were cooled to room temperature and neutralized with excess amount of HCl. The amount of hydrolyzed PnBA groups depends on the duration of hydrolyzation. After hydrolyzation, the samples were dried using a rotary evaporator to ensure complete removal of n-butanol. The salt and polymer mixture were washed multiple times in ethyl acetate and water consecutively. Finally, the polymer solutions were washed with water and dried using a rotary evaporator. Extent of reaction, i.e. the number of nBA side groups hydrolyzed to AA, was quantified using ^1HNMR spectroscopy. A general scheme of hydrolysis is shown in Fig. 2.1

The extent of hydrolysis was determined by high field proton NMR in solution of approximatively 10 mg polymer/1 ml CDCl3 using >200 scans separated by recycling times > 5 relaxation times of the polymer. A b071 - AVANCE 500 MHz aimant Oxford spectrometer was used for recording 1H-NMR. The average fraction of hydrolyzed monomers was determined by using the ratio of triplet methyl (<0.9 ppm) and methylene (≈4.3 ppm) protons to the rest of the protons in the backbone

and side chain (1<chemical shift<2.4 ppm).

In the presence of metallic salts, such hydrogen bonding systems behave like ionomers, in which acid groups are adsorbed to the ionic aggregates. In carboxylic acid containing ionomers, the association strength and consequently both linear and non-linear rheology strongly depend on the nature of the cation as well as the counter ion. Hence it is imperative for the purpose of this study to purify the sample from metallic contaminations, before any measurements. Purification was performed by successive washing of the samples. Energy dispersive X-ray spectrometry analysis (EDX) was used in order to quantify the residual metallic contamination after synthesis and purification of the copolymers. EDX measurements were carried out using a JEOL FEG SEM 7600F scanning electron microscope equipped with an EDX system (Jeol JSM2300 with a resolution <129 eV) operating at 15 keV with a working distance of 8 mm. The acquisition time for the chemical spectra lasted 300 s with a probe current of 1 nA. Specimens for EDX were mounted on stubs and analyzed without metallization. All samples showed less than 0.6% metallic content after washing. Most samples showed less athan 0.1% metallic content after washing.

The samples and their characteristics are shown in Table 2.1. Given that the $Z = 5$, an examination of Table 2.1 shows that even for Ref(PnBA) there are several AA groups per entanglement section.

Table 2.1: Percentage and number of AA side groups on backbone

Sample Name	%sticky groups/chain	Number of AA side groups/chain
Ref (PnBA)	3	49
AA6	5.5	90
AA13	13	207
AA38	38	615

Rheology

Linear Viscoelasticity

Linear visoelastic properties of the PnBA-AA copolymers were investigated by small amplitude oscillatory shear (SAOS) rheology using a MCR 301 (Anton Paar, Germany) rheometer. Temperature was controlled using a convection oven operating under nitrogen. Three different (8, 15 or 20mm-diameter) parallel plate geometries were used depending on the viscosity level of the system at the given temperature. Furthermore, the different geometries were used to ensure proper accounting for tool compliance. No slippage problem was observed due to good adhesion of the polymers to the surface of the steel geometries. For samples pure PnBA, AA6, the linear viscoelastic data were measured between -25^{o}C and 45^{o}C and time temperature superposition was used to create master curves. For samples AA13 and AA38, the linear viscoelastic data were measured between -15^{o}C and 30^{o}C and time temperature superposition

was used to create master curves. Outside of this range (more specifically above 15^oC) samples with acrylic acid content above 6% show thixotropic behavior, do not follow TTS, and therefore are not included in generation of a master curve. The thixotropic behavior of these samples is a discussion for a future article.

Extensional viscosity measurements

The extensional stress growth coefficient as a function of time was measured using a filament stretching rheometer (DTU-FSR). Cylindrical stainless steel sample plates with a diameter of 5.4mm were used for all measurements. The mass of each sample varied from 0.04g to 0.06g. The aspect ratio,$\Lambda_0 = L_0/R_0$, varied from 0.36 to 0.75. Measurements were performed at a constant Hencky strain rate imposed at the mid-filament diameter using an online control scheme [Román Marín et al. (2013)]. All experiments were performed at 21.5°C. The imposed strain rates were varied from $0.0006s^{-1}$ to $1s^{-1}$. All samples except AA38, were relatively fluid like and were formed into an approximate cylindrical test specimen manually using a steel spatula. After considerable time, the sample relaxed to form an axisymmetric cylindrical shape due to surface tension. It is very important that sufficient time is allowed for the sample to completely relax before performing any measurement. This was ensured by monitoring the force on the sample and waiting for the force to be sufficiently close to zero, i.e. zero within the noise ($\pm$0.05 g) of the force transducer. Since sample AA38 has extremely long relaxation times (see LVE data in Results), it was annealed at 80°C under a nitrogen rich environment for approximately half an hour. Nitrogen was used during annealing to prevent sample oxidation. Prior to performing elongational measurements, sample AA38 was pre-stretched at 80°C to a diameter between 2.48mm and 4.4mm depending on the applied strain rate. At which point, the temperature was reduced to the desired temperature and the stress was allowed to relax for up to 2 hours depending on the sample. Such practice ensures that the maximum force during the experiment was low enough to avoid sample detachment from the plates.

2.3 Results

The linear viscoelasticity (LVE) measured using small amplitude oscillatory shear is presented in Fig. 2.2 for all four samples. Fig. 2.2a shows the response for the PnBA as received from the supplier. At high frequency, G' and G'' show the classical frequency dependence expected for a monodisperse entangled linear polymer melt. There is a power law dependence of G'' in the glassy regime near the high-frequency crossover, ω_H, a discernible plateau modulus in G', and an inflection in G'' just before the low frequency cross-over, ω_L. However, at frequencies below ω_L, known as the terminal regime, G' and G'' deviate from the expected power law dependence of two and one, respectively. This deviation is surprising to the authors, since no data for a monodisperse entangled linear polymer melt is known to show such a deviation in the terminal regime. An explanation for the observed discrepancy is due to hydrogen

bonding via the small amount of AA/chain, 3%, present in the sample measured via NMR, see Table 2.1.

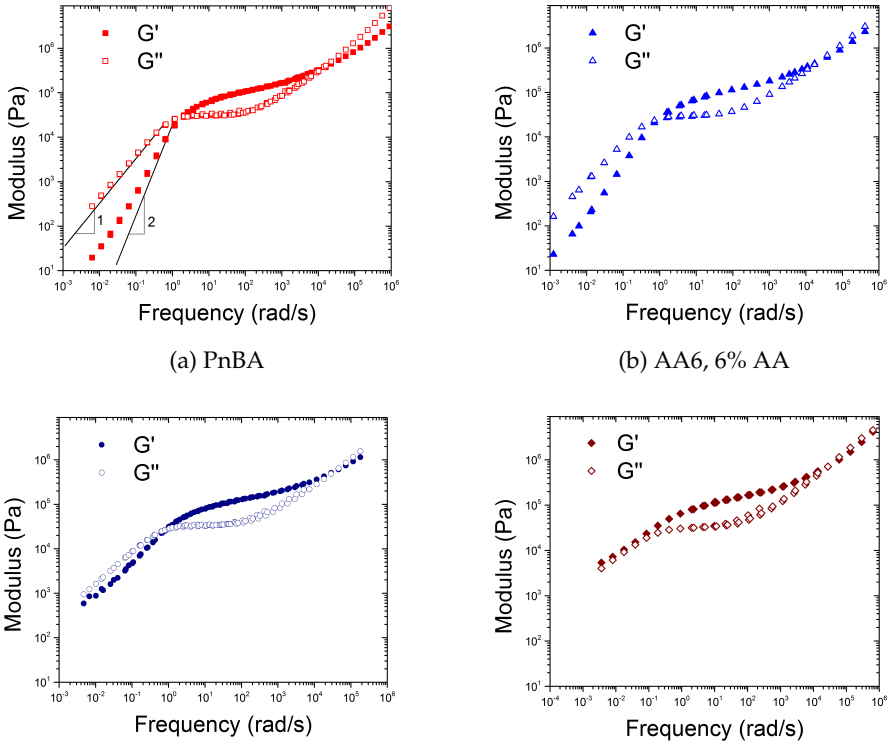

(a) PnBA

(b) AA6, 6% AA

(c) AA13, 13% AA

(d) AA38, 38% AA

Figure 2.2: shows the linear viscoelastic response of all four samples measured using small amplitude oscillatory shear. The lines in (a) represent the expected power law dependence of G' and G'' for a monodisperse linear polymer melt in the low frequency, terminal regime.

Fig. 2.2b shows LVE data for sample AA6, which is composed of 6% AA along the backbone. Even though the amount of AA is doubled, Fig. 2.2b shows very similar LVE behavior to the PnBA sample in Fig. 2.2a. Qualitatively, the only difference between the two data sets appears to be a slight shift in the frequency dependence of G' and G'' at frequencies below, ω_L. Fig. 2.2c, shows LVE data for sample AA13, which is composed of 13% AA along the backbone. Again Fig. 2.2c shows similar LVE behavior at high frequency, but a much more pronounced change in low frequency dynamics. The greatest change in LVE behavior is shown in Fig. 2.2d, for sample AA38, wherby G' and G'' lie parallel and on top of each other for low frequencies.

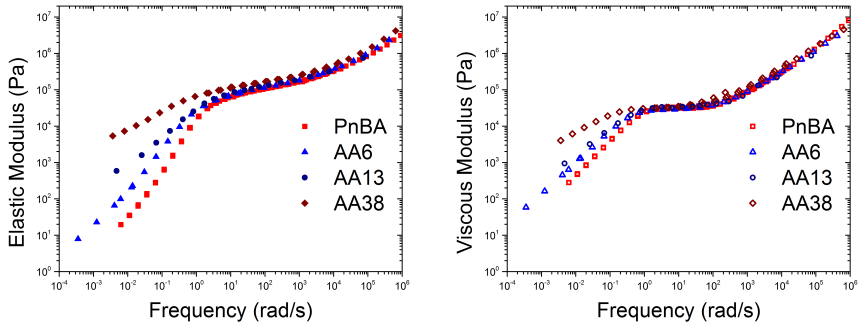

(a) Elastic Modulus (b) Viscous Modulus

Figure 2.3: Shows an overlay of all data presented in Fig 2.2 split into (a) G', elastic modulus, and (ii) G'', viscous modulus.

This is indicative of a weak network, i.e. gel, or Rouse dynamics. It would appear from Figs. 2.2a-2.2d that the existence of AA side groups strongly alter the behavior of G' and G'' at frequencies lower than ω_L.

Fig. 2.3 shows a closer examination of (a) the elastic modulus and (b) the viscous modulus. What is now evident from Fig. 2.3a is that there is a slight shift in the plateau modulus with increasing AA content. Furthermore, by comparing Fig. 2.3a and 2.3b there is a shift in the low frequency crossover. Therefore, hydrolyzing the nBA side group to AA along the backbone has the following three effects on LVE, (i) increases the plateau modulus, (ii) decreases the low frequency crossover, ω_L, and (iii) changes the power law dependence and increases the overall magnitude of G' and G'' at frequencies lower than ω_L. These three dependencies will be examined in greater detail in the discussion section.

We now examine the extensional rheology of the four samples in the context of the LVE data presented above. Fig. 2.4 shows the extensional rheology of all four samples for various strain rates. The strain rates are always increasing from right to left, i.e. the farthest curve to the right in Fig. 2.4a corresponds to the smallest strain rate 0.3 s^{-1} and the farthest to the left corresponds to the highest strain rate 3 s^{-1}. The solid line in all figures represent the corresponding LVE envelope determined from a multi-mode Maxwell fit to the LVE data shown in Fig. 2.2. The dashed lines in Fig. 2.4b-2.4d represents the LVE envelope for PnBA, i.e. the solid line shown in Fig. 2.4a is replicated for reference in all three figures. Typically in extensional rheology of monodisperse entangled linear polymer meltss, the measured stress growth coefficient follows the LVE envelope for strain rates less than the inverse of the disengagement time, $1/\tau_d$. For strain rates greater than $1/\tau_d$, the stress growth coefficient deviates upwards from the LVE envelope. This upwards deviation is referred to as strain hardening. $\tau_R = 0.038$ s for the PnBA studied here, which is calculated using BSW parameters, the BSW model and parameter

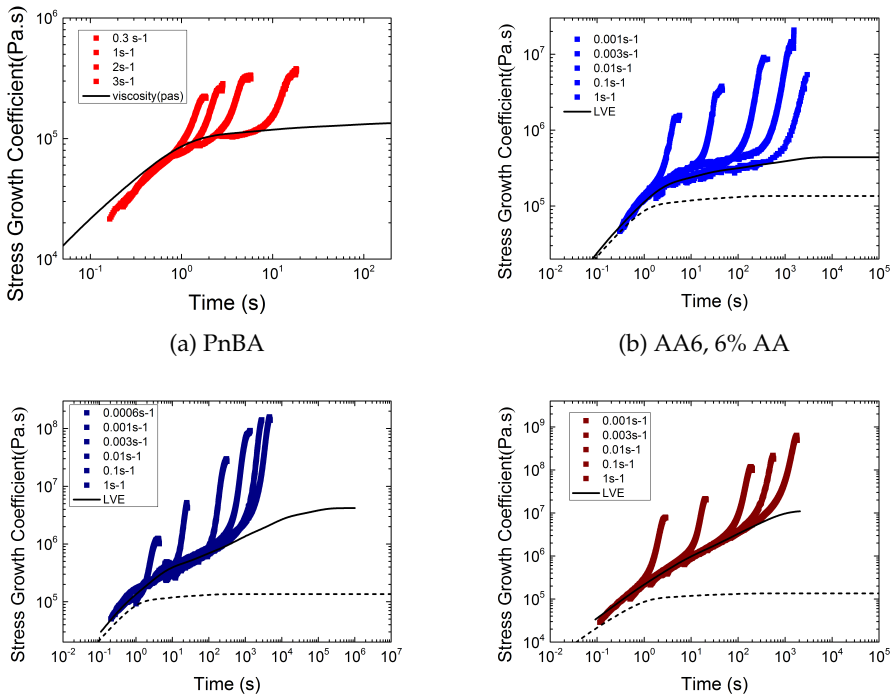

(a) PnBA

(b) AA6, 6% AA

(c) AA13, 13% AA

(d) AA38, 38% AA

Figure 2.4: shows the stress growth coefficient measured using the filament stretching rheometer. The solid lines represent the best fit of the multi-mode Maxwell model to the LVE data shown in Fig. 2.2. The dashed lines in (b)-(d) represent the multi-mode Maxwell model for the PnBA sample (solid line in (a)) for comparison.

estimation are explained in more detail in the discussion section. Thus, for PnBA, strain hardening is not expected for strain rates $\dot{\epsilon} < 13\ s^{-1}$. It is convenient to discuss the relative magnitude of $\dot{\epsilon}$ to τ_R in terms of the Weissenberg number, $Wi = \dot{\epsilon}\tau_R$ i.e. when $Wi < 0.5$ no strain hardening is expected and when $Wi \geq 0.5$ strain hardening is expected. It is evident from Fig. 2.4a that even for the lowest $Wi = 0.01$, strain rate $0.3\ s^{-1}$, strain hardening is observed. The strain hardening plateaus at a value approximately a factor of three higher than the zero shear rate viscosity. We hypothesize that this deviation is most likely due to the small presence of AA, 3%, in the PnBA as received. Note that if this is indeed the case, one should be careful to use PnBA as a model linear polymer system assuming no association groups.

Fig 2.4b shows the extensional rheology of sample AA6 for five increasing strain rates from 0.001-1 s^{-1}. At small times, all curves follow the LVE envelop. At larger times there is a sharp strain hardening behavior observed for all measured strain

rates. The strain hardening achieves a magnitude an order higher than the LVE envelope and two orders of magnitude higher than the zero shear rate viscosity of PnBA denoted by the dotted line. The same strain hardening behavior is observed for samples AA13 and AA38, see Fig. 2.4c-2.4d. The main difference is that a doubling of the number of AA side groups per chain causes an order of magnitude increase in the strain hardening behavior. Sample AA6, AA13 and AA38 achieve stress growth coefficients two, three and four orders of magnitude above the zero shear rate viscosity of PnBA, respectively.

It is important to note that the greatest strain hardening behavior is observed for strain rates much lower than the strain rates applied to PnBA in Fig. 2.4a. Assuming the same Rouse time, $Wi \leq 4 \times 10^{-5}$ for the lowest strain rates in Fig 2.4b-2.4d. For such extremely low Wi, the stress growth coefficient is expected to follow the LVE envelope for all relevant strains. The significant deviation from LVE of pure PnBA demonstrates the influence of hydrogen bonding on the nonlinear response of an entangled linear polymer melt at low strain rates. In other words, addition of hydrogen bonding side groups help to prevent creeping of the material. It is for the similar reasons that the acrylic acid groups in acrylic based pressure sensitive adhesives (PSA's) are employed to stabilize the fibrils during debonding [Lakrout et al. (2001); Ahn and Shull (1998)]. The above mentioned data offers promising route for tailoring strain hardening in PSA's to avoid sticky polymer residue on the substrate.

2.4 Discussion

It was noted above that hydrolyzation of nBA to AA affected the LVE behavior by (i) increasing the plateau modulus, G_{N0}, (ii) decreasing the low frequency crossover, ω_L, and (iii) increasing G' and G'' and altering their power law dependence at frequencies lower than ω_L. Recall that these are the same three observations drawn from the work of Stadler and Freitas regarding modified polybutadienes [Stadler and Freitas (1986)]. At least for these two systems, these observations seem to be general and independent of chemistry. We are interested in discerning which of these three changes can be attributed to the existence of hydrogen bonding and which are an effect of changes in chemical structure via hydrolysis. Since all hydrolyzed samples are derived from the same PnBA molecule the changes in chemistry can be accounted for by taking into account changes in packing length of the polymer molecule. The packing length of a polymer chain is given by the equation,

$$P = \frac{\nu_0}{b^2}, \tag{2.1}$$

where ν_0 is the volume of the polymer repeat unit and b is the Kuhn length. Since ν_0 depends on the molecular weight of the repeat unit, then it is expected that the packing length will depend on the percentage of nBA hydrolyzed to AA. We assume that since the backbone chemistry is left unchanged via hydrolysis the kuhn length

is not a function of the number of AA side groups (see argument in preceding paragraph). The molecular weight of a nBA repeat unit is M_{nBA}=128 g/mol. After hydrolysis, the nBA is converted to AA with a a molecular weight of M_{AA}=72 g/mol. The Mw of the chain after hydrolysis is given by $Mw_H = \alpha Mw$, where

$$\alpha = (1 - 0.44f) \tag{2.2}$$

where f is the mol fraction of AA side groups and α represents the transition in Mw from pure nBA, α=1, to pure AA, α=0.56. Note that in what follows the superscript "0" denotes the property with respect to pure PnBA. We therefore define an average packing length per chain for a given fraction of AA,

$$\bar{P} = \frac{\alpha v_0}{b^2}. \tag{2.3}$$

Following from Fetters et al. (2007), a change in packing length will yield the following effect on the original G_{N0} and disengagement time (i.e. reptation time), τ_{d0},

$$G_N = \frac{G_{N0}}{\alpha^3} \tag{2.4}$$

$$\tau_d = \frac{\tau_{d0}}{\alpha^{6.8}}. \tag{2.5}$$

Therefore, by knowing f, α can be calculated via Eq. 2.2 and the expected change in plateau modulus and disengagement time can be easily calculated via Eqs. 2.4 and 2.5. Note that a small change in α has a very large effect on G_N and an even larger effect on τ_d.

The above argument assumes that the Kuhn length does not change with a change in side group chemistry. It is not clear that this is a good assumption and therefore we think it is best to demonstrate that this assumption is in fact supported by our current knowledge of polymer physics. *Argument in support of unchanged Kuhn length*: Suppose that we have a backbone of poly(ethylene), PE, and could somehow put a benzene ring on every second C-atom, forming poly(styrene). Using Fetters et al. this would result in a change of Kuhn length from 13.7 $\dot{A}$, see Table in Fetters, to 18 $\dot{A}$, calculated using equation:

$$b = \frac{< R^2 >_0}{M} \frac{m_b}{l \cos(\theta/2)} \tag{2.6}$$

where $< R^2 >_0 / M$=0.437, m_b =54, $\cos(\theta/2)$ =0.83 for CC bond angle, and l =1.5$\dot{A}$ for CC bond length [Fetters et al. (2007)]. This means that going from PE to PS only yields a 30% change in Kuhn length, this is in comparison to the 130% change in the packing length, p, estimated from Eq. 2.3. One could additionally argue that going from PE to PS is a dramatic change compared to the chemical change from PAA to PnBA, since the chemical change for PnBA is further away from the CC backbone. These arguments strongly support the assumption of a constant Kuhn

length. Therefore, it can be argued that the major influence of changing the chemistry will be the ability to tie knots, i.e. the entanglement length or packing length.

If our simple arguments are correct, then the observed changes in LVE behavior (i) and (ii) above, should be accounted for by changes in chemistry and not hydrogen bonding between chains. The Baumgaertel-Schausberger-Winter (BSW) relaxation spectrum is a model that has been shown to accurately fit and predict LVE behavior of monodisperse entangled linear polymer melts. The BSW model has five parameters: n_e and n_g, which represent empirical slopes of G'' immediately after ω_L and immediately before ω_H, respectively, and G_N, τ_d, and τ_c, which are related to the theoretical tube model parameters: plateau modulus, disengagement time, and the relaxation time of one entanglement, respectively [Huang et al. (2013)]. For a monodisperse linear polymer, n_e=-0.23 and n_g=0.7. We perform a nonlinear least squares fit of the BSW model to the LVE data of PnBA in order to determine the values of G_{N0}, τ_{d0}, and τ_c. The best fit parameters are given in Table 2.2. The best fit BSW spectrum is plotted in Fig. 2.5a. It is evident from this figure that the BSW model fits the data very well, except in the terminal regime below ω_L, as expected.

Using Eqs. 2.4 and 2.5, we can predict the BSW parameters as a function of AA fraction. The predicted values are given in Table 2.2. Fig. 2.5b-2.5d shows LVE data for samples AA6, AA13, and AA38 along with the BSW predictions accounting for the number of AA side groups per chain. The excellent agreement between the BSW predictions and the experimental data shows that our simple model is able to predict quantitatively the observed change in G_N for increasing number of AA side groups. Furthermore, the simple model is able to capture the increase in the low frequency crossover as seen from Fig. 2.5a-2.5b. This is less evident in Fig. 2.5c-2.5d due to the convolution that occurs at low frequency for increased AA content. However, it is clear that that low frequency crossover is decreasing in the experimental data, which is the same trend predicted by Eq. 2.5, i.e. increasing τ_d. One can conclude from these results that observations (i) and (ii) are strongly due to hydrolysis of nBA to AA and not hydrogen bonding. However, changes in packing length cannot explain observation (iii) whereby a change in power law dependence of G' and G'' occurs. We therefore conclude that hydrogen bonding between chains is giving rise to this particular phenomenon. With regard to the data presented by Stadler and Freitas, we hypothesize that if one could account for how G_{N0} and τ_d would change with their chemistry, the same conclusions would be drawn.

Assuming that superposition holds, we subtract the corresponding BSW spectrum from the experimental data in order to examine the hydrogen bonding contribution to linear viscoelasticity. The remaining G' and G'' contribution due to hydrogen bonding is shown in Fig. 2.6a and 2.6b, respectively. Note that in these figures a larger frequency window for the data set is included than shown in Figure 2.2. The solid black line is an indicator of 0.5 power law scaling, which is indicative of a gel or Rouse dynamics. In Fig. 2.6a, the power law scaling of G' for PnBA is slightly greater than 0.5 and decreases with increasing AA content. In Fig. 2.6b, the power law of G'' for PnBA is also slightly higher than 0.5 and decreases with increasing AA content. For sample AA38, the power law scaling of G' and G'' appears to be

	BSW Parameters				
	G_N [Pa]	τ_d [s]	τ_c [s]	n_e	n_g
PnBA(3% AA)	1.71×10^5	1.06	3.5×10^{-4}	-0.23	0.7
AA6	1.78×10^5	1.16	3.5×10^{-4}	-0.23	0.7
AA13	1.92×10^5	1.45	3.5×10^{-4}	-0.23	0.7
AA38	2.84×10^5	3.37	3.5×10^{-4}	-0.23	0.7

Table 2.2: The parameters for PnBA were determined from nonlinear least squares fit. Parameters for AA6, AA13, and AA38 were calculated using Eqs. 2.4 and 2.5 using PnBA parameters taking into account that PnBA has 3% AA. The theoretically pure PnBA can be calculated using the parameters for 3% AA to be $G_N = 1.64 \times 10^5$ Pa and $\tau_m = 0.97$ s, which is then used to make the parameter estimations for AA6, AA13, and AA38.

precisely 0.5. Moreover, G' and G'' overlap each other for samples AA13 and AA38, which is indicative of a gel or Rouse dynamics.

Another observation from Fig. 2.6a and Fig. 2.6b is that there appears to be a steady increase in the magnitude of G' and G'' as a function of the number of AA groups per chain. Fig. 2.7a shows the magnitude of G' plotted as a function of the number of AA groups per chain for two frequencies. There appears to be a linear dependence of $|G'|$ on the number of AA groups per chain for both frequencies. This linear dependence is in stark contrast to the highly nonlinear dependence of extensional stress as a function of the number of AA groups/chain in nonlinear rheology. Fig. 2.7b shows the extensional stress taken at the plateau seen in Fig. 2.4 plotted as a function of the number of AA groups for different strain rates. It is evident from this figure that this dependence is a strong function of strain rate. For example, for a $\dot{\epsilon} = 0.01\text{s}^{-1}$ the dependence appears linear for the concentrations of AA examined. However, for $\dot{\epsilon} = 0.003\text{s}^{-1}$ the trend is concave and for $\dot{\epsilon} = 0.1\text{s}^{-1}$ the trend is convex for increasing values of f.

We speculated in the results section that the deviation of PnBA LVE from the classical power law scaling in the terminal regime was due to the presence of hydrogen bonding. It is clear from the results presented here that indeed hydrogen bonding for a monodisperse linear polymer manifests itself in the terminal regime of LVE. Surprisingly, hydrogen bonding has little effect on the LVE at frequencies above ω_L. This suggests that the relaxation time of hydrogen bonding is slower than the inverse disengagement time of the polymer chains and therefore at frequencies larger than $1/\tau_d$ the dynamics of the hydrogen bonds are irrelevant and classical polymer dynamics of the entangled chains dominate. This important observation is also evident in the nonlinear response of the samples. In Fig. 2.4, one observes that the largest strain hardening is observed for the slowest strain rates. In other words, when the strain rate is much less than $1/\tau_d$ the hydrogen bonds contribute strongest to the stress. However, for increasing strain rate, e.g. $\dot{\epsilon}$=0.1 s^{-1}, sample AA6, AA13, and AA38 show decreasing degrees of strain hardening. Note that these conclusions

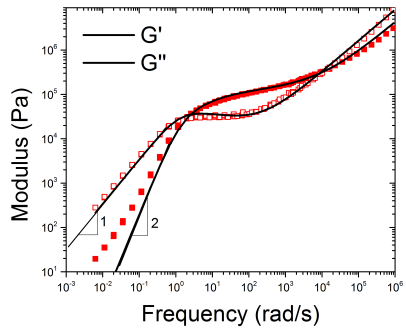

(a) PnBA

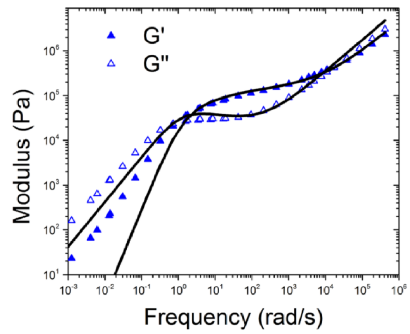

(b) AA6, 6% AA

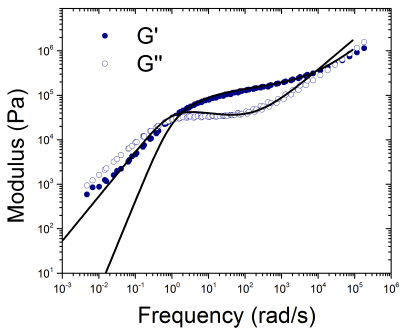

(c) AA13, 13% AA

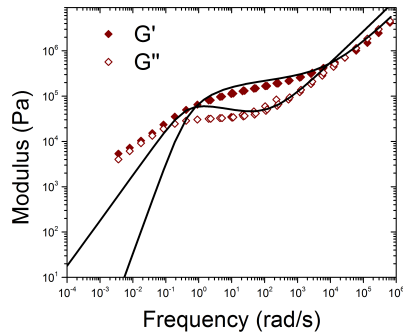

(d) AA38, 38% AA

Figure 2.5: shows the linear viscoelastic response of all four samples measured using small amplitude oscillatory shear as presented in Fig. 2.2 along with BSW predictions (solid lines) assuming Eq. 2.4 and 2.5 hold.

can only hold for the number of AA side groups studied here, i.e. up to 38%.

Recall from the introduction that Lewis and coworkers in their study considering four different hydrogen bonding groups concluded that dimerization of a single side group was not enough to induce the formation of a network. This trend seems to hold true in the results presented here for the weakly entangled networks and low fraction of AA side groups studied by them. However, it is evident from this study that for an entangled linear polymer network with more than 12% AA side groups, the formation of a weak network/gel is possible. It is still not clear whether this is due to the large percentage of AA side groups or the fact that the chains are sufficiently entangled. The mechanism responsible for the network/gel formation is the subject of a future article, whereby the data is discussed in terms of a physical model.

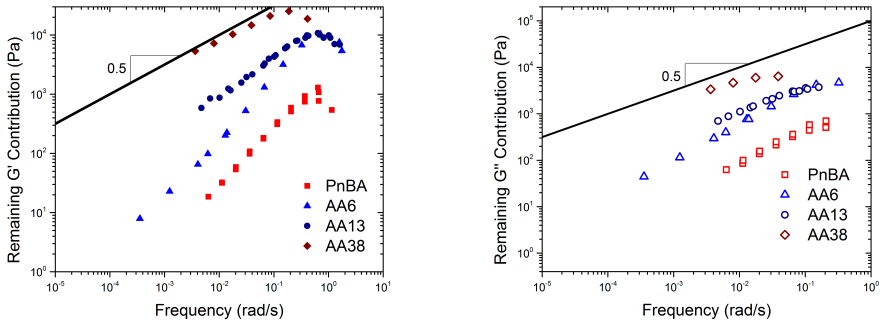

(a) (b)

Figure 2.6: shows the remaining contribution of (a) G' and (b) G'' to LVE after subtraction of the corresponding BSW spectrum, see Fig. 2.5. The solid line indicates a power law scaling of 0.5.

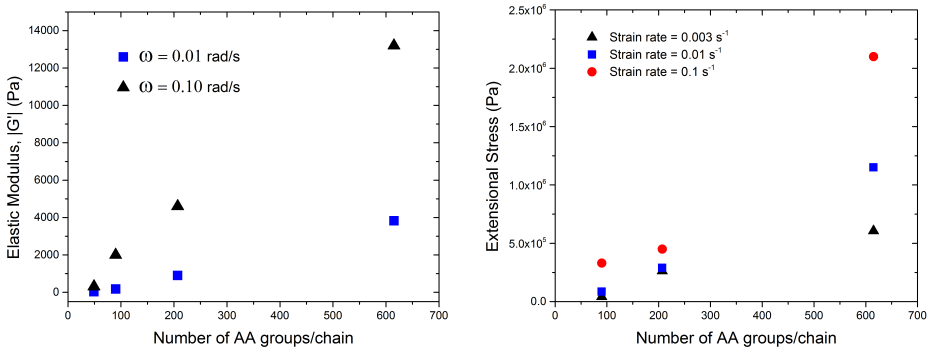

(a) (b)

Figure 2.7: (a) shows the magnitude of G' as a function of the number of AA groups per chain for the given frequency shown in the legend and (b) shows the magnitude of extensional stress at the plateau as a function of the number of AA groups per chain for the given strain rate shown in the legend.

2.5 Conclusions

We present linear and nonlinear rheological results for a model monodisperse linear polymer, PnBA, which has been hydrolyzed to different extents to determine the impact of hydrogen bonding on polymer dynamics. There are two contributions to the observed trends in linear viscoelasticity as a function of increasing AA side groups,

(i) changes in packing length and (ii) hydrogen bonding between chains. Using a simple model, we were able to account for changes in packing length and therefore explicitly show the effect of hydrogen bonding. Hydrogen bonding specifically alters the power law dependence of G' and G'' in the LVE terminal regime, i.e. frequencies below ω_L, of an entangled linear polymer network. More specifically, hydrogen bonding increases the magnitude of G' with respect to G'' such that at sufficiently high concentrations, i.e. 12% in our case, G' and G'' are parallel (power law 0.5) and equal in magnitude. For frequencies above ω_L, hydrogen bonding has little to no effect on the LVE response. This suggests that there is a relaxation time associated with the hydrogen bonding groups that is greater than $1/\omega_L$. For frequencies above ω_L the hydrogen bonds are too slow to effect LVE behavior. Extensional rheology was used to probe the contribution of hydrogen bonding to nonlinear dynamics. It was evident that for strain rates below ω_L, the samples exhibited impressive strain hardening behavior. The magnitude of strain hardening decreases as the strain rate approached ω_L. This trend supports the hypothesis that above a critical strain rate the hydrogen bonds become irrelevant. There is a need for better understanding of the action and strength of hydrogen bonding. Hopefully the data and analysis presented here will guide the foundation of theory work in this area.

2.6 Bibliography

Ahn, D. and Shull, K. R. (1998). Effects of methylation and neutralization of carboxylated poly(n-butyl acrylate) on the interfacial and bulk contributions to adhesion. *Langmuir*, 14(13):3637–3645.

Brunsveld, L., Folmer, B. J. B., Meijer, E. W., and Sijbesma, R. P. (2001). Supramolecular Polymers. *Chem. Rev.*, 101(12):4071–4098.

Chen, Q., Tudryn, G., and Colby, R. (2013). Ionomer dynamics and the sticky Rouse model. *J. Rheol.*, 16802(August):1441–1462.

Corbin, P. and Zimmerman, S. (1998). Self-association without regard to prototropy. A heterocycle that forms extremely stable quadruply hydrogen-bonded dimers. *J. Am. Chem. Soc.*, 7863(98):9710–9711.

Eisenberg, A. and Kim, J. (1998). *Introduction to Ionomers*. Wiley.

Feldman, K. E., Kade, M. J., Meijer, E. W., Hawker, C. J., and Kramer, E. J. (2009). Model Transient Networks from Strongly Hydrogen-Bonded Polymers. *Macromolecules*, 42(22):9072–9081.

Fetters, L. J., Lohse, D. J., and Colby, R. H. (2007). *Chain Dimensions and Entanglement Spacings*, pages 447–454. Springer New York, New York, NY.

Huang, Q., Mednova, O., Rasmussen, H. K., Alvarez, N. J., Skov, A. L., Almdal, K., and Hassager, O. (2013). Concentrated Polymer Solutions are Different from Melts: Role of Entanglement Molecular Weight. *Macromolecules*, 46:5026–5035.

Jullian, N., Leonardi, F., Grassl, B., Peyrelasse, J., and Derail, C. (2010). Rheological characterization and molecular modeling of poly (n-butyl acrylate). *Appl. Rheol*, 20(3):1–11.

Lakrout, H., Creton, C., Ahn, D., and Shull, K. R. (2001). Influence of molecular features on the tackiness of acrylic polymer melts. *Macromolecules*, 34(21):7448–7458.

Lange, R. F. M., Van Gurp, M., and Meijer, E. W. (1999). Hydrogen-bonded supramolecular polymer networks. *J. Polym. Sci. A Polym. Chem.*, 37(19):3657–3670.

Leong, K. and Butler, G. (1980). Chemical Reactions on Polymers - 2. Modification of Diene Polymers with Triazolinediones via the Ene Reaction. *J.Macromol. Sci. A.*, 14:287.

Lewis, C., Stewart, K., and Anthamatten, M. (2014). The Influence of Hydrogen Bonding Side-Groups on Viscoelastic Behavior of Linear and Network Polymers. *Macromolecules*, 47:729–740.

Montarnal, D., Tournilhac, F., Hidalgo, M., Couturier, J.-L., and Leibler, L. (2009). Versatile one-pot synthesis of supramolecular plastics and self-healing rubbers. *J. Am. Chem. Soc.*, 131(23):7966–7.

Mugemana, C., Guillet, P., Hoeppener, S., Schubert, U. S., Fustin, C.-A., and Gohy, J.-F. (2010). Metallo-supramolecular diblock copolymers based on heteroleptic cobalt(III) and nickel(II) bis-terpyridine complexes. *Chem. Commun.*, 46(8):1296–8.

Nair, K., Breedveld, V., and Weck, M. (2011). Multiresponsive reversible polymer networks based on hydrogen bonding and metal coordination. *Macromolecules*, 44:3346–3357.

Nair, K. P., Breedveld, V., and Weck, M. (2008). Complementary Hydrogen-Bonded Thermoreversible Polymer Networks with Tunable Properties. *Macromolecules*, 41(10):3429–3438.

Román Marín, J. M., Huusom, J. K., Alvarez, N. J., Huang, Q., Rasmussen, H. K., Bach, A., Skov, A. L., and Hassager, O. (2013). A control scheme for filament stretching rheometers with application to polymer melts. *J Nonnewton Fluid Mech.*, 194:14–22.

Rossow, T. and Seiffert, S. (2014). Supramolecular polymer gels with potential model-network structure. *Polym. Chem.*, 5(8):3018.

Sijbesma, R. and Meijer, E. (1999). Self-assembly of well-defined structures by hydrogen bonding. *Curr. Opin. Colloid Interface Sci.*, 4:24–32.

Sivakova, S., Bohnsack, D. A., Mackay, M. E., Suwanmala, P., and Rowan, S. J. (2005). Utilization of a combination of weak hydrogen-bonding interactions and phase segregation to yield highly thermosensitive supramolecular polymers. *J. Am. Chem. Soc.*, 127(51):18202–11.

Stadler, R. and de Lucca Freitas, L. (1988). Dynamics of hydrogen bond complexes in polymer melts. *Colloid Polym. Sci.*, 266(12):1102–1109.

Stadler, R. and Freitas, L. D. L. (1986). Thermoplastic Elastomers by Hydrogen Bonding 2. IR-Spectroscopic Characterization of the Hydrogen Bonding. *Polym. Bull.*, 15:173–179.

Weiss, R. A. and Yu, W.-C. (2007). Viscoelastic Behavior of Very Lightly Sulfonated Polystyrene Ionomers. *Macromolecules*, 40(10):3640–3643.

Yan, X., Wang, F., Zheng, B., and Huang, F. (2012). Stimuli-responsive supramolecular polymeric materials. *Chem. Soc. Rev.*, 41(18):6042–65.

Zhang, L., Brostowitz, N. R., Cavicchi, K. A., and Weiss, R. A. (2014). Perspective: Ionomer Research and Applications. *Macromol. React. Eng.*, 8(2):81–99.

CHAPTER 3

Linear Viscoelastic and Dielectric Relaxation Response of Unentangled UPy based Supramolecular Networks

3.1 Introduction

Polymer networks utilizing hydrogen bonding as transient physical interactions hold a prominent place in the field of associating polymers. Although isolated hydrogen bonding interactions are typically not as strong as other non-covalent interactions such as ionic interactions [Chen et al. (2013, 2014); Ling et al. (2012); Stadler et al. (2009); Gonzlez et al. (2013); Shabbir et al. (2015)] or metal-ligand coordination [Kumpfer et al. (2012); Rossow and Seiffert (2014)], their ability to form highly directional and versatile associations make them very useful [Bosman et al. (2004)]. The association strength of an isolated hydrogen bond in a polymer melt depends on the nature of donor and acceptor. Weak hydrogen bonding associations lead to viscoelastic liquids, whereas strong hydrogen bonds result in rubbery like polymer networks. The association energies of hydrogen bonds typically span from one to tens of $k_B T$, which makes the nature of these interactions thermally reversible [Tang et al. (2015)]. At high temperatures, hydrogen bonds become weak leading to Newtonian like fluid properties, whereas at low temperatures they form elastic networks spanning many decades in frequency [Lewis et al. (2014); Feldman et al. (2009)]. Understanding the rich dynamics of such associating polymers offers opportunities for property manipulation and is thus interesting from both fundamental and applied standpoints.

The process of breaking and reformation of reversible associations (stickers) controls the dynamics of supramolecular polymers [Rubinstein and Semenov (2001)].

Baxandall (1989) and Green and Tobolsky (1946) showed that the stress relaxation *via* breaking and reformation of reversible associations is essentially Rouse like on timescales larger than the association lifetime [Baxandall (1989); Green and Tobolsky (1946); Chen et al. (2013)]. Chain reptation can complicate the situation in case of entangled polymer melts [Rubinstein and Semenov (2001)]. In this study, our focus is on unentangled polymer melts. The viscoelastic response of unentangled reversible networks near and above the gel point has been described by the modified Rouse model called the sticky Rouse model [Rubinstein and Semenov (1998)]. According to this theory, reversible associations act as a second source of friction for the polymer chain thus delaying the terminal relaxation [Leibler et al. (1991); Chen et al. (2013)].

While a few recent studies have examined the applicability of Green and Tobolsky ideas on ionomers [Chen et al. (2013)], very few studies have investigated its applicability in hydrogen bonded systems. Chen et al. (2013) were the first to quantitatively describe the LVE response of unentagled poly-ether-ester sulphonate copolymer ionomers using the sticky Rouse model [Chen et al. (2013)]. Feldman et al. (2009), used the theory by Rubinstein and Semenov, which considers a single mode Rouse model for frequencies lower than the inverse association lifetime [Feldman et al. (2009)]. A recent paper from Tang et al. (2015) has shown the LVE rheological response of protein hydrogels to be dominated by sticky Rouse dynamics [Tang et al. (2015)]. In their case, the sticky Rouse signature is due to the hindered motion of associative protein molecules in an aggregated state.

The strength and reversibility of hydrogen bonds can be tailored by exploiting multiple hydrogen bond (MHB) arrays [Bosman et al. (2004); Sijbesma et al. (1997)]. Supramolecular polymers based on multiple hydrogen bonds which exploit the trait of co-operativity have gained large interest recently, showing remarkable properties since they combine directionality and versatility. Since the introduction of 6-methyl-2-ureido-4[1*H*]-pyrimidone-bearing methacrylate (UPyMA) by Yamauchi et al. (2003), several polymers with hydrogen bonding groups have been synthesized. For example, hydrogen bonding copolymers of UPyMA with *n*-butyl acrylate [Yamauchi et al. (2003); Lewis et al. (2014)], 2-ethylhexyl methacrylate [Elkins et al. (2005)], and 2-hydroxyethyl methacrylate [Lewis and Anthamatten (2013)] have been synthesized by making use of either free or controlled radical polymerization method. With thermally tunable strength of association, these hydrogen bonding copolymers display stimuli responsive rheological behavior, and may be employed as shape memory, self-healing, and adhesive materials.

This paper is a continuing work in the effort to fully understand the dynamics of hydrogen bonding associating polymers. Here, we report the synthesis and characterization of copolymers based on 2-methoxyethyl acrylate (MEA) incorporating UpyMA. More specifically, we examine two copolymers with increasing amount of UPyMA groups: 3 % UPyMA, and 8 % UPyMA. The percentage of UPyMA groups is determined using NMR spectroscopy. PMEA is chosen due to its FDA approval in medical devices and applications [Tanaka et al. (2014)]. The inherent freezing bound water bestows excellent blood compatibility to the intermediately hydrophilic PMEA [Tanaka et al. (2014)] , and allows its exploitation as coating material for cir-

cuits and tubes in cardiopulmonary bypass and catheters for central veins of blood vessels [Tanaka et al. (2014)] as well as for artificial oxygenators [Tinius et al. (2003)]. MEA has been employed as one of the building blocks in preparation of random [Javakhishvili et al. (2013b)], block [Javakhishvili et al. (2013a); Røn et al. (2014)], and graft copolymers [Javakhishvili et al. (2012, 2014)] by means of controlled radical polymerizations.

In this paper, MEA and UPyMA copolymers are synthesized via free radical polymerization resulting in a random distribution of the UPy (hydrogen bonding) sites. Note that this is in contrast with the polycondensation process where the distance between the sticker groups is strictly controlled by the length of the monomer unit (see Chapter 4). A key difference between the systems studied in this Chapter compared to Chapter 1 is that here the systems are un-entangled so that the effect of entanglements on the rheological properties be minimal. This study examines the effect of UPyMA density on the copolymer's linear viscoelasticity. The experimental data is compared to the sticky Rouse model considering both polydispersity of the copolymer and polydispersity in the number of stickers per chain. The latter represents a novel analysis to address the open question regarding the effect of associating group dispersion on the terminal regime power-law. The model is parameterized to the fullest extent via experimental data in an effort to minimize adjustable parameters. For example, we independently determine the association lifetime of hydrogen bonds via dielectric relaxation spectroscopy (DRS). The original sticky Rouse model is compared to experimental data and is shown to work reasonably well in predicting the viscoelasticity for low density of UPyMA units, it has difficulty at high UPyMA density. The modified sticky Rouse model taking into account polydispersity in the number of stickers works very well in fitting the experimental data via one adjustable parameter, the standard deviation of stickers per chain. The comparison of our results with other studies in the literature suggest that associating groups regardless of association mechanism (i.e. ionic, hydrogen bonding, etc) have three common characteristics in linear viscoelasticity depending on polydispersity of chain molecular weight (MW), number of stickers per chain, and dispersion of stickers.

3.2 Experimental Section

Materials

2-Methoxyethyl acrylate (MEA; Aldrich, 98 %) was passed through a short aluminum oxide column (Sigma-Aldrich, activated, basic, Brockmann I, standard grade, $\sim$ 150 mesh, 58 Å) before use. N,N-Dimethylformamide (DMF; Sigma-Aldrich, $\geq$ 99.9 %) was dried over molecular sieves. α,α' -Azoisobutyronitrile (AIBN; from Ventron) was recrystallized from methanol. 2-Isocyanatoethyl methacrylate (Aldrich, 98 %), 2-amino-4-hydroxy-6-methylpyrimidine (Aldrich, 98 %), tetrahydrofuran (THF; Sigma-Aldrich, 99.9 %), diethyl ether (Sigma-Aldrich, $\geq$ 99.8 %), heptane (Sigma-Aldrich, 99 %), methanol (Sigma-Aldrich, 99.9 %), dimethyl sulfoxide (DMSO; SAFC, $\geq$ 99 %), $CDCl_3$ (Aldrich, 99.8 atom % D), and DMSO-d_6 (Aldrich, 99.9 atom% D)

were used as received. 6-Methyl-2-ureido-4[1*H*]-pyrimidone-bearing methacrylate (UPyMA) was synthesized as reported in literature [Yamauchi et al. (2003)].

Analytical Techniques

NMR experiments were carried out on a Bruker Avance 300 MHz spectrometer. Chemical shifts are reported in ppm.

Molecular weights, MW, and polydispersity indices (PDI) were estimated by size exclusion chromatography (SEC) using an HLC-8320GPC from Tosoh Corporation Bioscience Division equipped with refractive index and UV detectors employing three PFG micro columns (100 Å, 1000 Å, and 4000 Å) from Polymer Standards Service (PSS). The samples were run in DMF (5 mM LiCl) at 50 °C (0.3 mL min^{-1}). Molecular weights were calculated using WinGPC Unity 7.4.0 software and poly(methyl methacrylate) (PMMA) standards from PSS. The copolymer composition, F_{UPyMA}, and the average number of stickers, n_s, were estimated from ^{1}H NMR experiments and number average molecular weights estimated by SEC. The molecular weight of a sticky segment, M_s, was determined using the weight average molecular weights from SEC.

Attenuated total reflectance Fourier transform infrared (ATR FTIR) spectra in the range of 4000-350 cm^{-1} were recorded on a Nicolet iS50 ATR spectrometer with a diamond crystal from Thermo Scientific.

Thermal transitions were measured in a range of -90 °C to 100 °C at a heating rate of 10 °C min^{-1} on a differential scanning calorimeter (DSC) Q1000 from TA. Glass transition temperatures were obtained from the second heating curve. All analytically determined values are tabulated in Table 3.1.

Synthetic Procedures

All reactions were carried out under nitrogen flow.
General polymerization protocol. A Schlenk tube was charged with MEA, AIBN, and DMF along with comonomer UPyMA where applicable. The reaction mixture was stirred and deoxygenated by bubbling nitrogen through for 30 min. The tube was then immersed in an oil bath at 60 °C, and the polymerization was carried out for 5 h. Afterwards the tube was taken out of the bath, and the reaction mixture was exposed to air. It was then precipitated twice from THF or DMF in diethyl ether-heptane (1:1) mixture. The product was dried in the vacuum oven until no residual solvent was detected by spectroscopic means. Yield: 66-76 %.

E.g.: **P(MEA-*co*-UPyMA) 8**%. MEA (2.6 mL, 20.2 mmol), UPyMA (215 mg, 0.77 mmol), AIBN (16 mg, 0.10 mmol), and DMF (15 mL) were taken. SEC: $\overline{M}_w$ = 68.6 kDa, $\overline{M}_w$ / $\overline{M}_n$ = 3.6. IR (neat): 2931, 2885, 2820, 1727, 1662, 1588, 1526, 1448, 1404, 1384, 1333, 1249, 1198, 1160, 1125, 1097, 1028, 983, 952, 861, 764, 601, 532 cm^{-1}. ^{1}H NMR (300 MHz, DMSO-d_6, δ): 11.20-12.00 (*b*, N*H*C(CH_3)CH); 9.60-10.20 (*b*, N*H*C(NH)N); 7.10-7.80 (*b*, CH_2N*H*C(O)); 5.77 (*s*, C(O)C*H*C(CH_3)NH); 3.85-4.32 (*b*, OCH_2CH_2OC(O) and

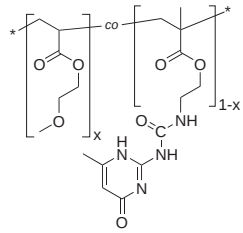

Figure 3.1: Copolymer of MEA and UPyMA

NHCH$_2$CH_2OC(O)); 3.38-3.65 (*b*, OCH_2 CH$_2$OC(O) and NHCH_2 CH$_2$OC(O)); 3.14-3.30 (*b*, CH_3O); 2.15-2.43 (*b*, CH$_2$C*H*C(O)O; 2.10 (*s*, C(O)CHC(CH_3)NH); 0.75-1.95 (*b*, CH_2CHC(O)O, CH_2C(CH$_3$)C(O)O, and CH$_2$C(CH_3)C(O)O).

LVE Measurements

Linear viscoelasticity for the three P(MEA-*co*-UPyMA) polymers was measured via SAOS performed with an ARES-G2 (TA instruments) rheometer. Temperature was controlled using a convection oven operating in nitrogen. 8 mm diameter parallel plate geometry was used for all experiments. No slippage problem was observed due to good adhesion of the sample and the plate geometry. For PMEA, LVE segments were measured between -30 °C and 100 °C . For P(MEA-*co*-UPyMA) 3%, LVE segments were measured between -25 °C and 100 °C . For P(MEA-*co*-UPyMA) 8%, LVE segments were measured between -20 °C and 120 °C . When possible, time temperature superposition was used to create master curves. Since instrument compliance is known to influence the LVE data in the glassy regime (10^8 Pa), measurements were corrected following the method reported by Schrter et al. (2006) for 8 mm plates on an ARES-G2 rheometer.

DRS Measurements

To measure the complex dielectric permittivity, $\epsilon^*(\omega) = \epsilon^{'}(\omega) - i\epsilon^{''}(\omega)$, we have used a Novocontrol Alpha-Analyzer with a Quatro Cryosystem temperature control. Each sample was melted on the dielectric electrodes with a Teflon spacer of 0.1 mm. The sample diameter was 30 mm. The dielectric measurements were done approximately from (T_g + 90 K) to (T_g 10 K)

3.3 Results

Figure 3.1 depicts the structure of the copolymer P(MEA-*co*-UPyMA).

Together with the homopolymer, PMEA, two copolymers with varying UPyMA content have been synthesized by adjusting the monomer feed ratio in free radical

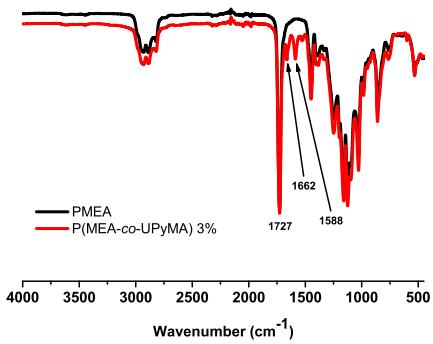

Figure 3.2: Overlay of FTIR spectra of PMEA and P(MEA-*co*-UPyMA)3%

polymerization. Formation of the copolymer has been verified by FTIR spectroscopy, which reveals absorption bands at $1727\,cm^{-1}$, $1662\,cm^{-1}$, $1588\,cm^{-1}$ that are attributed to ester, urea, and pyrimidone groups, respectively (Figure 3.2).

The band at $1588\,cm^{-1}$ is characteristic to the dimerized UPy, which implies that the presence of the multitude of methoxyethyl fragments along the polymeric backbone does not disrupt the hydrogen bond formation [Lewis and Anthamatten (2013); de Greef et al. (2010)]. The copolymer composition is further elucidated by NMR spectroscopy. ^{1}H NMR spectroscopy experiments corroborate incorporation of the UPyMA repeating units; resonance signals **10** and **11** at 5.77 ppm and 2.10 ppm, respectively, are unambiguously ascribed to the methine and methyl groups of the pyrimidone fragment (Figure 3.3). A heteronuclear single quantum coherence (HSQC) experiment substantiates the assignment revealing the coupled carbons at 104 ppm and 23 ppm, respectively. The UPyMA molar fractions in the two copolymers are estimated to be 3% and 8%, respectively. This estimation is made by comparing the integrals of the resonance signals **2** and **5** in Figure 3.3, attributed to the MEA repeating unit, with the integrals of the overlapping peaks **3**, **8** and **4**, **9** originating from the MEA and UPyMA repeating units.

The weight average molecular weights ($\overline{M}_w$) and molecular weight distributions (MWD) of the homo- and copolymers have been obtained by SEC. SEC measurements show a PDI $\geq$ 2.9, which is intrinsic to free radical polymerizations.

Influence of the content and nature of the H-bonding units on the Tg has been probed by DSC. Tg increases from -35°C for PMEA to -31 °C and -28 °C for P(MEA-*co*-UPyMA) 3% and P(MEA-*co*-UPyMA) 8%, respectively. Characteristics of the homo- and copolymers are summarized in Table 3.1.

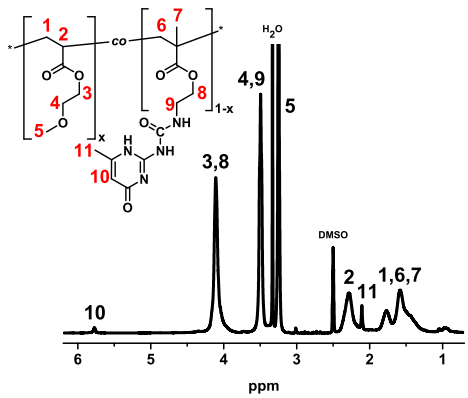

Figure 3.3: ^{1}H NMR spectrum of P(MEA-*co*-UPyMA)8% acquired in DMSO-d_6

Table 3.1: Molecular weight characteristics, composition, and thermal properties of homo- and copolymers

Sample Name	$M_w{}^a$ kDa	PDI	$F_{UPyMA}{}^b$ mol %	$n_s{}^b$ Stickers/chain	T_g	$M_s{}^b$ kDa
PMEA	65.3	2.9	0	-35	-	
P(MEA-co-UPy MA) 3%	32.1	2.9	3.0	2	-31	12.9
P(MEA-co-UPy MA) 3%	68.6	3.6	8.0	11	-28	6.4

^{a} Obtained by SEC; ^{b} estimated by combining results from ^{1}H NMR spectroscopy and SEC.

Linear Viscoelasticity

Master curves representing linear viscoelasticity for all three samples are presented in Figure 3.4. More specifically, Figure 3.4 shows $G^{'}(\omega)$ and $G^{''}(\omega)$ for PMEA, P(MEA-*co*-UPyMA) 3%, and P(MEA-*co*-UPyMA) 8% as a function of frequency, ω, at $T_{ref} =$ 25 °C. The rheological response of PMEA shows a power-law dependence of G' and G'' at relatively high frequency, followed by a terminal regime at relatively low frequency (i.e. G' and G'' of powerlaw 2 and 1, respectively). This is the typical response of an unentangled polymer melt and is typically referred to as Rouse dynamics in the literature. Also in Figure 3.4, the rheological response of UPyMA containing copolymers is represented in colored symbols. The presence of hydrogen bonds produces a substantial change in the measured linear viscoelastic response. At moderate frequencies, a discernible plateau modulus in $G^{'}(\omega)$ is noted which spans approximately four decades in frequency. The width of the rubbery plateau increases with the number of UPy side groups. Furthermore, the magnitude of the

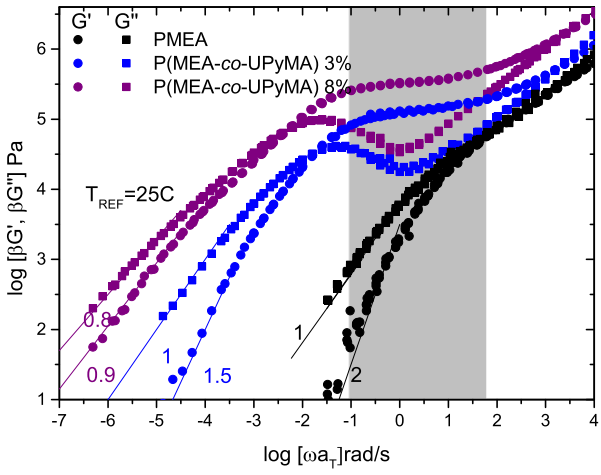

Figure 3.4: Comparison of linear viscoelastic master curves of PMEA and P(MEA-*co*-UPyMA) systems shifted to $T_{ref} = 25\ ^{\circ}\mathrm{C}$. The gray region represents the accessible time frame of a single experiment

rubbery plateau also increases with the number of UPy side groups suggesting the strength of the network to be a function of concentration of hydrogen bonds. At low frequencies, there is an evident deviation from terminal power law slopes for UPyMA containing copolymers. This observation has been previously observed in LVE of several hydrogen bonding associating polymers [Feldman et al. (2009); Lewis et al. (2014); Hackelbusch et al. (2013); Lange et al. (1999); Shabbir et al. (2015)]. This could be due to either, (i) the relatively large PDI of the polymer, (ii) the polydispersity in UPy side group spacing along the backbone, or (iii) the signature response of hydrogen bonding polymers. Although concrete evidence is lacking, we hypothesize that the lack of a terminal response is most likely due to (ii), the polydisperse UPy side group spacing along the backbone.

The time temperature superposition (TTS) shift factors a_T are shown in Figure 3.5. As expected, PMEA follows typical Williams-Landel-Ferry (WLF) behavior. Shift factors for the two UPyMA containing polymers show a transition from WLF to Arrhenius-like behavior as a function of temperature. More specifically, WLF like behavior at low temperatures and Arrhenius-like behavior at higher temperatures. The transition to Arrhenius behavior is suggestive of kinetics of association/disassociation dynamics of hydrogen bonds. At low temperatures the hydrogen bonds can be thought of as being static. However at temperatures above which the thermal energy $(k_B T)$ becomes comparable to the activation energy of hydrogen bond disassociation,

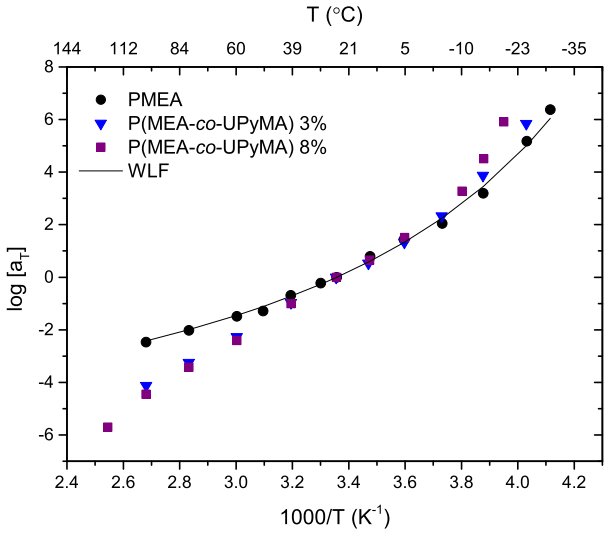

Figure 3.5: Temperature dependence of apparent shift factors for PMEA and P(MEA-*co*-UPyMA) systems shifted to $T_{ref} = 25\,^{\circ}\mathrm{C}$

the hydrogen bonds are dynamic. The data was plotted as suggested by Liu et al. in order to see a second transition corresponding to T_g, however the temperature range of the LVE data was not low enough to observe one [Chen-Yang Liu and Bailly (2006)].

For the two UPyMA copolymers, the gray shaded region in Figure 3.4 signifies the failure in time-temperature-superposition (TTS). We hypothesize that the breakdown of TTS is due to a competition of timescales, one for each molecular mechanism: (i) the dynamics of the polymer chain, and (ii) the fluctuations of hydrogen bonds. At 25 °C, both polymer chain dynamics (denoted by PMEA LVE) and hydogen bond fluctuations (denoted by rise in plateau modulus) occur in the same frequency range. The breakdown of TTS is most likely related to the coinciding of these two mechanisms occurring in the same frequency range. Thermorheological complexibility has been observed for other hydrogen bonding associating polymers [Lewis et al. (2014); Noro et al. (2008); McKee et al. (2005)] and ionomers [Ling et al. (2012); Chen et al. (2013, 2014); Stadler et al. (2009)].

The activation energies, E_a, calculated from Arrhenius relationship:

$$\ln a_T = -\frac{E_a}{RT} + C \tag{3.1}$$

are 110 and 125 kJ/mol for P(MEA-*co*-UPyMA) 3% and P(MEA-*co*-UPyMA) 8% respectively.

Dielectric relaxation spectroscopy (DRS)

Broadband dielectric spectroscopy is a technique based on the interaction of an external field with the electric dipole entities in the sample [Kremer and Schnhals (2003)]. The relaxation phenomena are related to molecular fluctuations of dipoles due to the movements of molecules or their parts in a potential field. Additional contributions to the observed relaxation can be caused by motion of mobile charge carriers and polarization of the electrode itself. If the frequency of the applied oscillatory field corresponds to reorientation times, τ, of the molecular dipoles, there is a characteristic response of the storage permittivity, $\epsilon^{'}$, and loss permittivity, $\epsilon^{''}$. $\epsilon^{'}(\omega)$ decreases with increasing ω depicting a characteristic step, while $\epsilon^{''}(\omega)$ exhibits a maximum with increasing ω. The essential quantity, τ can be extracted from this behavior. The frequency corresponding to the maximum loss, ν_p, is related to the characteristic relaxation time, $\tau = 1/2\pi\nu_p$. $\epsilon^{'}$ and $\epsilon^{''}(\omega)$ for PMEA are shown in Figure 3.6 for varying temperature. It is evident from this data that PMEA shows a single characteristic relaxation time (i.e. one maximum in $\epsilon^{''}$ and one step-like shoulder in $\epsilon^{'}$) for the measured frequency range and the temperatures measured. This single and primary relaxation process is referred to as the α-relaxation process and is attributed to segmental motion of the chain near the glass transition.

Figure 3.7(a-c) shows both the storage and loss permittivity as a function of frequency and derivative formalism for P(MEA-*co*-UPyMA) 8 % at different temperatures above T_g. The real part of the complex permittivity, $\epsilon^{'}(\omega)$ (Figure 3.7a) shows two steps indicating two relaxation processes. However, only one relaxation process is observed in $\epsilon^{''}(\omega)$, as shown in Figure 3.7b. This is due to a strong electrode polarization and/or ionic conductivity which masks $\epsilon^{''}$ in the frequency regime of interest. To overcome the issue observed in loss permittivity due to electrode polarization and/or ionic conductivity, it is standard procedure to use the derivative analysis of $\epsilon^{'}$: [Wbbenhorst and van Turnhout (2002); Chen et al. (2013); Kremer and Schnhals (2003)]

$$\epsilon_{der}(\omega) = -\frac{2}{\pi}\frac{\partial\epsilon^{'}(\omega)}{\partial\log\omega} \tag{3.2}$$

The derivative analysis for P(MEA-*co*-UPyMA) is shown in Figure 3.7c. From this analysis, it is clear that two relaxation processes are occurring (i.e. two maximums observed). The fast process is related to the glass transition and therefore referred to as α-relaxation. The slow process, not present in pure PMEA, is presumably due to hydrogen bonds and is referred to as the α^*-relaxation in Figure 3.7c.

Although one can crudely determine the frequency corresponding to the maximum in ϵ_{der}, a more quantitative approach is to fit a model to the permittivity data. In this case, the complex dielectric permittivity is described by the superposition of a Havriliak-Negami function, two Cole-Cole functions [Cole and Cole (1942)], and a dc

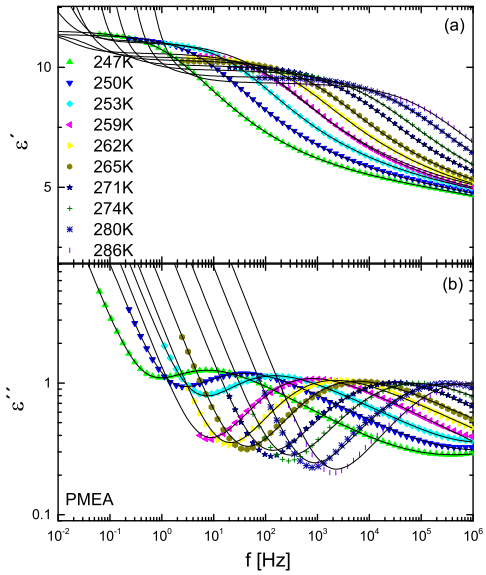

Figure 3.6: The storage permittivity (a) $\epsilon^{'}$ and (b) loss permittivity $\epsilon^{''}$ as a function of frequency for pure PMEA (no UPy groups). Note that only one step-like shoulder and one maximum are observed in (a) and (b), respectively, indicating a single relaxation time in this frequency and temperature range. This characteristic relaxation time is denoted as the α-relaxation time. The lines represent the best fit to the data using Eqn. 3.3, which is used to quantitatively determine the relaxation timescale.

conductivity term. The total fit function was given by

$$\epsilon^*(\omega) = \epsilon_\infty + \frac{\Delta\epsilon}{[1+(i\omega\tau_0)^\alpha]^\beta} + \sum_{j=1}^{2} \frac{\Delta\epsilon_j}{1+(i\omega\tau_j)^{\alpha_j}} + i(\frac{\sigma_0}{\epsilon_0\omega}) \tag{3.3}$$

where $\Delta\epsilon$ is the dielectric strength ($\Delta\epsilon = \epsilon_s - \epsilon_\infty$, ϵ_∞ and ϵ_s are the unrelaxed and relaxed values of the dielectric constant respectively), τ_0 is the relaxation time for the α relaxation mechanism, and τ_j corresponds to the electrode polarization ($j = 1$) and α^* relaxation ($j = 2$), α and β are the shape parameters which describe the symmetric and the asymmetric broadening of the spectrum, and $\omega = 2\pi f$ is the angular frequency. ϵ_0 denotes the vacuum permittivity and σ is the static ionic conductivity. Both CC functions were used to describe the α^*-relaxation and the electrode polarization observed in $\epsilon^{'}(\omega)$ (EP) respectively, whereas the HN function takes into account the α-relaxation. The shape parameters, α and β in equation are approximately $\alpha \approx 0.5$ and $\beta \approx 0.4$ for the α-relaxation whereas for α^*-relaxation, α parameter is close to 0.95 and therefore almost Debye-like. The most relevant

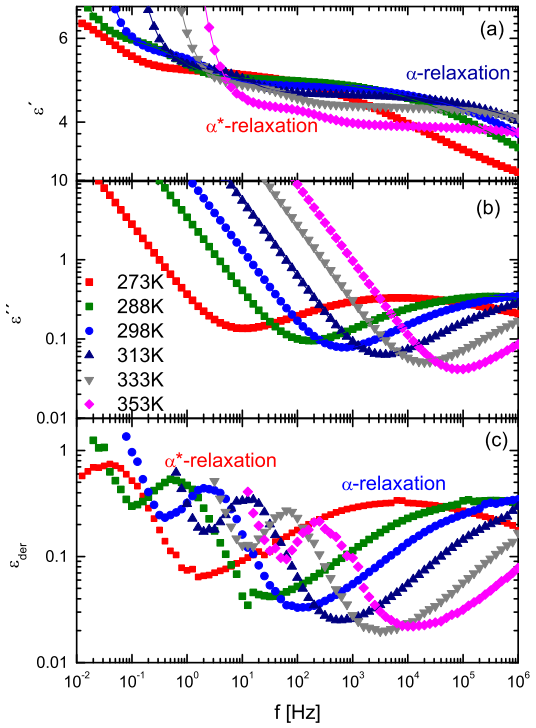

Figure 3.7: (a) storage permittivity, (b) loss permittivity and (c) derivative formalism spectra for P(MEA-*co*-UPyMA) 8 %. Solid lines through the data points represent the fits to the experimental data using Eqn. 3.3

parameter derived from the fitting procedure is the relaxation time τ, describing the dynamical behavior of the polymeric system. Relaxation processes usually follow the empirical Vogel-Fulcher-Tammann (VFT) equation [Vogel (1921); Fulcher (1925)],

$$\tau(\alpha) = \tau_H \exp\left(\frac{DT_0}{T - T_0}\right) \tag{3.4}$$

where τ_H is the high temperature limit of the relaxation time, T_0 is the Vogel temperature, and D is the strength parameter inversely related to the fragility. On the other hand, for a thermally activated behavior, the temperature dependence of the relaxation time follows the Arrhenius law.

The temperature dependence of the relaxation times τ_0, and τ_2 are plotted in

Figure 3.8 for the three samples in order to determine the dominating relaxation mechanisms for P(MEA-*co*-UPyMA) systems. As expected, the α-relaxation (fast times, high frequency) is well described by the VFT equation. Note that the temperature values at which the relaxation times reach 100 s, i.e., the dielectric $T_{g,100s}$ show a good agreement with the corresponding calorimetric values for all the investigated samples, supporting the idea that this relaxation corresponds with the glass transition timescale. On the other hand, τ_2 is well described by the Arrhenius equation suggesting that this process is kinetic in nature. In other words, the molecular relaxation process characterized by τ_2 is most likely due to hydrogen bond dynamics. This interpretation is inline with previous studies of UPy containing supramolecular polymers [Wubbenhorst et al. (2001)] and other similar systems [Lou et al. (2013)].

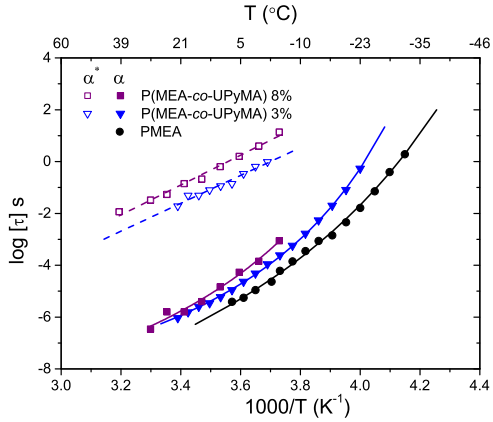

Figure 3.8: Extracted relaxation times for PMEA and P(MEA-*co*-UPyMA) polymers as a function of inverse temperature. The timescale associated with α^*-relaxation shows a distinct powerlaw, indicative of Arrhenius behavior (dotted lines), while timescale associated with α-relaxation follows the VFT model (solid lines).

3.4 Discussion

The concept of chain relaxation *via* repetitive breaking and reforming of reversible bonds along the backbone dates back to early work from Green and Tobolsky (1946). This concept was extended by Rubinstein and Semenov (1998) in their theoretical work on unentangled associating polymer solutions [Rubinstein and Semenov (1998)]. Recently Chen et al. (2013) have experimentally tested these ideas on ionomer melts. We are interested in testing the sticky Rouse model on the LVE of unentangled polymer melts with hydrogen bonding. The sticky Rouse model first proposed by Rubinstien, Semenov, Leibler and Colby assumes that the normal Rouse modes (higher order modes, $p > N_s$, where N_s is the number of sticky Rouse segments per

chain) exist for length scales up to the order of the distance between two associations, known as the sticky Rouse segment. However, the chain dynamics on length scales larger than the length of a sticky Rouse segment is only controlled by the association lifetime, τ_s. Thus, the lower order Rouse modes ($p \leq N_s$) are delayed. The Rouse relaxation modulus taking into account a known molecular weight distribution is given in the time domain as [Chen et al. (2013); Ferry (1980)]:

$$G_R(t) = \sum_i \frac{\rho w_i RT}{M_i} \sum_{p=1}^{N_i} \frac{-tp^2}{\tau_{R,0} N_i^2} \tag{3.5}$$

The first summation term takes into account polydispersity in molecular weight, which can be determined independently using SEC.

Eq. 4 in Chen *et al.* is given as,

$$G_{stickyRouse}(t) = \sum_i \frac{\rho w_i RT}{M_i} \left(\sum_{p=1}^{N_{s,i}} \frac{-tp^2}{\tau_s N_{s,i}^2} + \sum_{p=N_{s,i}+1}^{N_i} \frac{-tp^2}{\tau_0 N_i^2} \right) \tag{3.6}$$

Considering Eq. 3.6 can be converted to the frequency domain using a Fourier transform [Chen et al. (2013)]:

$$G'_{stickyRouse}(\omega) = \sum_i \frac{\rho w_i RT}{M_i} \left(\sum_{p=1}^{N_s} \frac{(\tau_s N_s^2 p^{-2}\omega)^2}{1+(\tau_s N_s^2 p^{-2}\omega)^2} + \sum_{p=N_s+1}^{N_i} \frac{(\tau_{R,0} N_i^2 p^{-2}\omega)^2}{1+(\tau_{R,0} N_i^2 p^{-2}\omega)^2} \right) \tag{3.7}$$

$$G''_{stickyRouse}(\omega) = \sum_i \frac{\rho w_i RT}{M_i} \left(\sum_{p=1}^{N_s} \frac{(\tau_s N_s^2 p^{-2}\omega)}{1+(\tau_s N_s^2 p^{-2}\omega)^2} + \sum_{p=N_s+1}^{N_i} \frac{(\tau_{R,0} N_i^2 p^{-2}\omega)}{1+(\tau_{R,0} N_i^2 p^{-2}\omega)^2} \right) \tag{3.8}$$

where w_i and M_i are weight fraction and molecular weight of the ith component, respectively. $\tau_{R,0}$ is the relaxation time of the elementary Rouse segment, τ_s is the relaxation time of the sticky segment, $N_i = M_i/M_0$ is the number of elementary Rouse segments per chain and $N_{s,i} = M_i/M_s$ is the number of sticky Rouse segments per chain. M_0 and M_s are the weight average molecular weight of the elementary Rouse segment and sticky Rouse segment, respectively. M_s is defined as the ratio of the weight average molecular weight estimated by SEC divided by the average number of stickers determined from NMR spectroscopy.

While Eqs. 3.7 and 3.8 take into account polydispersity in molecular weight, data in the literature suggests that dispersity in the distribution of associating groups along the polymer backbone are responsible for shallowing of the low frequency power-law [Seiffert (2016)]. In Eqs. 3.7 and 3.8 N_s for a given M_i is assumed a single value equal to that determined from NMR. In reality, there is a distribution of N_s per chain due to the uncontrolled free radical polymerization of the two monomers used in this work. The discrete distribution of N_s is potentially represented by a binomial distribution

determined by the number of monomer units per chain, $n_c = M_i/M_m$, where M_m is the molecular weight of the MEA repeat unit, and the probability of an UPy group adding to a growing chain is defined as, $p = n_s/n_c$ where n_s is the number of stickers per chain determined from NMR reported in Table 3.1. Application of the binomial distribution to N_s leads to a discrete distribution represented by:

$$\sum_{j}^{n_c} f_j N_{s,j} = n_s \tag{3.9}$$

Eqns. 3.10 and 3.11 are altered to take the distribution of sticky Rouse groups per chain into account via:

$$G'_{stickyRouse}(\omega) = \sum_i \frac{\rho w_i RT}{M_i} \sum_j f_j \left(\sum_{p=1}^{N_{s,j}} \frac{(\tau_s N_{s,j}^2 p^{-2}\omega)^2}{1+(\tau_s N_{s,j}^2 p^{-2}\omega)^2} + \sum_{p=N_{s,j}+1}^{N_i} \frac{(\tau_{R,0} N_i^2 p^{-2}\omega)^2}{1+(\tau_{R,0} N_i^2 p^{-2}\omega)^2} \right) \tag{3.10}$$

$$G''_{stickyRouse}(\omega) = \sum_i \frac{\rho w_i RT}{M_i} \sum_j f_j \left(\sum_{p=1}^{N_{s,j}} \frac{(\tau_s N_{s,j}^2 p^{-2}\omega)}{1+(\tau_s N_{s,j}^2 p^{-2}\omega)^2} + \sum_{p=N_{s,j}+1}^{N_i} \frac{(\tau_{R,0} N_i^2 p^{-2}\omega)}{1+(\tau_{R,0} N_i^2 p^{-2}\omega)^2} \right) \tag{3.11}$$

.

The characteristic modulus corresponding to the sticky Rouse segments is defined as $k_B T$ per sticker and is given as $G_c = P_0 k_B T$, where $P_0 = \rho N_A/M_s$ is the number density of stickers, k_B is the Boltzmann constant, ρ is the mass density and N_{Av} is the Avogadro number. The corresponding timescale is the sticky Rouse segment time or the sticker lifetime and is evaluated as $\tau_s \sim 1/\omega_c$, where ω_c is the characteristic frequency at which $G^{'}(\omega_c) = P_0 k_B T$ [Chen et al. (2013)]. A comparison of the mean sticker lifetime extracted from SAOS rheology ($\tau_s \sim 1/\omega_c$) and DRS (peak corresponding to α^*-relaxation process) is shown in Figure 3.9 a. A fairly good agreement is found between the two techniques. The activation energies obtained using DRS and rheology are also comparable.

The gel point represents the point at which physical junctions percolate over the system [Chen et al. (2015)]. According to the sticky Rouse model above the gel point, multiple associations and disassociations of a given pair of stickers are required before the sticker finds another partner different from its previous partner. This leads to an effective lifetime of the sticker, τ_s^*. As a consequence this renormalized lifetime, τ_s^*, is larger than the bare sticker lifetime, τ_s [Rubinstein and Semenov (2001, 1998)]. The mean-field prediction of the gel point, p_c, for P(MEA-*co*-UPyMA) 3% is estimated to be around 1 mol% of UPyMA content, while in case of P(MEA-*co*-UPyMA) 8% it is around 0.7 mol%. This implies that the content of the UPyMA repeating units in either copolymer is above the gel point. Therefore, τ_s^* will be used in the sticky Rouse model to capture the LVE response. As previously done in other studies, τ_s^* is determined from the frequency at which the storage modulus has dropped 10 % of the plateau modulus [Feldman et al. (2009)]. There should be a linear relationship

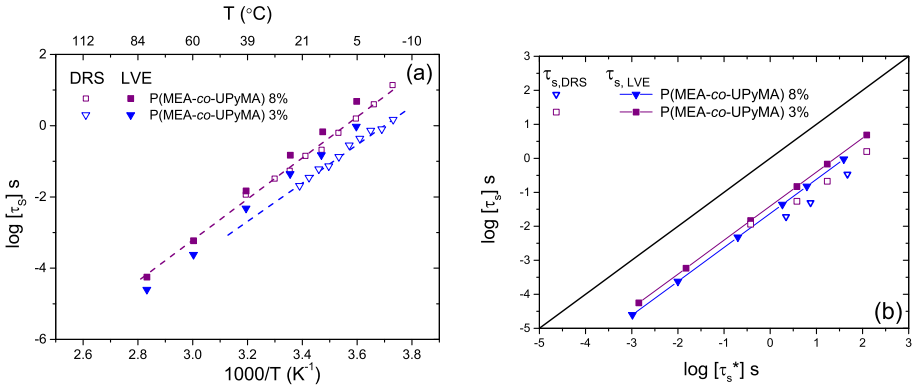

Figure 3.9: Comparison of (a) bare lifetime of hydrogen bonds obtained using dielectric relaxation spectroscopy/rheology as a function of inverse temperature, and (b) bare lifetime with renormalized lifetime of hydrogen bonds. The solid line represents hypothetical situation in which bare lifetime and renormalized time is equal.

between the timescale measured using DRS, the bare sticker lifetime, τ_s, and the effective lifetime τ_s^* whose slope corresponds to the proportionality constant between them. In Figure 3.9 b, there is a clear linear relationship between τ_s and τ_s^*. τ_s^* is larger than τ_s by a factor of ~ 40 for P(MEA-*co*-UPyMA) 3%, and by a factor of ~ 25 for P(MEA-*co*-UPyMA) 8%. Surprisingly, the proportionality constant decreases with increasing UPy content, which has no explanation at present.

The fast Rouse (higher order) and slow sticky Rouse (lower order) model contributions to the dynamic moduli are shown by dashed and dashed-dot-dashed lines in Figure 3.10. The sticky Rouse parameters are tabulated in Table 3.2. Since the sticky Rouse model does not take into account the glass mode relaxation, the Kohlrausch-Williams-Watts (KWW) model has been included to account for the glassy part of the dynamic rheological spectra. The Fourier transform of KWW model is given as,

$$G'_{KWW}(\omega) = \omega G_g \int_0^\infty \exp(-[t/\tau_{KWW}]^\beta) \sin(\omega t) dt \tag{3.12}$$

$$G''_{KWW}(\omega) = \omega G_g \int_0^\infty \exp(-[t/\tau_{KWW}]^\beta) \cos(\omega t) dt \tag{3.13}$$

where G_g is the glassy modulus, β is the stretch parameter of the exponential function, and τ_{KWW} defines the characteristic time of glassy relaxation. The empirical KWW fit is shown by dotted lines in Figure 3.10. Modes larger than a Kuhn segment is evidenced in the glassy-rubbery transition where the KWW model deviates from the experimental data. The corresponding modulus ~ 15 MPa at deviation between experiment and theory gives an estimation of M_0=200 g/mol, the Kuhn segment molecular weight. $\tau_{R,0}$ is another parameter obtained from LVE, which roughly corresponds to the high frequency crossover and is different for the three

samples because of different T_g. This completes the list of parameters to predict the experimental data using the sticky Rouse model described above. In general there

Table 3.2: Parameters used in the sticky Rouse model

Sample Name	Rouse		sticky Rouse	
	$\tau_{R,0}$ (s)	M_0 (kDa)	τ_s^* (s)	$M_s{}^a$ (kDa)
PMEA	8×10^{-9}	0.2		
P(MEA-co-UPy MA) 3%	1×10^{-8}	0.2	0.01	2
P(MEA-co-UPy MA) 3%	4.5×10^{-8}	0.2	0.014	6.4

[a] estimated by combining results from ^{1}H NMR spectroscopy and SEC.

are three effects of increasing interaction strength and number of associations per chain on linear viscoelasticity: (i) the longest relaxation time increases, (ii) the plateau modulus increases, and (iii) the power law scaling in the terminal regime deviates towards lower magnitudes [Shabbir et al. (2015)]. Seiffert hypothesizes that (iii) is predominately due to polydispersity in the dispersion of associating groups along the backbone and not polydispersity in polymer molecular weight [Seiffert (2016)]. Figure 3.10a-c shows the best fit model prediction via Eqs. 3.7 and 3.8 considering a monodisperse polymer molecular weight $M_1 = \overline{M}_w$ measured from SEC. It is evident from Figures 3.10a-c that the model does an excellent job at predicting the shape of the experimental curve for timescales shorter than the longest relaxation time. For example, the model captures the plateau modulus quantitatively in Figures 3.10b-c. However the model does a poor job of predicting the experimental data for longer timescales. In Figure 3.10a, which has no hydrogen bonding groups present, the discrepency between experiment and model is hypothesized to be explicitly due to effects of polydispersity in molecular weight.

The effect of polydispersity in molecular weight can be easily incorporated into the sticky Rouse model by discretizing the SEC molecular weight distribution and using Eqs 3.7 and 3.8 as explained above. The molecular weight probability distribution function (pdf) from SEC was discretized into 540 points. Figures 3.11a-c (solid lines) show the model predictions taking into account MW polydispersity only. It is evident by comparing Figure 3.10a and Figure 3.11a that polydispersity in molecular weight does not account for the discrepancy between model and data. For the case of pure PMEA, the inability of the model to capture the data quantitatively could be due to the presence of entanglements, which are not explicitly taken into account in the model. Furthermore, there is divergence between model prediction and data for Figures 3.11b-c. For example, the predicted plateau modulus is lowered and the low frequency crossover is shifted to higher frequency. This observed divergence between model and data is explained by noting that the polydispersity model will statistically favor the more prevalent lower molecular weight species (lower modulus and higher crossover frequency), while the calculations made in Figure 3.10a-c uses only $\overline{M}_w$ which is skewed by larger molecular weight species. Moreover, this trend could be

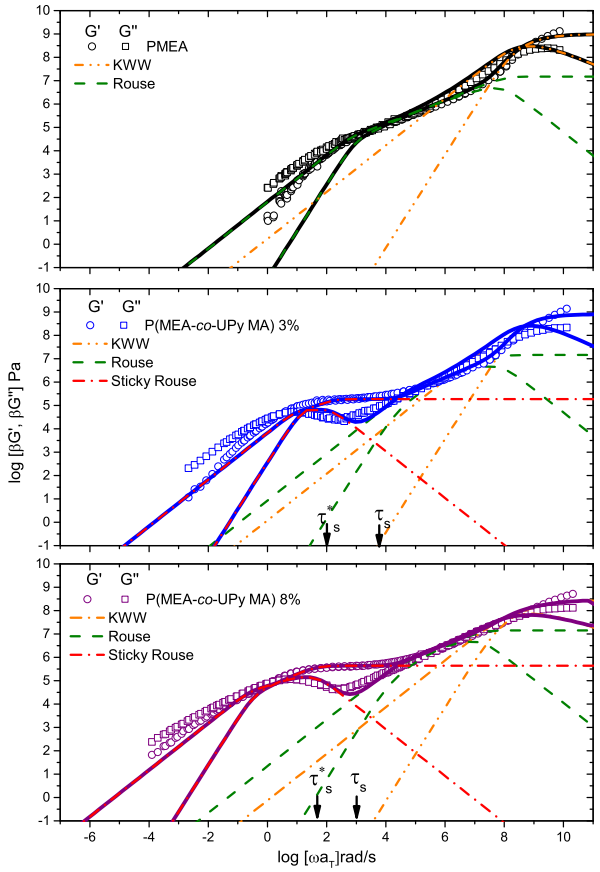

Figure 3.10: linear viscoelastic master curves of PMEA and P(MEA-*co*-UPyMA) systems shifted to $T_{ref} = 60$ °C. and the model prediction (solid lines) considering a monodisperse molecular weight.

explained from the fact that SEC most likely gives an artificially lower average MW since a proper standard for calibration is not available for polymers with associating groups. For example, if the polymer interacts with the column via some association kinetics, then retention is delayed and the MW compared to PMMA standards would appear artificially small. The inclusion of polydispersity however, clearly shows a shallowing of the power-law scaling for low frequency due to the presence of large molecular weight species with larger number of sticky groups. This suggest that improved agreement between model and data must consider the distribution in number of sticky groups for a given MW.

We thus hypothesize that the inclusion of polydispersity in the number of sticky groups per chain will lead to close agreement of the model with the experimental data. Using Eqs. 3.10 and 3.11, we now consider the sticky Rouse model taking into account polydispersity in the number of stickers per chain via a binomial distribution as discussed above. The results are shown in Figures 3.11b-c (dashed lines). It is evident in the 3% UPy case that the inclusion of a distribution in the number of stickers has stretched the model's low frequency crossover closer to the experimental data. However, it is evident that a distribution of stickers considering a binomial distribution cannot fully account for the low frequency response of the sample. Additionally, we find that in the 8% UPy case the result considering a distribution in N_s is almost identical to the result considering only polydispersity in MW. In fact, the two curves are almost indistinguishable. The insets in Figures 3.11b-c show the calculated binomial distribution considering the $\overline{M}_w$ determined from SEC. Note, there are several arguments as to why the binomial distribution may not be applicable, such as the assumed constant probability of monomer addition for the entire reaction. The binomial distribution may not be the accurate distribution in the case of the free radical polymerization carried out in this work.

One can speculate that the reduced power-law dependence of the moduli is due to the presence of a small number of molecules with a large number of stickers. In other words, the distribution of N_s for a given MW follows a skewed distribution tending to large numbers. To generate such a distribution, we generate a normal distribution for $M_{s,j}$ around the mean value M_s determined from NMR and SEC. We then generate a discrete distribution on the number of stickers via

$$N_{s,j} = \frac{M_i}{M_{s,j}} \tag{3.14}$$

The resulting distribution is shown in the insets of Figures 3.12a-b for the mean $\overline{M}_w$ determined from SEC. The parameters used to generate the distributions are $\sigma(3\%) = 4.5$ kDa $M_s = 12.9$kDa and $\sigma(8\%) = 3$ kDa $M_s = 6.4$ kDa with the constraint that $M_{s,j} > M_m$ (where M_m is the molecular weight of one repeat unit). The distribution calculated above is coupled with Eqs. 3.10 and 3.11 to predict the experimental data. Comparison of model predictions and experimental data are shown in Figure 3.12a-b.

It is evident from Figures 3.12a-b that there is improved agreement of the model with experimental data. Specifically, the model more readily captures the shallowing

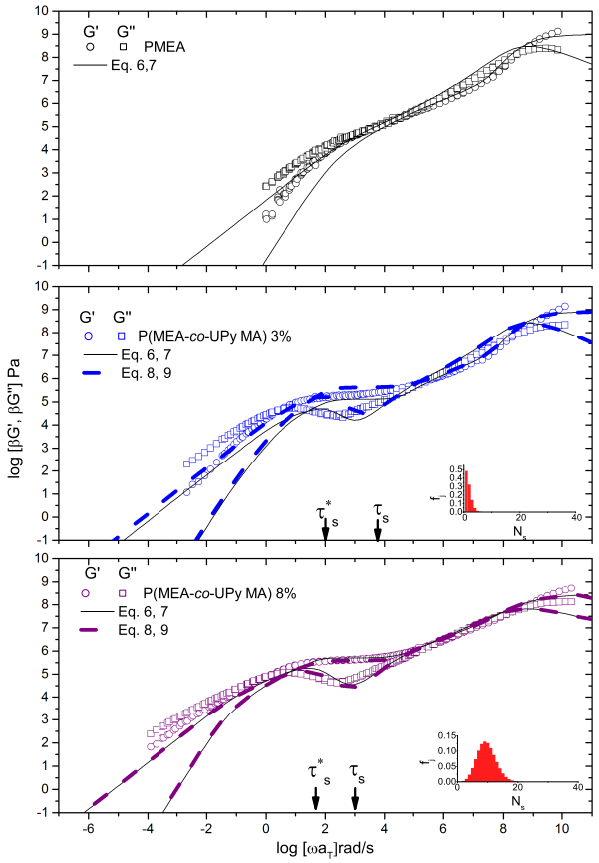

Figure 3.11: linear viscoelastic master curves of PMEA and P(MEA-*co*-UPyMA) systems shifted to $T_{ref} = 60$ °C. and the model prediction (solid lines) considering a polydispersity effects in MW as measured from SEC and (dotted lines) considering polydispersity effects in MW and $N_{s,j}$ via a binomial distirbution. Inset in b.) and c.): Binomial distribution function considering $\overline{M}_w$ from SEC.

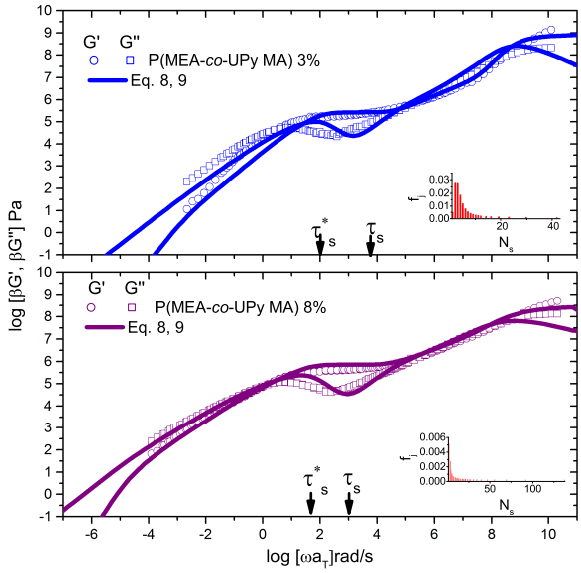

Figure 3.12: linear viscoelastic master curves of P(MEA-*co*-UPyMA) systems shifted to $T_{ref} = 60$ °C. and the model prediction (solid lines) considering both polydispersity in MW and a skewed distribution of $N_{s,j}$. Inset: Skewed distribution function of N_s for $\overline{M}_w$.

of the low frequency power-law when a skewed distribution in N_s is considered. This strongly suggests that a small number of molecules with a large number of stickers can strongly affect the low frequency response of the melt. In the case of chemistry where a distribution in N_s are irrelevant, such as in the work performed considering ionic associating polymers where the spacing was highly controlled, the sticky Rouse model of Eqs. 3.7 and 3.8 showed excellent agreement for the entire LVE [Chen et al. (2013)]. It would appear that when the spacing of the associating groups are not highly controlled, a distribution in N_s smears the low frequency behavior to lower power-laws, which must be taken into account when modeling such as in Eqs. 3.10 and 3.11. Overall the model does an excellent job of capturing the observed changes in LVE with increasing degree of association group density. These results suggest that indeed changes in LVE with association group density appear to be universal regardless of associating chemistry (e.g. ionic, hydrogen, etc.)

3.5 Conclusions

We present a detailed study of the linear viscoelastic and DRS response of a series of unentangled linear polymers: PMEA, P(MEA-*co*-UPyMA) containing 3% UPy,

and P(MEA-*co*-UPyMA) containing 8% UPy, with approximately the same molecular weight. Linear viscoelasticity clearly shows the formation of hydrogen bonding polymer networks with a distinct plateau modulus, an increase in the terminal relaxation timescale, and a shallowing of the low frequency power-law dependence. DRS was used as an independent (non-rheological) technique to measure the association lifetime of hydrogen bond units. The timescale obtained from DRS represents a bare lifetime of hydrogen bond units which is order k_BT per sticker. The timescale observed in rheology, the effective sticker lifetime, scales very well with the bare sticker lifetime, but is an order of magnitude larger than that measured via DRS. We argue that the difference is due to decreased probability of sticker disassociation above the gel point. The sticky Rouse model using parameters extracted from experimental data was predicted and compared to G' and G''. It is evident from the comparison that the sticky Rouse model accounting for polydispersity in MW is not sufficient in capturing the experimental trends. However, a modified sticky Rouse model where a distribution in N_s is taken into account does an excellent job of capturing the low frequency power-law dependence. Furthermore, these results strongly suggest that a small number of chains with a large number of stickers can account for a lowering of the power-law scaling in the expected terminal regime. Overall, the comparison of model and experimental data suggest and support the hypothesis that the linear viscoelastic response of unentangled polymers is not unique to a given type of bond association. In other words, the associating bond chemistry does not have a profound effect on the linear viscoelastic response; allowing for the same theoretical analysis regardless of associating chemistry.

3.6 Bibliography

Baxandall, L. G. (1989). Dynamics of Reversibly Cross-Linked Chains. *Macromolecules*, 22:1982–1988.

Bosman, A. W., Sijbesma, R. P., and Meijer, E. W. (2004). Supramolecular polymers at work. *Mater. Today*, 7(4):34–39.

Chen, Q., Huang, C., Weiss, R. A., and Colby, R. H. (2015). Viscoelasticity of Reversible Gelation for Ionomers. *Macromolecules*, 48(4):1221–1230.

Chen, Q., Masser, H., Shiau, H.-S., Liang, S., Runt, J., Painter, P. C., and Colby, R. H. (2014). Linear Viscoelasticity and Fourier Transform Infrared Spectroscopy of PolyetherEsterSulfonate Copolymer Ionomers. *Macromolecules*, 47(11):3635–3644.

Chen, Q., Tudryn, G. J., and Colby, R. H. (2013). Ionomer dynamics and the sticky Rouse model a). *J. Rheol.*, 16802(August):1441–1462.

Chen-Yang Liu, Jiasong He, R. K. and Bailly, C. (2006). New linearized relation for the universal viscositytemperature behavior of polymer melts. *Macromolecules*, 39(25):8867–8869.

Cole, K. S. and Cole, R. H. (1942). Dispersion and absorption in dielectrics ii. direct current characteristics. *J. Chem. Phys.*, 10(2).

de Greef, T. F. A., Nieuwenhuizen, M. M. L., Sijbesma, R. P., and Meijer, E. W. (2010). Competitive intramolecular hydrogen bonding in oligo(ethylene oxide) substituted quadruple hydrogen bonded systems. *J. Org. chem.*, 75(3):598–610.

Elkins, C. L., Park, T., McKee, M. G., and Long, T. E. (2005). Synthesis and characterization of poly(2-ethylhexyl methacrylate) copolymers containing pendant, self-complementary multiple-hydrogen-bonding sites. *J. Polym. Sci. Polym. Chem.*, 43(19):4618–4631.

Feldman, K. E., Kade, M. J., Meijer, E. W., Hawker, C. J., and Kramer, E. J. (2009). Model Transient Networks from Strongly Hydrogen-Bonded Polymers. *Macromolecules*, 42(22):9072–9081.

Ferry, J. (1980). *Viscoelastic Properties of Polymers, 3rd ed.* Wiley, New York.

Fulcher, G. A. (1925). Analysis of recent measurements of the viscosity of glasses. *J. Am. Ceram. Soc.*, 8:339–355.

Gonzlez, L., Ladegaard Skov, A., and Hvilsted, S. (2013). Ionic networks derived from the protonation of dendritic amines with carboxylic acid end-functionalized pegs. *J. Polym. Sci. Polym. Chem.*, 51(6):1359–1371.

Green, M. S. and Tobolsky, A. V. (1946). A New Approach to the Theory of Relaxing Polymeric Media. *J. Chem. Phys.*, 14:80–92.

Hackelbusch, S., Rossow, T., and Assenbergh, P. V. (2013). Chain Dynamics in Supramolecular Polymer Networks. *Macromolecules*, 46:6273–6286.

Javakhishvili, I., Jankova, K., and Hvilsted, S. (2013a). Neutral, anionic, cationic, and zwitterionic diblock copolymers featuring poly(2-methoxyethyl acrylate) hydrophobic segments. *Polym. Chem.*, 4(3):662–668.

Javakhishvili, I., Kasama, T., Jankova, K., and Hvilsted, S. (2013b). RAFT copolymerization of itaconic anhydride and 2-methoxyethyl acrylate: a multifunctional scaffold for preparation of "clickable" gold nanoparticles. *Chem. Commun.*, 49(42):4803–4805.

Javakhishvili, I., Røn, T., Jankova, K., Hvilsted, S., and Lee, S. (2014). Synthesis, characterization, and aqueous lubricating properties of amphiphilic graft copolymers comprising 2-methoxyethyl acrylate. *Macromolecules*, 47(6):2019–2029.

Javakhishvili, I., Tanaka, M., Ogura, K., Jankova, K., and Hvilsted, S. (2012). Synthesis of Graft Copolymers Based on Poly (2- Methoxyethyl Acrylate) and Investigation of the Associated Water Structure. *Macromol. Rapid Commun.*, pages 319–325.

Kremer, F. and Schnhals, A. (2003). *Broadband Dielectric Spectroscopy*. Springer Berlin Heidelberg.

Kumpfer, J. R., Wie, J. J., Swanson, J. P., Beyer, F. L., Mackay, M. E., and Rowan, S. J. (2012). Influence of Metal Ion and Polymer Core on the Melt Rheology of Metallosupramolecular Films. *Macromolecules*, 45:473–480.

Lange, R. F. M., Van Gurp, M., and Meijer, E. W. (1999). Hydrogen-bonded supramolecular polymer networks. *J. Polym. Sci. Polym. Chem.*, 37(19):3657–3670.

Leibler, L., Rubinstein, M., and Colby, R. H. (1991). Dynamics of Reversible Networks. *Macromolecules*, 24:4701–4707.

Lewis, C. L. and Anthamatten, M. (2013). Synthesis, swelling behavior, and viscoelastic properties of functional poly(hydroxyethyl methacrylate) with ureidopyrimidinone side-groups. *Soft Matter*, 9(15):4058.

Lewis, C. L., Stewart, K., and Anthamatten, M. (2014). The Influence of Hydrogen Bonding Side-Groups on Viscoelastic Behavior of Linear and Network Polymers. *Macromolecules*, 47:729–740.

Ling, G. H., Wang, Y., and Weiss, R. A. (2012). Linear Viscoelastic and Uniaxial Extensional Rheology of Alkali Metal Neutralized Sulfonated Oligostyrene Ionomer Melts. *Macromolecules*, 45:481–490.

Lou, N., Wang, Y., Li, X., Li, H., Wang, P., Wesdemiotis, C., Sokolov, A. P., and Xiong, H. (2013). Dielectric relaxation and rheological behavior of supramolecular polymeric liquid. *Macromolecules*, 46(8):3160–3166.

McKee, M. G., Elkins, C. L., Park, T., and Long, T. E. (2005). Influence of Random Branching on Multiple Hydrogen Bonding in Poly(alkyl methacrylate)s. *Macromolecules*, 38:6015–6023.

Noro, A., Matsushita, Y., and Lodge, T. P. (2008). Thermoreversible Supramacromolecular Ion Gels via Hydrogen Bonding. *Macromolecules*, 41:5839–5844.

Røn, T., Javakhishvili, I., Patil, N. J., Jankova, K., Zappone, B., Hvilsted, S., and Lee, S. (2014). Aqueous lubricating properties of charged (abc) and neutral (aba) triblock copolymer chains. *Polymer*, 55(19):4873 – 4883.

Rossow, T. and Seiffert, S. (2014). Supramolecular polymer gels with potential model-network structure. *Polym. Chem.*, 5(8):3018–3029.

Rubinstein, M. and Semenov, A. N. (1998). Thermoreversible Gelation in Solutions of Associating Polymers. 2. Linear Dynamics. *Macromolecules*, 31:1386–1397.

Rubinstein, M. and Semenov, A. N. (2001). Dynamics of Entangled Solutions of Associating Polymers. *Macromolecules*, 34:1058–1068.

Schrter, K., Hutcheson, S. A., Shi, X., Mandanici, A., and McKenna, G. B. (2006). Dynamic shear modulus of glycerol: Corrections due to instrument compliance. *J. Chem. Phys.*, 125(21):214507.

Seiffert, S. (2016). Effect of supramolecular interchain sticking on the low-frequency relaxation of transient polymer networks. *Macromol. Rapid Commun.*, 37(3):257–264.

Shabbir, A., Goldansaz, H., Hassager, O., van Ruymbeke, E., and Alvarez, N. J. (2015). Effect of hydrogen bonding on linear and nonlinear rheology of entangled polymer melts. *Macromolecules*, 48(16):5988–5996.

Sijbesma, R. P., Beijer, F. H., Brunsveld, L., Folmer, B. J. B., and Hirschberg, J. H. K. K. (1997). Reversible Polymers Formed from Self-Complementary Monomers Using Quadruple Hydrogen Bonding. *Science*, 278:1601–1604.

Stadler, F. J., Pyckhout-Hintzen, W., Schumers, J.-M., Fustin, C.-A., Gohy, J.-F., and Bailly, C. (2009). Linear Viscoelastic Rheology of Moderately Entangled Telechelic Polybutadiene Temporary Networks. *Macromolecules*, 42(16):6181–6192.

Tanaka, M., Sato, K., Kitakami, E., Kobayashi, S., Hoshiba, T., and Fukushima, K. (2014). Design of biocompatible and biodegradable polymers based on intermediate water concept. *Polym. J.*, 47(2):114–121.

Tang, S., Wang, M., and Olsen, B. D. (2015). Anomalous self-diffusion and sticky Rouse dynamics in associative protein hydrogels. *J. Am. Chem. Soc.*, 137(11):3946–57.

Tinius, J. A., Dragomer, D., Klutka, F., Vanbebber, A., and Cerney, K. (2003). The Capiox RX05 oxygenator : pediatric clinical observations. *Perfusion*, 18:321–323.

Vogel, H. (1921). The law of the relationship between viscosity of liquids and the temperature. *Phys. Z*, 22:645–646.

Wbbenhorst, M. and van Turnhout, J. (2002). Analysis of complex dielectric spectra. i. one-dimensional derivative techniques and three-dimensional modelling. *J. Non-Cryst. Solids*, 305(13):40 – 49.

Wubbenhorst, M., Turnhout, J. V., Folmer, B. J. B., Sijbesma, R. P., and Meijer, E. W. (2001). Complex Dynamics of Hydrogen Bonded. *IEEE Trans. Dielectr. Electr. Insul.*, 8:365–372.

Yamauchi, K., Lizotte, J. R., and Long, T. E. (2003). Thermoreversible Poly (alkyl acrylates) Consisting of Self-Complementary Multiple Hydrogen Bonding. *Macromolecules*, 36:1083–1088.

CHAPTER 4

Non-linear Shear and Uniaxial Extensional Rheology of Polyether-Ester-Sulfonate Copolymer Ionomer Melts

4.1 Introduction

Ionomers represent a family of polymers where ionic groups are covalently attached to the polymer backbone. Due to the strong dipolar interaction between the ion pairs, ionic groups have a tendency to bond into nanometer-sized aggregates (which can microphase separate into ionic clusters) within the nonpolar polymer matrix and thus act as temporary crosslinks [Tierney and Register (2002)]. Bulk properties of such supramolecular polymer systems are governed by these ionic clusters. Viscosity and elasticity of ionomer melts are typically several orders of magnitude higher compared to their nonionic counterparts because of retarded diffusional motion of polymer chains. The ion pairs attached to the polymer chains relax by a mechanism which involves many jumps from one cluster to another, often termed as 'ionic hopping', before the whole chain can relax completely [Tierney and Register (2002); Chen et al. (2014)].

Linear rheology of ionomer melts has been studied quite extensively by many research groups [Stadler et al. (2009); Weiss and Yu (2007); Weiss and Zhao (2009); Vanhoorne and Register (1996); Tierney and Register (2002); Chen et al. (2013, 2014)]. In contrast, little is known about the nonlinear viscoelasticity of ionomers in particular under extensional flows. [Connelly et al. (1982)] were the first to study extensional properties of ionomers in 1982. [Takahashi et al. (1994)] investigated effects of ionic interaction on uniaxial extensional flow of ethylene-based ionomer melts. [Stadler et al. (2010)] studied extensional behavior of entangled telechelic polybutadiene

carboxylate ionomers and showed qualitatively the dependence of strain hardening on various counterions (Rb, Na, K, and Li). The authors qualitatively discuss the influence of cohesive strength of ionic clusters on the strain hardening behavior. Weak ionic clusters (largest, Rb) exhibit fluid like behavior, medium strength clusters (K) exhibit noticeable strain hardening, and strong ionic clusters (Na, Li) are too brittle to study strain hardening [Stadler et al. (2010)]. More recently, Ling et al. (2012) have studied extensional rheology of nearly monodisperse alkali metal neutralized oligomeric sulfonated polystyrene ionomers. The effect of ionic associations was isolated since the systems studied were below the entanglement molecular weight of polystyrene. Their work has reported strain hardening for extension rates greater than the inverse of sticker lifetime. They conclude that a maximum in engineering stress under extensional deformation results from the catastrophic failure of the transient network and is nearly independent of extension rate. Ionomers have been shown to exhibit equilibration time dependence of rheological properties [Stadler et al. (2009)]. While the above mentioned studies may have suffered from the inability to anneal the samples in-situ in order to obtain results from equilibrated structures, the results are useful.

A filament stretching rheometer with state of the art temperature control provides for in-situ annealing prior to performing uniaxial extensional flow, with minimal experimental errors [Bach et al. (2003b)]. Investigation of ionomers in nonlinear shear are limited as well, in part due to the experimental difficulties to overcome artifacts such as edge fracture [Snijkers and Vlassopoulos (2011)]. Takahashi et al. (1995) have investigated systematically the nonlinear stress relaxation in ethylene-co-methacrylic acid ionomers as a function of ion content. They found that the damping function $h(\gamma) = \frac{G(t,\gamma)}{G(t)}$, a measure of material's nonlinear response, was unaffected by ionic interactions at low ion content, whereas strong strain softening was reported at higher ion content. The implementation of the cone-partitioned plate (CPP) geometry on strain- controlled rheometers has opened the route for advancing the polymer melt rheology field by performing artifact-free nonlinear shear experiments, and shall be used in this work [Snijkers and Vlassopoulos (2011); Schweizer (2003)].

Recently, single-ion conducting polymers, or ionomers, have found great interest as candidate materials in energy storage devices, such as lithium ion batteries [Chen et al. (2013); Armand et al. (1981); Chen et al. (2014); Tudryn et al. (2012)]. Polymer electrolytes without volatile solvents as materials for battery applications are safer when compared to conventional liquid electrolytes. However, the ionic conductivity of these materials is still far below the 1 mS/cm target for practical applications [Wang et al. (2014)]. The coupling between the segmental chain dynamics and ionic conductivity leads to a conflict between them [Wang et al. (2012); Tudryn et al. (2012)]. Consequently, enhancing mechanical performance (elasticity and glass transition temperature, T_g) often lowers conductivity, making it challenging to find the right balance. Poly (ethylene oxide) [PEO] based ionomers have been studied quite extensively due to superior cation solvation ability [Armand et al. (1981); Chen et al. (2014, 2013); Tudryn et al. (2012); Lin et al. (2013)]. Recently, Chen et al. (2014)

have investigated linear viscoelastic properties of amorphous copolyester ionomers synthesized via condensation of sulfonated phthalates with mixtures of PEO and poly(tetramethylene glycol) [PTMO] [Chen et al. (2014)]. This study is based on unentangled ionomer systems where the rich LVE properties are attributed to the ionic clusters. By introducing low T_g PTMO along the backbone of the PEO ionomer, the elasticity was remarkably improved due to stronger ionic clusters formed in the PTMO-rich domain.

This article is part of a continuing investigation on viscoelastic properties of polyether-ester ionomers initiated by Colby and coworkers [Chen et al. (2013); Tudryn et al. (2012)]. In this work, we examine non-linear shear and uniaxial extensional rheology of PTMO- Na/Li ionomers and one coionomer PEO25-PTMO75- Na/Li. In the case of the coionomer, 25 molar percentage of the diols are PEO, and 75 molar percentage are diols of PTMO. The effect of PEO phase on shear and extensional melt behavior is elucidated by comparing the properties of PTMO-ionomer and the PEO25-PTMO75-coionomer melts at similar flow conditions.

4.2 Experimental Section

Materials

Amorphous copolyester ionomers were synthesized via condensaiton of sulfonated phthalates with mixtures of poly (ethylene glycol) with $M = 600$ kg/mol and poly(tetramethylene glycol) with $M = 650$ kg/mol [Chen et al. (2014)]. The structures of PEO-PTMO-Na (Li) coionomers and PTMO-Na (Li) ionomers are shown in Figure 4.1. The LVE was remeasured and shown to be in good agreement with the published work [Chen et al. (2013)] except for the LVE of PTMO-Li ionomer which is shifted to lower frequencies (by factor of 4). This is likely due to one of the two reasons: either 1) the previously measured sample, which comes from a different batch, may contain small amount of moisture, or 2) the presence of some impurity in this particular batch due to imperfect ion exchange of PTMO-Li ionomer from PTMO-Na ionomer. Previous X-ray scattering results have shown that crystallization only occurs at low temperatures below 0°C[Tudryn et al. (2012)], here our samples are amorphous at room temperature. The samples used in this work and their characteristics are given in Table 4.1.

Moisture Content

Recent studies on ionomers have shown that the presence of moisture can modify the rheological properties by lowering the viscosities and accelerating the terminal relaxation time [Chassenieux et al. (2000); Nishioka et al. (2008)]. Therefore, the samples were dried in a vacuum oven at 100°C overnight prior to direct loading to the rheometer. Instrument quality Argon gas (Argon 99.999%, $O_2 < 2ppm$, $N_2 < 5ppm$, $H_2O < 3ppm$) was used instead of air for releasing the vacuum inside the vacuum oven. This step minimizes oxidation of the sample. However, the samples

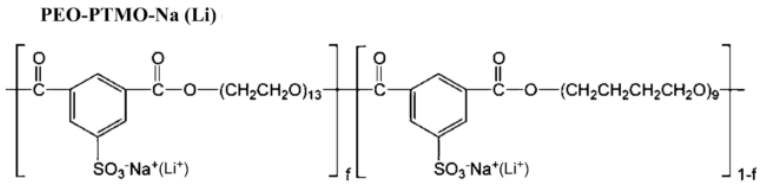

Figure 4.1: Chemical structure of PEO-PTMO-Na (Li) coionomers with the fraction f of PEO spacer varied from 0.25 (PEO25-PTMO75-Na (Li)) to 0 (PTMO-Na (Li)).

Table 4.1: Molecular weight M_n, number density of ionic groups p_0, and T_g for the ionomers with Li and with Na counterions

sample	M_n	Li		Na	
	g/mol	$p_0(nm^{-3})$	$T_g(C)$	$p_0(nm^{-3})$	$T_g(C)$
PEO25-PTMO75	6500	0.67	-48	0.67	-47
PTMO	6700	0.66	-63	0.66	-64

oxidize over long residence times in the rheometer making data reproducibility a major challenge. Overall, all samples investigated were very sensitive to humidity, temperature and oxygen conditions. However, all reported data are obtained with the same protocol and reproducible.

Uniaxial Extensional Rheology Measurements

The extensional stress growth coefficient was measured as a function of time using filament stretch rheometers: (DTU-FSR) and Rheofilament. Cylindrical stainless steel plates with a diameter of 5.4 mm were used for all measurements. Measurements were performed at constant Hencky strain rate imposed at the mid-filament diameter using an online control scheme [Román Marín et al. (2013)]. Samples were heated under nitrogen for 2 hours at 120°C prior to performing experiments. At such a temperature the ionomer flows easily and forms a nice axisymmetric shape when the top rheometer plate is brought in contact with the sample. All experiments were performed between 35°C and 90°C in a nitrogen controlled environment. The imposed stretch rates varied from $0.01s^{-1}$ to $1s^{-1}$.

Non-linear Shear Rheology Measurements

Selected measurements were performed in non-linear shear in order to compare the response of the ionomers (Table 4.1) in such a weaker flow (due to rotational contribution as well) against those in uniaxial extension. The same sample treatment

protocol was used in shear measurements as in extensional measurements. Shear rheology measurements were performed in a strain controlled rheometer (ARES 2kFRTN1, TA, USA) using a home-made stainless steel cone-partitioned-plate (CPP) geometry with the following characteristics: measuring plate diameter 6 mm, cone angle 0.1 rad, the outer partition with an outer diameter of 20 mm and an inner diameter of 6.16 mm; thus, the gap between the partitions is around 80 μm. For temperature control, the ARES convection oven with nitrogen flux was used, with a temperature control of $\pm$ 0.1 °C [Yan et al. (2016)].

Typically, a sample of diameter 6 mm and thickness 0.15 mm was placed in the rheometer and shaped at 100°C . Dynamic frequency sweeps (with linear strain amplitude γ_0=0.04 and imposed frequency range $\omega = 0.1 - 100$ rad/s) were performed in order to check the linear rheological data for consistency over a broad range of temperatures (0-100°C). Subsequently, start-up of steady shear was then performed at 60°C for PTMO-Na at constant values of shear rate ranging from $\dot{\gamma} = 0.02s^{-1} - 0.7s^{-1}$. Using the tTS frequency scale shift factor, the measurements at 60°C were shifted to 80°C . The maximum imposed deformation ($\dot{\gamma}t$) was limited to 4 strain units. Between consecutive tests the material was rejuvenated at 100°C for 15 min and the linear rheology was systematically measured to confirm the samples unchanged condition. A similar procedure was utilized for the PEO25-PTMO75-Na ionomer for which the start-up of steady shear was performed at 45°C at constant values of shear rate ranging from $\dot{\gamma} = 0.1s^{-1} - 1s^{-1}$, with a maximum imposed deformation limited to 20 strain units.

4.3 Results and Discussion

Linear viscoelasticity

LVE results are shown in Figure 4.2a-f, to highlight the regions investigated in nonlinear rheological measurements.

Figure 4.2a and 4.2c, show the influence of addition of PEO phase with Na and Li as the counterion, respectively. Our simple approach consists of comparing the LVE master curves at different temperatures to have an overlapped terminal flow regime. The effect of PEO phase can then be elucidated under a range of applied strain rates both in extension and nonlinear shear. Figure 4.2e, shows the ion dependence on LVE of the PTMO ionomers. To investigate the influence of ion on the physical mechanism of strain hardening in extensional flow, LVE master curves for PTMO-Li and PTMO-Na are shifted as shown in Figure 4.2f. For unentangled ionomers, the terminal relaxation time, τ, depends on the temporary ionic associations. The ionic groups attached to the chain, hop between aggregates with a characteristic time, $\tau_s = 1/\omega_s$, also called the lifetime of ionic associations. The higher the association lifetime, the longer is the terminal relaxation time. Polydispersity in molecular weight results in broadening in the lower crossover frequency because of a distribution in the number of polymer modes each associated with a contribution to the moduli [Shabbir et al. (2016)]. The ionomers used in this study are polydisperse ($PDI \approx 2.0$),

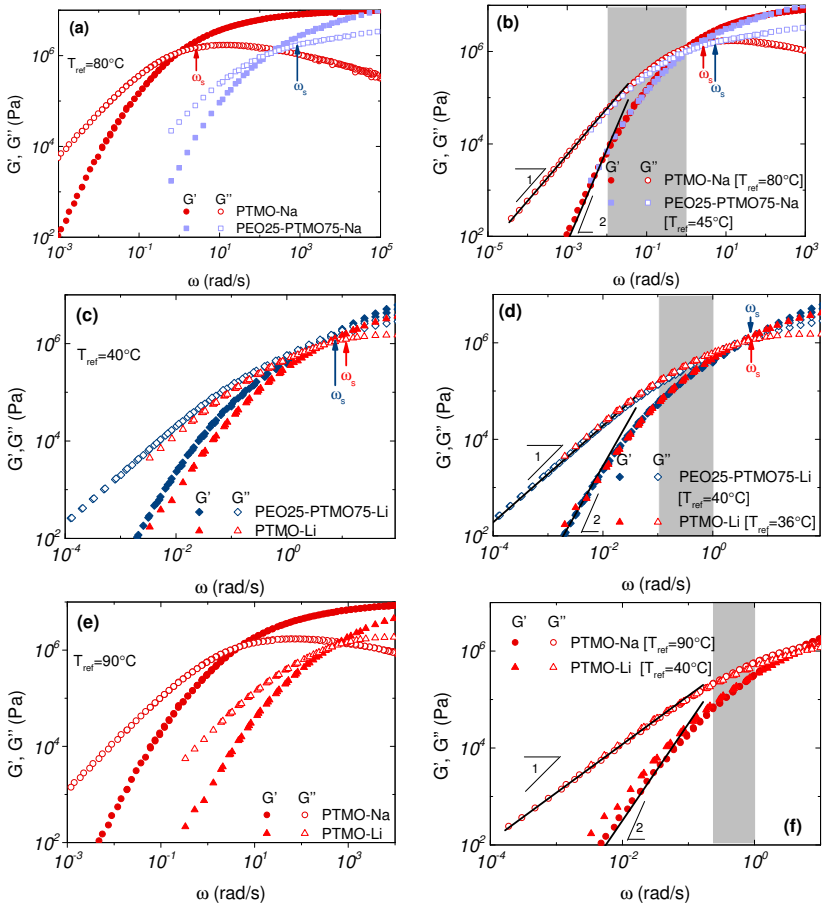

Figure 4.2: LVE master curves of (a) PTMO-Na and PEO25-PTMO75-Na at T_{ref} = 80°C, (c) PTMO-Li and PEO25-PTMO75-Li at T_{ref} = 40°C, (e) PTMO-Na and PTMO-Li at T_{ref} = 90°C. The corresponding master curves on the right (b,d,f) curves compared at different T in order to have an overlapped terminal regime

and they exhibit terminal slopes of one and two for $G^{''}(\omega)$, and $G^{'}(\omega)$, respectively (represented in black solid lines) at low frequency, ω as evident from Figure 4.2b, 4.2d, and 4.2f. The terminal relaxation time can be evaluated as,

$$\tau = \lim_{\omega \to 0} \left[\frac{G^{'}}{\omega G^{''}} \right] \tag{4.1}$$

The association lifetime can thus be obtained as

$$\tau_s = \frac{\tau}{N_s^2} \tag{4.2}$$

where $N_s = 7$ [Chen et al. (2013, 2014)] is the number of sticky Rouse segments per chain, which is the same for PTMO and PEO25-PTMO75 because the M_n and the spacer molecular weights are nearly identical (see Table 1). $\tau_s = 1/\omega_s$ is indicated by arrows in Figure 4.2a-d.

Uniaxial extensional rheology

Effect of PEO with Na counterion

We now examine the extensional rheology in the context of the LVE data presented above. Figure 4.3a and 4.3b show the stress growth coefficients, η_E^+, as a function of time for the PTMO-Na ionomer and the PEO25-PTMO75-Na coionomer at various strain rates, $0.01s^{-1} \leqslant \dot{\epsilon} \leqslant 1s^{-1}$. The strain rates are always increasing from right to left. The dashed line in Figure 4.3a, represents the LVE envelope of non-ionic PTMO, i.e. without any ionic groups. The zero extension rate viscosity is 5 orders of magnitude higher than the non-ionic PTMO for which $\eta_E = 100$ Pas at 80°C. The LVE envelope obtained using a multimode Maxwell fit from LVE oscillatory shear data is plotted as a solid line. The extensional data are consistent with the predictions of linear viscoelasticity at short extension times. All the samples, fracture into two halves in a brittle like fashion. The black arrows in Figure 4.3a, b indicate fracture of the filament. Detailed study of brittle fracture of ionomers is discussed in Chapter 5.

At very low strain rates ($<0.03s^{-1}$) the stress growth coefficient follows the LVE envelope attaining steady state at large Hencky strains. However, at higher strain rates, departure above the LVE envelope (often termed strain hardening) is noticed. The pattern of strain hardening observed here, i.e., decreasing strain hardening with increasing strain rate, resembles that of long chain branched polymers such as LCB-mLLDPE [Gabriel and Münstedt (2003)]. Similar trend was reported for entangled PBd-COORb telechelic ionomer by Stadler et al. (2010) For unentangled associative polymers, association lifetime defines the characteristic relaxation time scale. The extension rates probed in Figure 4.3a, b are smaller than the inverse of association lifetime (indicated in Figure 4.2b).

In order to elucidate the effect of addition of 25% PEO with Na as counterion, a comparison between PTMO-Na and PEO25-PTMO75-Na is shown in Figure 4.3c.

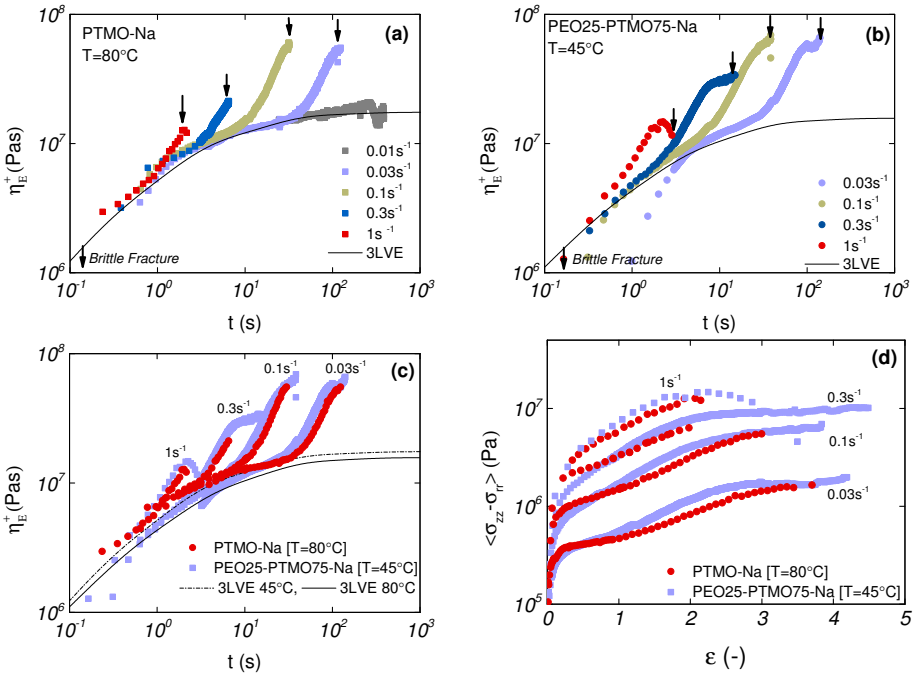

Figure 4.3: Top: Extensional stress growth coefficients at different Hencky rates as a function of time for (a) PTMO-Na at 80°C, and (b) PEO25-PTMO75-Na at 45°C, chosen because these temperatures have nearly identical LVE (see Figure 4.2b). Bottom: (c) comparison of stress growth coefficient as a function of time for PTMO-Na at 80°Cand PEO25-PTMO75-Na at 45°C, (d) Same data as in Figure 4.3c plotted as true extensional stress vs Hencky strain. Black arrows highlight end of experiment due to fracture of the filament.

Although PEO25-PTMO75-Na is chemically different than PTMO-Na, identical strain hardening is observed with and without PEO because the slowest associations in the coionomer are in the PTMO-rich phase. The plot of true extensional stress as a function of Hencky strain in Figure 4.3d indicates that incorporation of 25% PEO to the PTMO-ionomer increases the maximum Hencky strain at fracture. Although, for strain rates smaller than $1s^{-1}$, it appears that η_E^+ reaches a constant value, it does not represent a true steady state because the material fractures at the end of each experiment. Such a behavior is different from classical linear polymer melts where a steady state in η_E^+ is achieved at large Hencky strains followed by thinning of the filament rather than fracture [Bach et al. (2003a)].

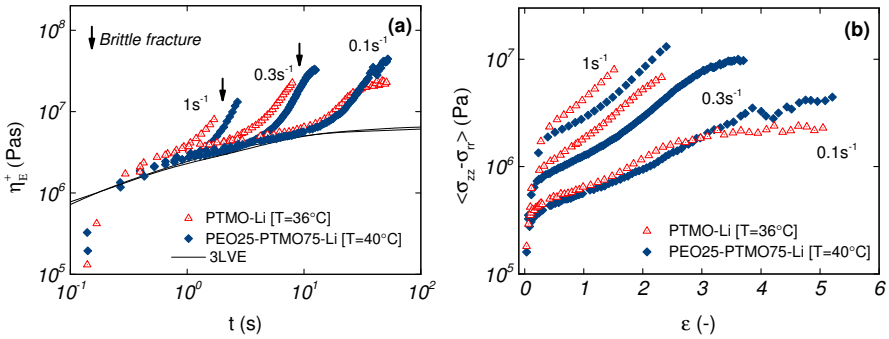

Figure 4.4: (a) Comparison of extensional stress growth coefficient as a function of time for PTMO-Li and PEO25-PTMO75-Li, (b) Same data plotted as true extensional stress vs Hencky strain

Effect of PEO with Li counterion

We now investigate the effect of PEO with Li as the counterion within the context of the LVE presented in Figure 4.2c and 4.2d above. With Li as the counterion the activation energy for ionic hopping is smaller than with Na counterion [Chen et al. (2014)]. Figure 4.4a, b compares PTMO-Li and PEO25-PTMO75-Li in extensional deformation. In Figure 4.4b, the material stretches more with the addition of PEO25% to the PTMO-Li ionomer. We conclude that addition of high solvating PEO makes the material significantly more ductile.

From previous study by Chen et al. (2014), the X-ray scattering revealed strong phase separation for PEO and PTMO in the coionomers [Chen et al. (2014)]. FTIR revealed the different aggregation status of the ions within the system. A combination of these two results suggest that the ionic groups can be classified into three groups: Taking a number fraction of PEO block as f, the ionic groups having both sides connected to the PEO spacers of a fraction of f^2 are well located in the PEO phase. Similarly, a fraction of $(1-f)^2$ ionic groups are well located in the PTMO phase, leaving a fraction $1-f^2-(1-f)^2 = 2f(1-f)$ ions at the PEO/PTMO interface. The higher ductility after the incorporating of EO block should be related to the non-uniform ionic dissociation times for the ionic groups of the coionomers. For the PEO25-PTMO75-Na and -Li, the fraction of ions within the PEO, PTMO domains and at the interface are 56%, 6%, and 38%, respectively. The ionic groups within the PEO phase are much more motile than those in the PTMO phase. For example, the lifetime of ionic groups was estimated from LVE to be $\tau_s = 4\mu s$ for PEO-Na at $T_{ref} = 45°C$ and $200\mu s$ for PEO-Li at $T_{ref} = 40°C$, which is much shorter than τ_s estimated for the sample as a whole shown earlier in Figure 4.2, which should be mainly controlled by those ionic groups that are strongly aggregated in the PTMO domains. The ionic groups at the interface should have lifetime in between those in PEO and PTMO domains. For the coionomer subjected to an elongation rate or shear rate less than

$1s^{-1}$ at T_{ref}, the ionic groups within the PEO phase and the interface should be able to move freely to adjust the conformation of a chain distributed around the PEO and PTMO microdomains, which should be responsible to the extra ductility seen for the PEO25/PTMO75-Na and Li at T_{ref}.

Effect of counterion (Na, and Li)

To investigate the ion dependence of strain hardening (see the respective LVE in Figure 4.2e and 4.2f), a comparison of PTMO-Na and PTMO-Li is presented in Figure 4.5. Identical strain hardening response suggests that Li and Na ions have similar interaction with the sulphonate-group. This result is different from that obtained for PBd-COOLi and PBd-COONa entangled telechelic ionomers for similar range of strain rates because strong solvation by ether oxygens greatly lowers the interaction energies. It was reported that strain hardening increased with increasing strain rate for PBd-COOLi, whereas strain hardening increased with decreasing strain rate for PBd-COONa. It was hypothesized that carboxy-group interacted differently with Li and Na, in the absence of solvation [Stadler et al. (2010)].

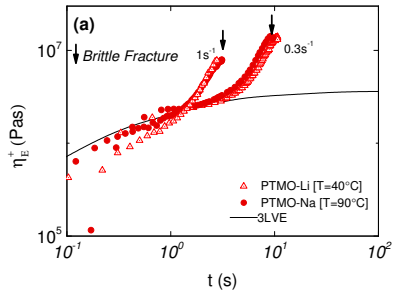

Figure 4.5: Comparison of extensional stress growth coefficient at two different Hencky rates as a function of time for PTMO-Na at 90°C, and PTMO-Li at 40°C.

Extensional deformation of PTMO-Na ionomer: from melt to a 'neo-Hookean' solid

We now turn our focus on the PTMO-Na ionomer. Figure 4.6a summarizes the results from extensional rheology measurements performed at $T = 40°C$, $T = 60°C$, $T = 80°C$, and $T = 90°C$. To test the validity of time-temperature-superposition for ionomers in non-linear extensional flows, a master plot is shown in Figure 4.6b at $T_{ref} = 80°C$. The stress growth coefficient and time have been reduced by the respective temperature dependent shift factors, a_T. In order to quantify the degree of nonlinearity, a dimensionless quantity called the Weissenberg number, Wi, is introduced which is the product of strain rate and relaxation time. Here we use the stciker lifetime such that $Wi = \dot{\epsilon}\tau_s$. Two regimes are noticeable: for $Wi < 1$ filaments undergo strain hardening before eventually breaking in brittle fashion (shown in top

right region), on the other hand for $Wi > 1$ no strain hardening is observed (shown in bottom left region). In fact, the filaments fracture right on top of the LVE envelope. This behavior is *opposite* to that of entangled linear polymer melts far above T_g, where strain hardening always increases with increasing strain rates. The inset plot shows the LVE of PTMO-Na ionomer in order to provide a guideline for the corresponding regions probed.

The strain rate dependence of true extensional stress as a function of Hencky strain is shown in Figure 4.6c. The black solid line indicates the neo-Hookean [Doi (1996)] stress prediction based on the plateau modulus, G_N^0, of PTMO-Na given by Eq.4.3

$$\sigma_{zz} - \sigma_{rr} = G_N^0(\lambda^2 - \lambda^{-1}) \tag{4.3}$$

Here σ_{zz} and σ_{rr} are the axial and radial components of stress respectively and $\lambda = e^{\epsilon}$. The Neo-hookean model does not take into account finite extensibility of polymer chains made up of N segments [Doi (1996)]. The neo-Hookean stress corresponds to affinely deforming a permanently cross-linked network and hence represents an upper limit because it does not account for the dissipative mechanisms during nonlinear deformation. In all cases, the experimental stress values are below those predicted from the neo-Hookean model. For $Wi > 1$, small Hencky strain values are achieved and the true extensional stress at fracture is close to the neo-Hookean stress prediction. On the other hand, for $Wi < 1$, the difference between true extensional stress at break and the model increases while the material is able to stretch to higher Hencky strain values. The emerging picture is that of a transition from a hard-brittle to soft-ductile state. In the hard-brittle state, the material shows a nearly strain-rate-independent response (see Figure 4.6b and c for $Wi > 1$) . This finding suggests that although these materials are elastic for $Wi > 1$, their response in extension is brittle in nature when stretched faster than the crosslink lifetime. Conventional polymer melts can be stretched to extensional stress levels much higher compared to the plateau modulus. For example, the maximum stresses reached with highly entangled polystyrene are about $40G_N^0$ [Bach et al. (2003a)]. However, maximum stress values that can be achieved with the PTMO-Na ionomer is in the order of $G_N^0(\approx 10^7)$ Pa (see dashed line in Figure 4.6c). This result highlights the difference in the nature of the physical interactions in ionomers compared to the entanglements in classical polymers.

Nonlinear shear rheology

Figure 4.7a, depicts the time evolution of shear stress at different shear rates for PTMO-Na, in the form of shear stress versus shear strain ($\gamma = t \times \dot{\gamma}$).

Note that the range of strains covered is small, with the maximum strain being 4 units (here we show data up to strain = 3 for clarity). The transient data at small strains (or short times) collapse onto the LVE envelope as shown in the shear stress growth coefficient of Figure 4.8 below. Furthermore, the same qualitative behavior

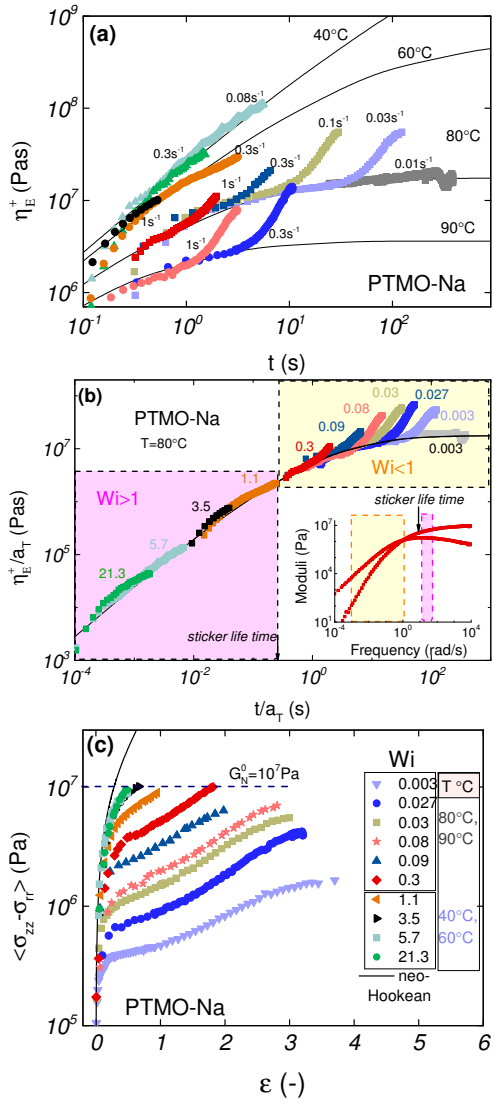

Figure 4.6: (a) Extensional stress growth coefficient as a function of time at four temperatures, 40°C, 60 °C, 80 °C, and 90 °C for PTMO-Na, (b) Master plot of extensional rheology at $T_{ref} = 80°C$, inset depicts LVE in order to provide a guideline for the corresponding regions probed, (c) True extensional stress vs Hencky strain for different rates and temperatures, corresponding to Figure 4.6a. The thin black line is the neo-Hookean stress prediction which is the stress level where the high rate ($Wi > 1$) samples break.

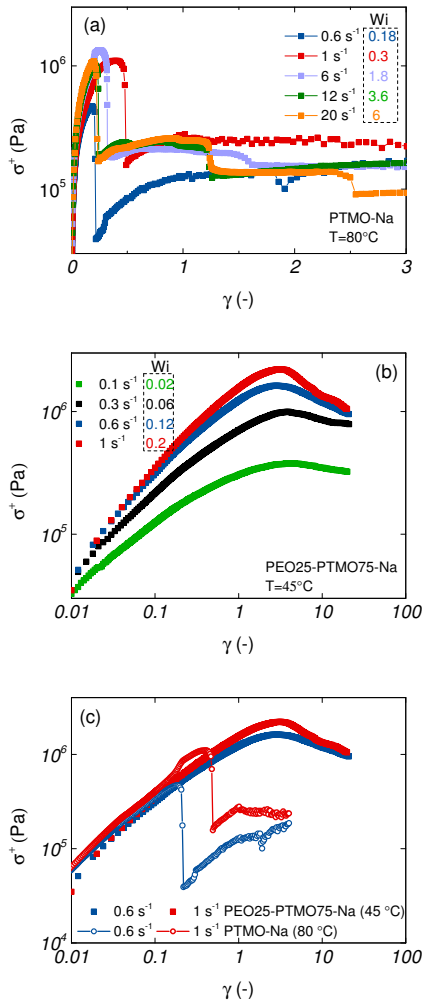

Figure 4.7: Transient nonlinear shear data at different shear rates for (a) PTMO-Na at $T = 80°C$, (b) PEO25-PTMO75-Na at $T = 45°C$, (c) Comparison of transient data shear stress vs shear strain as function of time for PTMO-Na at $T = 80°C$ and PEO25-PTMO75-Na at $T = 45°C$ where the temperatures were chosen so as to match LVE (see Figure 4.2b)

is observed for a wide range of applied shear rates (for 0.6 to 20 s^{-1}). In particular, the stress reaches a peak value (at the LVE envelope as seen in Figure 4.8) and then drops dramatically (by as much as one decade) before reaching steady state. More importantly, for $Wi > 1$ the stress reaches almost the same steady state value, independent of shear rate and drops stepwise, pointing to heterogeneous flow response. In fact, this strongly suggests the presence of instabilities and in particular wall slip and/or shear banding [Buscall et al. (1993)]. Given the high plateau modulus of this material (exceeding 10^7 Pa) we tentatively interpret this behavior as slip. Indeed, it is known that polymers with modulus of 10^6Pa (such as polybutadienes) or higher are prone to wall slip [Hatzikiriakos (2015)]. Therefore, the polymer can barely respond to shear and even at strains of just over 0.2 units it appears that it detaches from the plate of the rheometer (at least partly). This behavior is in contrast to the response of the same material in uniaxial extension (Figure 4.3) where in the absence of shear the material can deform but will eventually fracture at Hencky strains below 5 (see also Figure 4.8 below). Hence, our conclusion is that this brittle material cannot be sheared and the erratic behavior of Figure 4.7a is due to wall slip instabilities.

Remarkably, when we introduce 25% of PEO comonomer into the ionomer, the above picture alters substantially. This is shown in Figure 4.7b, where the transient shear stress is plotted against the accumulated strain. We note that much larger strains (by almost 2 decades) are achieved compared to pure PTMO-Na. More importantly, whereas at low strains (or early times up to about 0.3s) the transient stress data follow the LVE envelope, for higher strain we observe an overshoot, which becomes more evident as the shear rate increases. After the overshoot the stress approaches a steady state for 0.1 and 0.3 s^1, but this is not the case for the two higher shear rates. In the latter case the data suggest the influence of edge fracture, since the stress keeps on decreasing without evidence of steady state being approached [Snijkers and Vlassopoulos (2011)]. It is interesting to observe further that the stress overshoot occurs at strains between 2 and 3 for all rates; here, it is tempting to recall that entangled linear flexible polymers exhibit a peak strain value of about 2.3 at low rates due to orientation (the Doi-Edwards prediction), which increases eventually with shear rate due to stretching. Finally, the shear data corroborate the conclusions from the extensional data of Figure 4.3, where the same materials can deform (and eventually fracture) at higher Hencky strain compared to brittle PTMO-Na. Therefore, the overall picture is substantially different from that of Figure 4.7b. Clearly, the incorporation of ductile PEO makes the copolymer shear-processable. The latter can be appreciated in the comparative plot of Figure 4.7c.

Comparison of Nonlinear Shear and Extensional Rheology

We now compare the nonlinear rheological response of the PTMO-Na ionomer and the PEO25-PTMO75-Na coionomer under nonlinear shear and extensional deformations at identical conditions. This is shown in Figure 4.8, where the transient extensional stress growth coefficient and 3 times the stress growth coefficient are depicted as functions of time, along with the respective LVE envelope. The deformation rate is

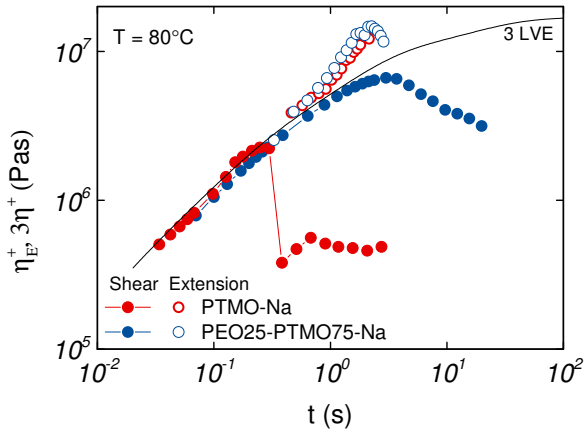

Figure 4.8: Comparison of PTMO-Na ionomer undergoing nonlinear shear and extension at $T = 80°C$ and rate of deformation fixed to $1s^1$.

fixed to $1s^1$ and the temperature is 80°C. Transient shear stress growth coefficient data (shown by closed symbols) are vertically shifted by a factor of 3 (Trouton ratio). In nonlinear shear flow, the PEO25-PTMO75-Na coionomer deforms up to the overshoot (at a strain of about 2.5 which can be considered as a yield strain), whereas the respective strain at which slip commences for PTMO-Na is about 0.3. We also observe the already discussed big difference in shear and extension for PTMO-Na. Whereas the brittle PTMO-Na ionomer cannot be sheared beyond $\gamma \cong 0.3$ and responds erratically, it deforms in extension, albeit weakly, and fractures at $\epsilon \cong 2$. The ductile PEO25-PTMO75-Na coionomer deforms uniformly to much larger strains in both shear and extension. Eventually, it fractures in extension at $\epsilon \cong 2.8$ and yields in shear at $\gamma \cong 2.5$ (subsequently being affected by edge fracture). The observation of fracture and the absence of steady state viscosity in transient shear and uniaxial extension highlights the difference in ionomer melts compared to entangled polymer melts. Ionic crosslinks lack the relaxation process and energy dissipation that is provided due to disentanglement of polymer chain by diffusional motion [Ling et al. (2012)].

4.4 Conclusions

In this study, the nonlinear shear and uniaxial extensional rheology of polyether-ester-sulfonate ionomers was investigated. The ionomers used in this study showed strain hardening at extension rates below the reciprocal of the sticker lifetime τ_s. The magnitude of strain hardening *decreased* as the Hencky strain rates approached $1/\tau_s$. Since the ionomers used in this study are unentangled, the strain hardening is attributed to the physical crosslinks which comprise ionic clusters. Despite significant elasticity of these ionomers, they fractured in a brittle fashion in extension. The high-

plateau modulus PTMO-Na exhibits a response akin to a brittle material: it fractures at low Hencky strains in extension and cannot be sheared homogeneously due to instabilities (predominantly wall slip). The effect of counterion on the extensional rheological response was also investigated by comparing PTMO-Na and PTMO-Li. Identical strain hardening and fracture showed that both Li and Na counterions have similar interaction with the sulphonate-group.

Further, the effects of 25% PEO addition on the extensional rheological properties was studied. Clearly, the coionomer is more ductile, as confirmed by its ability to deform more under both shear and extension. However, even the more ductile coionomer shows limits for how much it can deform. In uniaxial extension it always exhibits tensile fracture, while in shear flows it exhibits edge fracture at $\gamma \cong 2.5$. Results indicate that incorporating PEO comonomer into the PTMO-Na/Li ionomer increases the toughness of the material by increasing the maximum strain both in shear and extension.

The overall difference in nonlinear deformation and fracture between bulk PTMO and its PEO-based coionomer is attributed to the presence of PEO which makes the system more ductile. Since the PEO-rich domains offer better ion conduction, the coionomer has a better compromise between mechanical performance subject to large deformation and ion conduction.

4.5 Bibliography

Armand, M., Duclot, M., and Rigaud, P. (1981). Polymer solid electrolytes: stability domain. *Solid State Ion.*, 4:429–430.

Bach, A., Almdal, K., Rasmussen, H. K., and Hassager, O. (2003a). Elongational Viscosity of Narrow Molar Mass Distribution Polystyrene. *Macromolecules*, 36(14):5174–5179.

Bach, A., Rasmussen, H. K., and Hassager, O. (2003b). Extensional viscosity for polymer melts measured in the filament stretching rheometer. *J. Rheol.*, 47(2):429–441.

Buscall, R., McGowan, J. I., and MortonJones, A. J. (1993). The rheology of concentrated dispersions of weakly attracting colloidal particles with and without wall slip. *J. Rheol.*, 37(4).

Chassenieux, C., Tassin, J.-F., Gohy, J.-F., and Jerome, R. (2000). Elongation of Telechelic Ionomers under Shear : a Rheological and Rheo-optical Study. *Macromolecules*, 33:1796–1800.

Chen, Q., Masser, H., Shiau, H.-S., Liang, S., Runt, J., Painter, P. C., and Colby, R. H. (2014). Linear Viscoelasticity and Fourier Transform Infrared Spectroscopy of PolyetherEsterSulfonate Copolymer Ionomers. *Macromolecules*, 47(11):3635–3644.

Chen, Q., Tudryn, G. J., and Colby, R. H. (2013). Ionomer dynamics and the sticky Rouse model a). *J. Rheol.*, 16802(August):1441–1462.

Connelly, R. W., McConkey, R. C., Noonan, J. M., and Pearson, G. H. (1982). Melt rheology of ion-containing polymers. I. Effect of ionic content in a model polyesterionomer. *J. Polym. Sci. Part B: Polym. Phys.*, 20(2):259–268.

Doi, M. (1996). *Introduction to Polymer Physics*. Oxford University Press.

Gabriel, C. and Münstedt, H. (2003). Strain hardening of various polyolefins in uniaxial elongational flow. *J. Rheol.*, 47(3):619.

Hatzikiriakos, S. G. (2015). Slip mechanisms in complex fluid flows. *Soft Matter*, 11:7851–7856.

Lin, K.-J., Li, K., and Maranas, J. K. (2013). Differences between polymer/salt and single ion conductor solid polymer electrolytes. *R. Soc. Chem. Adv.*, 3(5):1564–1571.

Ling, G. H., Wang, Y., and Weiss, R. A. (2012). Linear Viscoelastic and Uniaxial Extensional Rheology of Alkali Metal Neutralized Sulfonated Oligostyrene Ionomer Melts. *Macromolecules*, 45:481–490.

Nishioka, A., Koda, T., Miyata, K., Murasawa, G., and Koyama, K. (2008). The Effects of Small Contents of Water on Melt Rheology for Ethylene-Methacrylic Zinc Ionomers. *Polym. J.*, 40(4):350–353.

Román Marín, J. M., Huusom, J. K., Alvarez, N. J., Huang, Q., Rasmussen, H. K., Bach, A., Skov, A. L., and Hassager, O. (2013). A control scheme for filament stretching rheometers with application to polymer melts. *J. Non-Newton. Fluid Mech.*, 194:14–22.

Schweizer, T. (2003). Comparing cone-partitioned plate and cone-standard plate shear rheometry of a polystyrene melt. *J. Rheol.*, 47(4).

Shabbir, A., Javakhishvili, I., Cerveny, S., Hvilsted, S., Skov, A. L., Hassager, O., and Alvarez, N. J. (2016). Linear viscoelastic and dielectric relaxation response of unentangled upy-based supramolecular networks. *Macromolecules*, 49(10):3899–3910.

Snijkers, F. and Vlassopoulos, D. (2011). Cone-partitioned-plate geometry for the ares rheometer with temperature control. *J. Rheol.*, 55(6):1167–1186.

Stadler, F. J., Pyckhout-Hintzen, W., Schumers, J.-M., Fustin, C.-A., Gohy, J.-F., and Bailly, C. (2009). Linear Viscoelastic Rheology of Moderately Entangled Telechelic Polybutadiene Temporary Networks. *Macromolecules*, 42(16):6181–6192.

Stadler, F. J., Still, T., Fytas, G., and Bailly, C. (2010). Elongational Rheology and Brillouin Light Scattering of Entangled Telechelic Polybutadiene Based Temporary Networks. *Macromolecules*, 43(18):7771–7778.

Takahashi, T., Watanabe, J., Minagawa, K., and Koyama, K. (1994). Effect of ionic interaction on elongational viscosity of ethylene-based ionomer melts. *Polymer*, 35(26):5722–5728.

Takahashi, T., Watanabe, J., Minagawa, K., Takimoto, J.-i., Iwakura, K., and Koyama, K. (1995). Effect of ionic interaction on linear and nonlinear viscoelastic properties of ethylene based ionomer melts. *Rheol. Acta*, 34(2):163–171.

Tierney, N. K. and Register, R. A. (2002). Ion Hopping in Ethylene - Methacrylic Acid Ionomer Melts As Probed by Rheometry and Cation Diffusion Measurements. *Macromolecules*, 35:2358–2364.

Tudryn, G. J., OReilly, M. V., Dou, S., King, D. R., Winey, K. I., Runt, J., and Colby, R. H. (2012). Molecular Mobility and Cation Conduction in PolyetherEsterSulfonate Copolymer Ionomers. *Macromolecules*, 45(9):3962–3973.

Vanhoorne, P. and Register, R. A. (1996). Low-Shear Melt Rheology of Partially-Neutralized Ethylene - Methacrylic Acid Ionomers. *Macromolecules*, 29:598–604.

Wang, Y., Agapov, A. L., Fan, F., Hong, K., Yu, X., Mays, J., and Sokolov, A. P. (2012). Decoupling of ionic transport from segmental relaxation in polymer electrolytes. *Phys. Rev. Lett.*, 108:088303.

Wang, Y., Fan, F., Agapov, A. L., Saito, T., Yang, J., Yu, X., Hong, K., Mays, J., and Sokolov, A. P. (2014). Examination of the fundamental relation between ionic transport and segmental relaxation in polymer electrolytes. *Polymer*, 55(16):4067 – 4076.

Weiss, R. a. and Yu, W.-C. (2007). Viscoelastic Behavior of Very Lightly Sulfonated Polystyrene Ionomers. *Macromolecules*, 40(10):3640–3643.

Weiss, R. a. and Zhao, H. (2009). Rheological behavior of oligomeric ionomers. *J. Rheol.*, 53(1):191–213.

Yan, Z.-C., Costanzo, S., Jeong, Y., Chang, T., and Vlassopoulos, D. (2016). Linear and nonlinear shear rheology of a marginally entangled ring polymer. *Macromolecules*, 49(4):1444–1453.

CHAPTER 5

Brittle fracture in associative polymers: the case of ionomer melts

5.1 Introduction

Viscoelastic fluids are complex materials with properties intermediate between a solid and a liquid. They behave as solid like on fast time scales and liquid like on slow time scales compared to the characteristic relaxation time [Ferry (1980)]. Fracture is expected at high deformation rates compared to the inverse of relaxation time of the material [Malkin and Petrie (1997)]. In solids this phenomenon is referred to as brittle fracture [Kausch (1978)]. Amongst viscoelastic fluids, associative polymeric systems including self-healing rubbers [Cordier et al. (2008)], and physical hydrogels [Baumberger et al. (2006)], have attracted the interest of researchers recently due to importance in processing and application as polymeric materials. Consequently, understanding fracture is important for tailoring such materials that are tougher and stronger for practical applications.

When a crack exists in a material, any external applied stress undergoes a large amplification at its tip [Bouchbinder et al. (2010)]. For linear elastic materials, the stress field close to an infinitely sharp line crack takes the form $\sigma \propto K/\sqrt{x}.f(\theta)$, where K is the stress intensity factor, x is the distance from the crack tip and $f(\theta)$ a function of the angle to the crack [Fischer-Cripps (2007); Bouchbinder et al. (2010)]. Displacement fields surrounding a crack tip (perpendicular to crack direction) predicts a parabolic crack tip opening $u \propto K.\sqrt{x}$ where x is the distance along the crack [Bouchbinder et al. (2010)]. For real materials, the stress singularity must be cut off to a finite value at least at the atomic scale, where it may or may not be large enough to snap bonds. Hence the prediction of a singular stress is itself insufficient to make a crack propagate. This lead to the early works of Griffith who provided a condition to determine whether the crack would propagate or not by noting that new surface must be created and that requires energy [Griffith (1921)]. On the other hand, fracture in viscoelastic materials has received less attention compared to solid materials. Modifications to Griffiths theory have been adapted to help understand fracture in viscoelastic

materials [Tabuteau et al. (2009); Skrzeszewska et al. (2010)].

Several groups have reported fracture in extensional deformation flow field for associative polymers [Bhardwaj et al. (2007); Tabuteau et al. (2011, 2009)]. Most of the work concerns either networks or solutions of worm-like micelles [Bhardwaj et al. (2007)]. Recently, Tabuteau et al. (2011) have studied fracture mechanisms of oil-in water emulsions linked by telechelic polymers using pendant drop experiments. More recently, Huang et al. (2016) have reported an experimental framework capable of quantifying time resolved crack propagation together with true stress measurements and applied this for linear homo-polymer melts. We use this framework to perform fracture experiments for ionomers at different viscoelastic regimes by employing different temperatures and strain rates.

Ionomers represent a family of polymers where ionic groups are covalently attached to the polymer backbone [Vanhoorne and Register (1996)]. Due to strong dipolar interactions, the ionic groups have a tendency to associate into ionic clusters [Tierney and Register (2002)]. These ionic clusters act as temporary crosslinks and restrict the motion of polymer chains thus leading to a delay in stress relaxation relative to the nonionic polymer. The terminal response of ionomers is governed by an association lifetime,τ_s, which is the average time for an ion pair to reside in the ionic cluster before its dissociation. The disassociated pair can associate back to its original cluster or randomly move to a nearby cluster: the later process leads to stress relaxation of the portion of chains between the ionic associations [Chen et al. (2013)]. Ionomers fracture in a brittle fashion under extensional deformation flow fields [Ling et al. (2012); Stadler et al. (2010)]. Although some work has been conducted to understand the fracture of ionomers, it has primarily focused on deformation and fracture below the glass transition temperature [Hara and Jar (1988); Hara et al. (1992)]. Fracture in the rubbery and flow states of ionomers has not been investigated at all. In the light of applications of ionomers as materials for toughening systems, coating and adhesives, batteries, and their importance in processing, it is surprising that no study has considered the fracture mechanisms from either theoretical or experimental perspectives [Zhang et al. (2014)].

We provide an experimental framework to investigate fracture mechanism of ionomer melts studied in Chapter 4. More specifically PTMO-Na ionomer is chosen for fracture study. This system provides an excellent model associative polymer melt (unentangled) where ionic associations attached to the polymer backbone act as physical crosslinks thus giving rich viscoelastic properties. The linear rheological response of the material resembles that of a well entangled polymer melt with a discernible plateau modulus. Despite being viscoelastic the material exhibits brittle fracture. Using a state of the art filament stretch rheometer coupled with high speed imaging camera, we demonstrate that the ionomer filaments rupture via edge fracture. Analysis of fracture profiles provide evidence that bulk viscous dissipation is minimal during the fracture event and has little impact on the crack profile. Results are in accordance with viscoelastic trumpet model of de Gennes [de Gennes (1996)]. Crack propagation velocities are quantified and compared to the speed of a shear wave in the medium [Bird et al. (1987)]. We employ Griffith's theory using Pomeau's criterion

[Pomeau (1992)] which reasons that the energy barrier to achieve crack growth can be overcome by thermal fluctuations. This allows for an estimation of the fracture energy needed to create two new air/polymer surfaces (dry fracture), which is found to be comparable to the surface tension of the ionomer. The use of Pomeau's criterion for such transient systems depends on the association/disassociation kinetics of temporary crosslinks (stickers) compared to the experimental time scales. When the average sticker lifetime, τ_s, is shorter than the experimental time scale, Pomeau's criterion is readily applicable. However, when the average sticker lifetime is much larger than the experimental time scale the material acts as a non-self-healing material within the experimental window and fractures. The driving force for fracture is not the thermal energy, and the origins of the problem become solid mechanics related. Finally, we examine the extensional rheological response over a wide range of flow rates to provide a rationale for understanding the nature of fracture for ionomer melts under uni-axial extensional flows.

5.2 Materials and Methods

Description of the ionomer melt

Amorphous polyester ionomer synthesized via condensation of sulfonated phtalates with poly(tetramethylene glycol) having $M = 650 g/mol$ with Na as the counterion was provided by [Chen et al. (2013)]. PTMO-Na ionomer exhibits microdomain separation as confirmed by X-ray scattering whereby Na^+ form dense aggregates with of the order of 15 ion pairs. The PTMO-Na ionomer exhibits glass transition temperature, $T_g = -60°C$ [Chen et al. (2014)].

Rheological experiments

The extensional stress growth coefficient as a function of time was measured using the VADER 1000 (Versatile accurate deformation extensional rheometer) from Rheo Filament ApS. Cylindrical stainless steel plates with a diameter of 5.4 mm were used for all measurements. The Hencky strain in the mid-filament is defined as $\epsilon = -2\ln(D(t)/D_0)$, where D_0 is the initial diameter. The diameter is measured by a laser micrometer during stretching and a control loop [Román Marín et al. (2013)] is used to adjust the plate motion to ensure a constant Hencky strain rate defined as $\dot{\epsilon} = d\epsilon/dt$. Samples were heated under nitrogen for 2 hours at 120°C prior to performing experiments. At such a temperature the ionomer flows easily and forms a nice axisymmetric shape when the top rheometer plate is brought in contact with the sample. All experiments were performed in a nitrogen controlled environment.

Fracture experiments

Fracture experiments were performed using a high speed camera Photron Mini UX100 with a Navitar Zoom6000 lens coupled with VADER 1000 operating in an open loop

control scheme configuration (at 60°C and 80°C). The imposed stretch rate was 1 s^{-1} (see open orange circles in Fig.5.7). The feedforward control parameters [Román Marín et al. (2013)]. which define the kinematic trajectory of the top plate motor were obtained by performing constant rate experiments on the VADER in a control loop scheme with an active feedback control and without coupling high speed camera. Only after that, VADER was coupled with the high speed camera to perform fracture experiments. Operating the VADER in open loop ensures avoiding interference between the laser micrometer and the light emitted from the illuminator used for the camera. Since the crack can nucleate and propagate in any direction of the filament surface, around 40 experiments were performed in order to capture crack propagation profiles orthogonal to the camera lens for the experimental data analysis.

5.3 Results

Shear rheology results were obtained from previous studies on PTMO-Na ionomer melts [Chen et al. (2014, 2013)].

Linear viscoelastic (LVE) response as shown in Fig.5.1a, resembles that of a well entangled polymer melt with a distinct plateau modulus. Since the PTMO-Na is unentangled, the plateau modulus, G_N^0, results from the ionic cluster density and is approximately 10^7 Pa. Polydispersity in molecular weight leads to a broadening in the lower crossover frequency because of a distribution in the number of polymer modes each associated with a contribution to the moduli [Chen et al. (2013); Shabbir et al. (2016)]. The PTMO-Na ionomers used in this study are polydisperse (*polydispersity* $\approx$ 2.0), they exhibit terminal tails (slope of 1 and 2 for loss modulus $G^{''}$ and storage modulus $G^{'}$, respectively) at low frequency, ω. The terminal relaxation time can be determined as,

$$\tau = \lim_{\omega \to 0} \left[\frac{G^{'}}{\omega G^{''}} \right] \tag{5.1}$$

The association lifetime can thus be obtained as [Chen et al. (2014)],

$$\tau_s = \frac{\tau}{N_s^2} \tag{5.2}$$

where $N_s = 7$ [Chen et al. (2013, 2014)] is the number of sticky Rouse segments per chain. Arrows in Fig.5.1 are indicative of association lifetime at the respective temperatures. Incidentally association lifetime is close to the maxima in loss moduli.

Extensional rheological response of the PTMO-Na ionomer is shown in Fig.5.1b. It shows the transient stress growth coefficient, η_E^+, as a function of time for fixed strain rate, $\dot{\epsilon} = 1\, s^{-1}$, at two different temperatures, 60 °C and 80 °C. The LVE envelope obtained using a multimode Maxwell fit from LVE oscillatory shear data is plotted as solid lines. The extensional data are seen to be consistent with the predictions of linear viscoelasticity. The inset shows transient extensional stress, σ_E^+, as a function

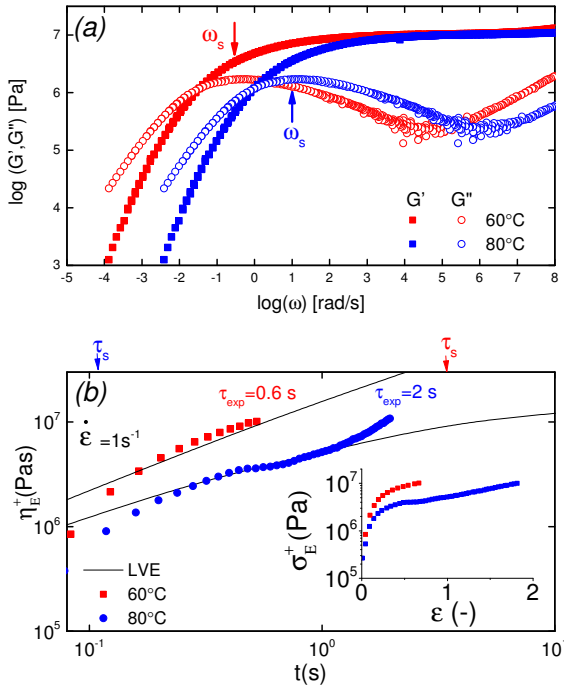

Figure 5.1: (a) LVE master curves of the PTMO-Na ionomer at $T_{ref} = 60°C$ and $T_{ref} = 80°C$ [Chen et al. (2013, 2014)] (b) Stress growth coefficient as a function of time at Hencky rate, $\dot{\epsilon} = 1\,s^{-1}$, for PTMO-Na at 60°C, and 80°C. The inset plot shows transient extensional stress as a function of Hencky strain. Solid lines represent the LVE envelope.

of Hencky strain, ϵ. The end of each experiment represents brittle fracture of the PTMO-Na filament. From Fig.5.1b, it is interesting to note the temperature dependent extensional rheological response. At $T = 60°C$, the experimental time scale is smaller compared to association lifetime, τ_s, and the material fractures at relatively lower Hencky strain without showing any departure from the LVE envelope (often termed as strain hardening). By contrast, at $T = 80°C$, the experimental time scale exceeds association lifetime, τ_s, and a noticeable strain hardening is observed before brittle fracture. From the inset, it is evident that the material fractures at the same level of stress 10^7 Pa which corresponds to the shear plateau modulus, G_N^0.

A complete evolution of the PTMO-Na ionomer filament at a Hencky strain rate, $\dot{\epsilon} = 1\,s^{-1}$ and $T = 60°C$ during extensional deformation is shown in Fig.5.2. During extensional deformation, a notch appears from the right edge of the filament orthogonal to the camera lens 0.32 ms before it fractures into two halves. Close inspection of the images reveals multiple cracks initially, but the crack shown in the

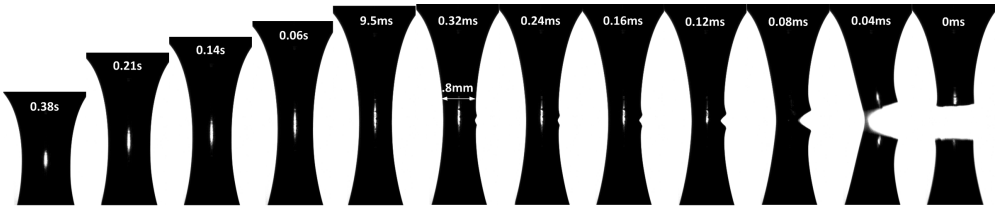

Figure 5.2: Sequence of images of PTMO-Na ionomer filament undergoing uniaxial extensional deformation at a constant Hencky strain rate, $\dot{\epsilon} = 1\,s^{-1}(Wi = 3)$ and $T = 60$ °C. The time specified is the time remaining to achieve complete brittle fracture of the filament.

picture prevails over the other cracks as can been seen in Fig. 5.3

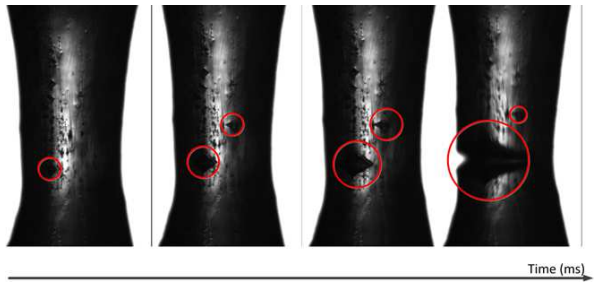

Figure 5.3: Sequence of images showing multiple cracks during stretching of PTMO-Na filament

The sequence of images demonstrates the decoupling of time scale associated with extensional deformation (of the order of seconds) from the fracture event time which is of the order of *ms*. The crack propagation at $T = 80$°C is shown in Fig. 5.4.

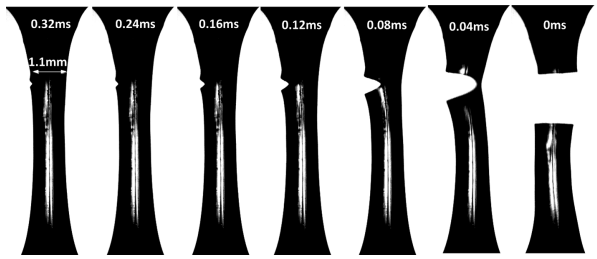

Figure 5.4: Crack propagation of PTMO-Na ionomer at $T = 80$°C, and $\dot{\epsilon} = 1\,s^{-1}$

In both cases, the fracture profile exhibits a parabolic shape from the beginning of crack propagation to complete fracture of the filament into two halves. This is an

attribute associated with fracture of solids under tension [Griffith (1921)]. It is worth mentioning that the position of fracture along the filament axis is completely random. This observation may indicate the stochastic nature of reversible microcracks. A microcrack corresponds to a domain across which there is no connection of polymer chains between crosslinks.

A quantitative analysis of fracture profiles is shown in Fig.5.5. Fig.5.5a, b shows fracture profiles (shifted to have the same crack tip position) at each moving frame with time spacing of 0.04 ms (corresponds to frame rate= 25000 fps). The overall fracture profile can be fit using an equation for a parabola $u(x) = a\sqrt{x}$, where a is a constant adjusted to fit the parabolic profile. The parabolic fit is shown in solid line. The fitting constant a, which is an indirect representation of amount of crack opening is higher for $T = 60$ °C compared to $T = 80$ °C.

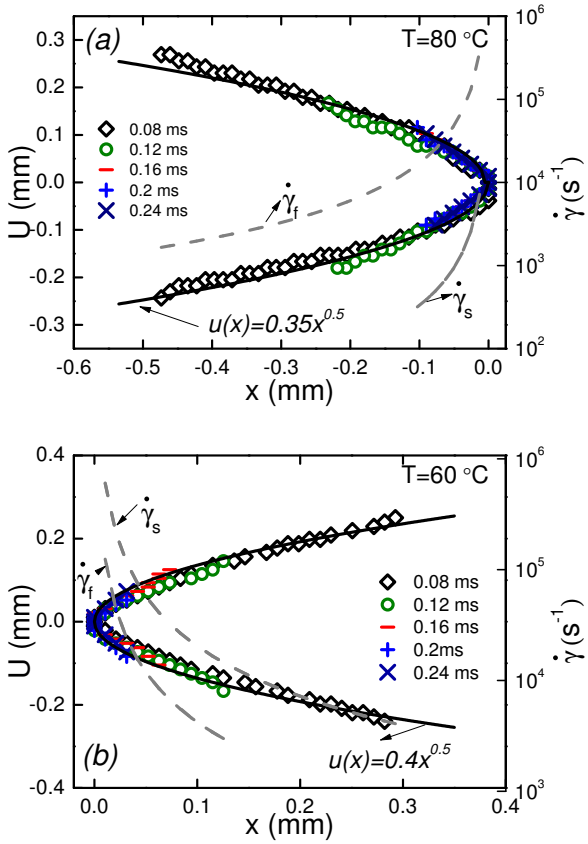

Figure 5.5: Fracture profiles $u(x)$ in the moving frame at different times before complete fracture of the filament at $T = 60$ °C, and $T = 80$ °C.

Crack length as a function of remaining time for the filament to disconnect into two halves is shown in Fig.5.6 at $T = 60\ ^{\circ}\mathrm{C}$, and $T = 80\ ^{\circ}\mathrm{C}$. We use the diameter of the filament just before opening of the crack, D, as the reference to define the crack length L from the crack tip. The velocity of the crack, V, is obtained from the slope of the plot. Two velocity regimes are evident:

i For $L < 0.05D$, a slow velocity regime, V_s, is noticed where the crack moves at almost $V = 0.1\ m/s$.

ii For $L > 0.05D$, a fast velocity regime, V_f, is observed in which the crack propagates dynamically at almost $V = 9.5\ m/s$.

The crack velocities are almost independent of temperature. An increase in crack velocity during crack propagation is to be expected because the stresses near the tip will increase thus driving faster crack growth. In addition, we speculate that in the slow velocity regime, multiple cracks shield one another from the external applied stress whereby they all propagate slowly together [Bowie (1973)], while in the fast velocity regime the leading crack takes off alone. While cracks achieve quite large velocities particularly close to complete fracture, the highest velocities are still an order of magnitude smaller than the elastic shear wave velocity for an incompressible material ($c_R \approx (|G^*|/\rho)^{1/2} = 96 m/s$), where ρ is the density and $|G^*| = (G^{'2} + G^{''2})^{1/2}$ is the absolute value of complex modulus [Bird et al. (1987)]. Slow crack velocities compared to shear wave velocity have been reported previously for non-associative polymers [Tabuteau et al. (2011); Baumberger et al. (2006); Persson (1998)]. What is different here compared to other reversible systems like gelatin [Baumberger et al. (2006)] and gels made from oil-in-water droplet emulsions bridged by telechelic polymers [Tabuteau et al. (2011)] is the absence of solvent drag. As a consequence the crack propagation velocities are in the range of 1-2 orders of magnitude faster compared to those in solvent containing reversible networks. It should be mentioned that the quantification of crack velocity was made assuming a 2D symmetry of the crack front and that the crack front is flat.

5.4 Discussion

It was noted above that the shape of the fracture profile was parabolic which is indicative of elastic like behavior. To provide a rationale of such a behavior of PTMO-Na ionomer during fracture, the viscoelastic trumpet model of de Gennes is employed [de Gennes (1996, 1988); Saulnier. et al. (2004)] This model demonstrates through scaling laws, the shape of the crack depends upon a characteristic relaxation time, τ, and crack propagation velocity, V. For a viscoelastic material, during crack propagation a transition from solid to liquid like response can be distinguished,

i $L \leq V\tau$: A strong elastic response is noticed and the viscous dissipation is negligible. For this case, $\sigma = G^{'} \frac{du}{dx} \sim Kx^{-1/2}$ yields

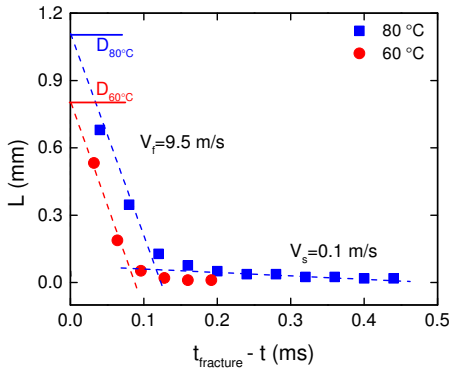

Figure 5.6: Variation of crack length as a function of time remaining for complete fracture of the filament at $T = 60$ °C, and $T = 80$ °C.

$$u(x) \sim K/G^{'} x^{1/2} \tag{5.3}$$

ii $L > V\tau$: In this region the modulus is purely imaginary and a Newtonian liquid response is expected. This region contributes to the bulk viscoelastic dissipation processes. For this case, $\sigma = \eta \frac{d}{dx}\frac{du}{dt} = \eta V \frac{d^2u}{dx^2} \sim Kx^{-1/2}$ yields

$$u(x) \sim (K/\eta V)x^{3/2} \tag{5.4}$$

If we define $\tau = \tau_s$, then the characteristic length scale, $V\tau$, for PTMO-Na ionomer is 10 mm and 300 mm at $T = 80$ °C, and $T = 60$ °C, respectively. Since the fracture length $L_{max} = D \sim 0.8 - 1.1$ mm, a purely elastic response is expected with the fracture profile given by a classical parabolic shape using Eq. (5.4).

During crack propagation, the local shear rate, $\dot{\gamma}$, experienced at the crack surface is high near the fracture tip, and lowers as the distance x to the tip increases because the material has time to relax the stresses [Saulnier. et al. (2004)]. We may thus define a relationship for $\dot{\gamma}$ as a function of distance x to the tip. For an elastic material, the local shear strain, γ, is defined as

$$\gamma = \frac{du}{dx} = \frac{1}{2}ax^{-1/2} \tag{5.5}$$

the local shear rate, $\dot{\gamma}$, during crack propagation is then given simply

$$\dot{\gamma} = \left|\frac{d}{dt}\gamma\right| = \frac{dx}{dt}\frac{d\gamma}{dx} = V\frac{d^2u}{dx^2} = V\frac{a}{4}x^{-3/2} \tag{5.6}$$

The local shear rates during crack propagation are plotted in Fig.5.5a, b as dashed lines. The shear rate, $\dot{\gamma}_s$, corresponds to the slow velocity regime ($V = 0.1\ m/s$) while shear rate, $\dot{\gamma}_f$, corresponds to the fast velocity regime ($V = 9.5\ m/s$).

A remarkable elastic recoil of the filament or strain recovery, defined as $r =$ (fracture strain-recovered strain)/(fracture strain-initial strain), of about 92% and 72% at $T = 60°$C and $T = 80°$C, respectively after fracture was noticed. This observation and that the fracture profile exhibits parabolic shape provide motivation to analyze data using Griffith's theory of brittle fracture [Griffith (1921)]. According to this theory, a surface energy, F_s, is required for the creation of free surface within the body counterbalanced by the bulk elastic energy released because of unloading of the newly created surface. Tabuteau et al. (2009) consider a disk-like crack for radius R. They state the energy to be,

$$W = \frac{\pi}{2}R^2F_s - \alpha\frac{\pi R^3}{3}\left(\frac{\sigma^2}{2Y}\right) \tag{5.7}$$

where $\alpha \simeq 1$ is constant depending on geometrical factors, R is the size of crack, and $Y = 3G_N^0$ is the Young modulus. However, there is one key difference to the situation for solids that are believed to contain a spectrum of micro-cracks. These may be the result of the fabrication process and will have a size distribution. As the stress increases, the crack size reaches the critical value, R_c, at which the crack begins to catastrophically grow leading to fracture. Mathematically, at this critical length, $dW/dR = 0$ which gives,

$$R_c = 2F_sY/\sigma^2 \tag{5.8}$$

The term $\sigma^2/2Y$ in Eq.(5.7), represents the elastic energy density, E, that may be released by the fracture opening. Since we have measured the stress as function of strain we prefer to use measurements to calculate this quantity directly in the form,

$$E = \frac{1}{V}\int f dx = \int \frac{f}{A}\frac{dx}{L} = \int_0^{\epsilon_c}(\sigma_{zz} - \sigma_{rr})d\epsilon \tag{5.9}$$

Only a fraction, r, of this energy is available for opening of the crack since part of the energy will be dissipated. We take, r, to be the percentage of strain recovery. We therefore replace $\sigma^2/2Y$ by rE.

The modified energy expression yields,

$$W = \frac{\pi}{2}R^2F_s - \frac{\pi}{3}rER^3 \tag{5.10}$$

Likewise, Eq.(5.8) is modified as $R_c = F_s/rE$ which may be substituted in the modified energy expression to obtain the critical energy,

$$W_c = \frac{\pi F_s^3}{6(rE)^2} \tag{5.11}$$

The critical energy derived above represents an energy barrier which can be overcome either by existing cracks of length, R_c, or by thermal fluctuations. The latter scenario would correspond to self-healing materials where the transient nature of physical crosslinks causes the crack length to reversibly increase. Microcracks in

self-healing materials always exist because of thermal energy fluctuations [Tabuteau et al. (2009)]. Recall that a microcrack is a domain without polymers connecting physical crosslinks. A crack can reversibly explore states with different crack lengths between the initial and critical ones [Ligoure and Mora (2013)]. For self-healing materials, we may thus assume that the critical energy can be overcome by thermal fluctuations as suggested by Pomeau (1992) which implies,

$$W_c = \beta k_B T \tag{5.12}$$

where β represents the height of energy barrier in units of $k_B T$. Comparison of Eq.(5.11) and Eq.(5.12) yields the expression for surface energy as,

$$F_s = (6/\pi\beta k_B T(rE)^2)^{1/3} \tag{5.13}$$

Recall from Fig.5.1b, the comparison of average sticker lifetime with the experimental time scale, τ_{exp} during out constant rate experiment. Clearly, the notion of self-healing works well for PTMO-Na ionomer at $T = 80$ °C since $\tau_s << \tau_{exp}$. In other words, the kinetics of association/dissociation is faster than experimental time scale. The activation energy barrier can be overcome by thermal fluctuations. From previous works [Chen et al. (2013)], the activation energy is approximated to be $E_a = 20 k_B T$ at $T = 80$ °C for the PTMO-Na ionomer. Plugging $\beta = 20$ in Eq.(5.13) yields $F_s = 20 mJ/m^2$ which is comparable to the surface tension estimated at $T = 80$ °C using a group contribution method [Quayle (1953a)] as describe below.

Parchors signifies a function of chemical composition and is a useful means of estimating surface tension [Agrawal (2005)]. It can be represented by the following formula:

$$\gamma = \Big(\frac{P_s}{V}\Big)^4 \tag{5.14}$$

where γ is surface tension, P_s represent additive group contribution values and V is the molar volume [Quayle (1953b)]. For PTMO-Na ionomer $P_s \approx 2004.8$ $(cm^3/mol)(erg/cm^2)^{1/4}$ as,

$P_s = 44 \times C + 75 \times H + 15 \times O + 1 \times S + 1 \times Na + 5 \times doublebond$

$P_s = 44 \times 9 + 75 \times 15.5 + 15 \times 19.8 + 1 \times 49.1 + 1 \times 54.8 + 5 \times 17$

$\rho \sim 0.994\ g/cm^3$ [Chen et al. (2013)] at $T = 20$°C which gives value of molar volume $V = M/\rho = 903.4\ cm^3/mol$ for molar mass $M = 898\ g/mol$. Temperature dependence of surface tension is obtained using the following formula:

$$\gamma = \rho(293)\Big(\frac{\rho(T)}{\rho(293)}\Big)^4 \tag{5.15}$$

The situation is slightly different at $T = 60$ °C where Fig.5.1b shows that $\tau_s >> \tau_{exp}$. In other words, kinetics of association/dissociation is slower than the experimental time scale. Although under equilibrium conditions, the material is still self-healing

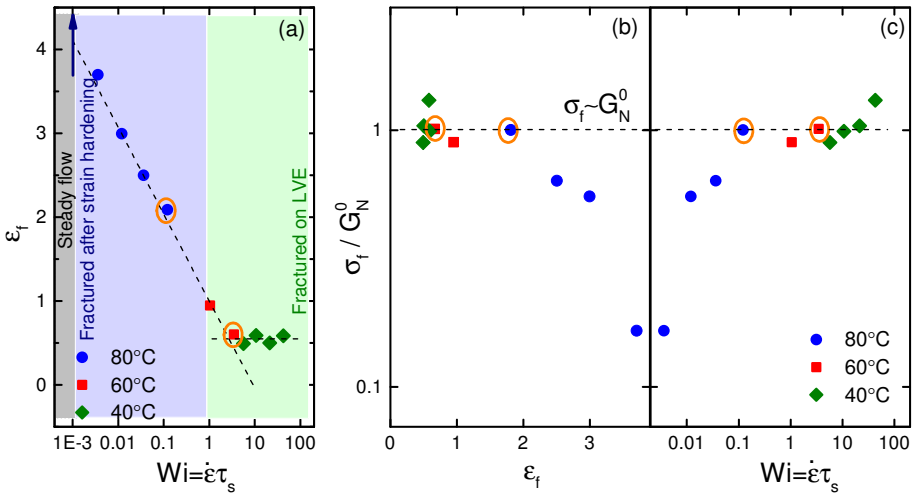

Figure 5.7: (a) Hencky strain at fracture, ϵ_f, as a function of, Wi, blue arrow shows measurement where a steady state in η_E was achieved. Orange circles point out measurements for which the time resolved study of fracture was carried out in the results section, (b) Fracture envelope: normalized fracture stress, σ_f / G_N^0, vs. Hencky strain at fracture over a range of temperatures, (c) Normalized fracture stress as a function of Wi. Dashed lines are to guide the eye.

at $T = 60$ °C, it is viewed as a non-self-healing material on the experimental time scale. To simplify, defects in the network (due to thermal fluctuations) exist under equilibrium conditions, but these pre-existing cracks cannot explore different crack lengths between the initial and the critical ones during the experimental time scale. Henceforth, use of Eq.(5.12) is questionable. We speculate that at low temperatures mechanical pullout of chains from the ionic clusters leads to fracture but at the moment this still remains to be proven. So far we have only focused on two temperatures and one strain rate in Fig.5.1b. In order to probe a broader range of nonlinearity, we define a non-dimensional number called the Weissenberg number based on the average sticker lifetime as $Wi = \dot{\epsilon}\tau_s$. Fig.5.7a shows strain rate dependence of Hencky strain at fracture, ϵ_f. A monotonic decrease in the Hencky strain at fracture is noticed for $Wi < 1$. However, for $Wi > 1$ fracture strain is independent of Wi, and attains a constant value of ≈ 0.6. For $Wi \geq 1$, ionic crosslinks can be thought of as permanent junctions making the material elastic like. Note that for very low Weissenberg numbers, Newtonian behavior is seen with a steady state in η_E. The filament does not fracture in this regime and the ordinate of Fig.5.7a approaches infinity theoretically. Fig.5.7b shows non-dimensional extensional stress at fracture , σ_f / G_N^0, vs. Hencky strain at fracture over a range of temperatures. Such a plot has been referred to as the 'fracture envelope'[Kausch (1978); Smith (1964)]. Exploring this plot is vital to understand the underlying fracture mechanisms. Two different regimes are evident.

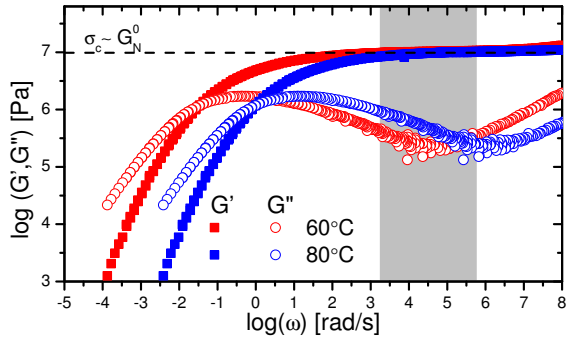

Figure 5.8: LVE master curves of PTMO-Na ionomer at $T_{ref} = 60°C$ and $T_{ref} = 80°C$ [Chen et al. (2013, 2014)]. The grey region highlights the local shear rates in Fig. 5.5 which are in the midst of the rubbery plateau, where the material behaves like a crosslinked network. The local shear rates during fracture were obtained using Eq.(5.6).

At high temperatures, the stress at fracture increases with increasing extension rate until $\sigma_f \simeq G_N^0$. At low temperatures, filaments fracture at a given critical stress $\sigma_f \simeq G_N^0$ independent of extension rate.

Finally, recall the local shear rates that were calculated in the results section (Fig. 5.5a, b). These shear rates are mapped on the LVE as shown in Fig. 5.8. The local shear rates close to the crack surface are 3 orders of magnitude higher than the strain rate imposed during uni-axial extension. It is evident that in the frequency regime which corresponds to the local shear rates during crack propagation (grey region in Fig. 5.8), the storage component dominates the loss component of complex modulus ($G' >> G''$). This is consistent with the finding that the crack profile follows the elastic part ($u(x) = a\sqrt{x}$) of the de Gennes trumpet model. Furthermore, from Fig. 5.8 it is evident that the critical stress observed in uni-axial extension is comparable to the storage modulus ($10^7 Pa$) of the sample in the LVE regime which is also the critical tensile stress of the material as discussed before. A comparison of fracture in ionomer melts with recently published work by Huang et al. (2016) on entangled polymer melts highlights key differences. A significantly low crack propagation speed of $2mm/s$ suggests higher dissipation in entangled PS melts. Shear rates across the fracture surface in their work correspond to frequencies where ($G'' > G'$). Consequently, much of the fracture profile is represented by viscous regime with scaling of $\sim x^{-3/2}$. Critical stress at fracture in polymer melts is orders of magnitude higher than the plateau modulus suggesting higher chain stretch in entangled polymer melts. A commonality between the current study on ionomer melts and the work by [Huang et al. (2016)] is the applicability Pomeau's ideas within a certain Wi.

5.5 Conclusions

In this study, we have demonstrated an original experimental framework to study fracture of one class of associative polymer melts called ionomers, using a high speed camera coupled with filament stretch rheometer under a constant strain rate deformation. The configuration allows for an excellent decoupling of extensional deformation from the fracture event.

It was shown that ionomers fail in a brittle fashion by edge fracture. Fracture profiles exhibit a parabolic shape which is indicative of solid like behavior. The absence of any significant bulk viscous dissipation was justified using the de Gennes viscoelastic trumpet model whereby the length of crack was smaller than the characteristic length $V\tau_s$, beyond which the viscous effects dominate. Quantification of crack propagation velocities showed that although these were not inertia limited, yet they were between one and three orders of magnitude slower compared to speed of shear waves in the material. Crack velocities were also insensitive to temperature variations. By combining fracture mechanics analysis (based on Pomeau's criterion) with constant rate uni-axial rheology, a common consensus was brought forward to understand the mechanism of fracture at different Wi. Two regimes corresponding to different fracture mechanisms were observed. For $Wi < 1$, defects originating from thermal density fluctuations can explore states with different crack lengths between the initial and critical ones thus overcoming the energy barrier. Fracture energy needed to create two new air/polymer surfaces in such a scenario corresponded to the surface tension of the material. Noticeable strain hardening was observed in this regime. On the other hand for $Wi \geq 1$, the pre-existing cracks due to thermal fluctuations cannot explore different crack lengths between the initial and the critical ones within the experimental time scale. Therefore, although these microcracks present the source for the crack nucleation, the driving force is not thermal energy. Classical Griffith's theory is applicable here to explain the crack propagation. No strain hardening was observed in this regime and the material fractured on the LVE envelope. We have speculated mechanical pullout of chains from the ionic clusters to be the reason for brittle fracture in this regime.

Given that the measured fracture speeds are between one and three orders of magnitude smaller than the shear wave speed, we conclude that some molecular dissipation process must be involved in setting the speed. However the precise nature of this process is not clear at present. It could of course be the same process that contributes to the loss modulus in the identified frequency range of the linear viscoelastic modulus (grey area in Fig.5.8). However it could also be some non-linear process near the fracture tip, where the linear analysis predicts a stress singularity and non-linear analysis will be needed ultimately. Related to this, the reason for the marked change of crack velocity by almost a factor of 100 is in our opinion also not fully resolved. We have offered a speculation in terms of crack competition, but other physical processes may be involved and more analysis will certainly be needed for a fully satisfactory explanation.

5.6 Bibliography

Agrawal, A. (2005). Surface tension of polymers.

Baumberger, T., Caroli, C., and Martina, D. (2006). Solvent control of crack dynamics in a reversible hydrogel. *Nat. Mater*, 5:552–555.

Bhardwaj, A., Miller, E., and Rothstein, J. P. (2007). Filament stretching and capillary breakup extensional rheometry measurements of viscoelastic wormlike micelle solutions. *J. Rheol.*, 51(4):693–719.

Bird, B., Armstrong, R. C., and Hassager, O. (1987). *Dynamics of Polymeric Liquids*. Wiley, New York.

Bouchbinder, E., Fineberg, J., and Marder, M. (2010). Dynamics of simple cracks. *Annual Review of Condensed Matter Physics*, 1(1):371–395.

Bowie, O. L. (1973). *Solutions of plane crack problems by mapping technique*, pages 1–55. Springer Netherlands, Dordrecht.

Chen, Q., Masser, H., Shiau, H.-S., Liang, S., Runt, J., Painter, P. C., and Colby, R. H. (2014). Linear Viscoelasticity and Fourier Transform Infrared Spectroscopy of PolyetherEsterSulfonate Copolymer Ionomers. *Macromolecules*, 47(11):3635–3644.

Chen, Q., Tudryn, G. J., and Colby, R. H. (2013). Ionomer dynamics and the sticky Rouse model a). *J. Rheol.*, 57(August):1441–1462.

Cordier, P., Tournilhac, F., Soulié-Ziakovic, C., and Leibler, L. (2008). Self-healing and thermoreversible rubber from supramolecular assembly. *Nature*, 451(7181):977–80.

de Gennes, P. G. (1988). *CR Acad. Sci. Paris Ser. II*, 307:1949.

de Gennes, P. G. (1996). Soft adhesives. *Langmuir*, 12(19):4497–4500.

Ferry, J. D. (1980). *Viscoelastic Properties of Polymers*. Wiley, New York.

Fischer-Cripps, A. C. (2007). *Introduction to Contact Mechanics*. Springer US.

Griffith, A. A. (1921). The phenomena of rupture and flow in solids. *Phil. Trans. R. Soc. A*, 221(582-593):163–198.

Hara, M., Bellinger, M., and Sauer, J. (1992). Deformation and fracture behavior of polystyrene ionomer and ionomer blends. *Colloid Polym. Sci.*, 270(7):652–658.

Hara, M. and Jar, P. Y. (1988). Deformation and fracture of ionomers under simple tension. 1. sulfonated polystyrene film from thf solution. *Macromolecules*, 21(11):3187–3190.

Huang, Q., Alvarez, N. J., Shabbir, A., and Hassager, O. (2016). Multiple cracks propagate simultaneously in polymer liquids in tension. *Phys. Rev. Lett.*, 117:087801.

Kausch, H. (1978). *Polymer Fracture*. Springer-Verlag Berlin Heidelberg.

Ligoure, C. and Mora, S. (2013). Fractures in complex fluids: the case of transient networks. *Rheol. Acta*, 52(2):91–114.

Ling, G. H., Wang, Y., and Weiss, R. A. (2012). Linear Viscoelastic and Uniaxial Extensional Rheology of Alkali Metal Neutralized Sulfonated Oligostyrene Ionomer Melts. *Macromolecules*, 45:481–490.

Malkin, A. Y. and Petrie, C. J. S. (1997). Some conditions for rupture of polymer liquids in extension. *J. Rheol.*, 41(1):1–25.

Persson, B. N. J. (1998). Model study of brittle fracture of polymers. *Phys. Rev. Lett.*, 81:3439–3442.

Pomeau, Y. (1992). *CR Acad. Sci. Paris Ser. II*, 314:553.

Quayle, O. R. (1953a). The parachors of organic compounds. an interpretation and catalogue. *Chem. Rev.*, 53(3):439–589.

Quayle, O. R. (1953b). The parachors of organic compounds. an interpretation and catalogue. *Chem. Rev.*, 53(3):439–589.

Román Marín, J. M., Huusom, J. K. b., Alvarez, N. J., Huang, Q., Rasmussen, H. K., Bach, A., Skov, A. L., and Hassager, O. (2013). A control scheme for filament stretching rheometers with application to polymer melts. *J. Non-Newtonian Fluid Mech.*, 194:14–22.

Saulnier., F., Ondaruhu., T., Aradian., A., and Raphal., E. (2004). Adhesion between a viscoelastic material and a solid surface. *Macromolecules*, 37(3):1067–1075.

Shabbir, A., Javakhishvili, I., Cerveny, S., Hvilsted, S., Skov, A. L., Hassager, O., and Alvarez, N. J. (2016). Linear viscoelastic and dielectric relaxation response of unentangled upy-based supramolecular networks. *Macromolecules*, 49(10):3899–3910.

Skrzeszewska, P. J., Sprakel, J., de Wolf, F. A., Fokkink, R., Stuart, M. A. C., and van der Gucht, J. (2010). Fracture and self-healing in a well-defined self-assembled polymer network. *Macromolecules*, 43(7):3542–3548.

Smith, T. L. (1964). Ultimate tensile properties of elastomers. ii. comparison of failure envelopes for unfilled vulcanizates. *J. Appl. Phys.*, 35(1):27–36.

Stadler, F. J., Still, T., Fytas, G., and Bailly, C. (2010). Elongational Rheology and Brillouin Light Scattering of Entangled Telechelic Polybutadiene Based Temporary Networks. *Macromolecules*, 43(18):7771–7778.

Tabuteau, H., Mora, S., Ciccotti, M., Hui, C.-Y., and Ligoure, C. (2011). Propagation of a brittle fracture in a viscoelastic fluid. *Soft Matter*, 7:9474–9483.

Tabuteau, H., Mora, S., Porte, G., Abkarian, M., and Ligoure, C. (2009). Microscopic mechanisms of the brittleness of viscoelastic fluids. *Phys. Rev. Lett.*, 102:155501.

Tierney, N. K. and Register, R. A. (2002). Ion Hopping in Ethylene - Methacrylic Acid Ionomer Melts As Probed by Rheometry and Cation Diffusion Measurements. *Macromolecules*, 35:2358–2364.

Vanhoorne, P. and Register, R. A. (1996). Low-Shear Melt Rheology of Partially-Neutralized Ethylene - Methacrylic Acid Ionomers. *Macromolecules*, 29:598–604.

Zhang, L., Brostowitz, N. R., Cavicchi, K. A., and Weiss, R. A. (2014). Perspective: Ionomer research and applications. *Macromol. React. Eng.*, 8(2):81–99.

CHAPTER 6

Summarizing chapter

The overall objective of this project was to gain insight on the extensional rheology of supramolecular polymers. This understanding would allow for the development of supramolecular polymers with user defined properties. Most of the measurements were inherently unique because the extensional rheology of supramolecular polymer melts has not been investigated to great extent unlike the linear rheology. Extensional rheology is indeed interesting for all the supramolecular polymers with hydrogen bonding, ionic or metal-ligand associations. As such it was very important to narrow down the library of supramolecular polymer systems in order to follow a clear objective. In this thesis, three categories of samples were characterized: a) entangled hydrogen bonding system with weak associations, b) unentangled hydrogen bonding system with strong associations, and c) unentangled ionomers.

In the first category, we have characterized linear and nonlinear rheology of a model system of pure poly(*n*-butyl acrylate), PnBA, homopolymer and four poly(acrylic acid), PnBA-PAA, copolymers with varying AA side groups (0%-38%). The beauty of these systems is that the length of the polymer backbone is unaltered in the copolymer compositions. This systematic unravels the effect of changes in chemistry (affecting packing length) and influence of hydrogen bonding on the linear rheology of the copolymer systems using a simple model with no adjustable parameters. It is found that hydrogen bonding specifically changes the power law dependence of storage moduli and loss moduli in the terminal regime (time scales larger than the inverse of low crossover frequency ω_L in the LVE). For frequencies above ω_L hydrogen bonding has little to no effect on the LVE response. DTU-FSR was employed to characterize the extensional rheological response of these systems. Impressive strain hardening is noticed for strain rates below ω_L. The magnitude of strain hardening decreases as the strain rates approach ω_L. This supports the hypothesis that above a critical strain rate the hydrogen bonding associations become irrelevant.

In the second category, we have characterized linear viscoelastic and dielectric response of unentangled 2-ureido-4[1*H*]-pyrimidones (UPy) based supramolecular networks. This work is inspired from the results mentioned above and by the work of Chen et al. (2013). We have been particularly interested in the change of slopes in storage and loss moduli at time scales larger than ω_L for hydrogen bonding supramolecular systems. Green and Tobolsky (1946) have showed that the stress relaxation via breaking and re-formation of reversible associations is essentially Rouse like on time scales larger than the association life time. We have hypothesized that the same theoretical analysis can be applied to unentangled polymers irrespective

of associating bond chemistry. In this case, we have modified the sticky Rouse model [Chen et al. (2013)] to take into account the distribution in the number of stickers in order to capture the lowering of the power-law scaling in the expected terminal regime. Furthermore, we have employed dielectric spectroscopy (DRS) as an independent (nonrheological) technique to measure the association lifetime of hydrogen bond units. We found that the time scale obtained from DRS corresponds to the bare lifetime of hydrogen bond units. The effective or renormalized time is much larger than the bare life time measured via DRS. We have argued that the difference is due to decreased probability of sticker dissociation above the gel point. It will be interesting to carry out a comparative study by combining rheology, DRS and nuclear magnetic relaxometry (NMR) to pick the association life time in a future study.

Third category is based on unentangled amorphous copolyester ionomers synthesized via condensation of sulfonated phthalates with: a) mixtures of poly (ethylene glycol) PEO and poly(tetramethylene glycol) PTMO i.e., PEO25-PTMO75.(called coionomers) , and b) PTMO100 (ionomer) [Chen et al. (2014)]. In the case of the coionomer, 25 molar percentage of the diols are PEO, and 75 molar percentage are diols of PTMO. The counterions are either Lithium (Li) or Sodium (Na). This inter-laboratory project combines the nonlinear shear and uniaxial extensional rheological study of the above mentioned ionomers. The measurements were performed on the DTU-FSR and on a strain controlled shear rheometer equipped with a cone-partitioned-plate (CPP) setup. These materials require great care in handling because they take up water very fast and are prone to oxidation. The high-plateau modulus PTMO-Na exhibits a response akin to a brittle material: it fractures at low Hencky strains in extension and cannot be sheared homogeneously due to instabilities (predominantly wall slip). Further, the effects of 25% PEO addition on the extensional rheological properties was studied. Clearly, the coionomer is more ductile, as confirmed by its ability to deform more under both shear and extension. However, even the more ductile coionomer shows limits for how much it can deform. In uniaxial extension it always exhibits tensile fracture, while in shear flows it exhibits edge fracture at 2.5. Results indicate that incorporating PEO comonomer into the PTMO-Na/Li ionomer increases the toughness of the material by increasing the maximum strain both in shear and extension.

Finally, we have studied the fracture mechanisms for the PTMO-Na ionomer by combining extensional rheometry with high speed imaging. This project was inspired by the fact that although ionomers find so many applications, a detailed study to delineate the fracture mechanisms was missing in literature [Zhang et al. (2014)]. It is shown that ionomers fail in a brittle fashion by edge fracture. Fracture profiles exhibit a parabolic shape which is indicative of solid like behavior. The absence of any significant bulk viscous dissipation has been justified using the de Gennes viscoelastic trumpet model [de Gennes (1996)]. By combining fracture mechanics analysis (based on Pomeau's criterion) with constant rate uni-axial rheology, a common consensus has been brought forward to understand the mechanism of fracture at different Wi. Microvoids can explore different crack lengths when $Wi < 1$ (noticeable strain hardening was observed in this regime) whereas for $Wi > 1$ this may not be the case.

Therefore, although these microcracks present the source for the crack nucleation, the driving force is not thermal energy. Classical Griffith's theory [Griffith (1921)] is applicable here to explain the crack propagation. No strain hardening has been observed in this regime and the material fractured on the LVE envelope. It could be interesting, to characterize extensional rheology of entangled ionomer melts in a future study. Validating the hypothesis that entanglements can make the material more tougher could be a nice study.

Overall, many open questions remain yet to be answered. Role of polymer architecture on extensional rheology of supramolecular polymers, effect of entanglements on fracture of ionomers, extensional rheology of metallo-supramolecular polymers and extensional creep of supramolecular polymer networks can be very interesting future studies.

6.1 Bibliography

Chen, Q., Masser, H., Shiau, H.-S., Liang, S., Runt, J., Painter, P. C., and Colby, R. H. (2014). Linear Viscoelasticity and Fourier Transform Infrared Spectroscopy of PolyetherEsterSulfonate Copolymer Ionomers. *Macromolecules*, 47(11):3635–3644.

Chen, Q., Tudryn, G. J., and Colby, R. H. (2013). Ionomer dynamics and the sticky Rouse model a). *J. Rheol.*, 57(August):1441–1462.

de Gennes, P. G. (1996). Soft adhesives. *Langmuir*, 12(19):4497–4500.

Green, M. S. and Tobolsky, A. V. (1946). A New Approach to the Theory of Relaxing Polymeric Media. *J. Chem. Phys.*, 14:80–92.

Griffith, A. A. (1921). The phenomena of rupture and flow in solids. *Phil. Trans. R. Soc. A*, 221(582-593):163–198.

Zhang, L., Brostowitz, N. R., Cavicchi, K. A., and Weiss, R. A. (2014). Perspective: Ionomer research and applications. *Macromol. React. Eng.*, 8(2):81–99.

APPENDIX A

Joint Author Statements

Technical University of Denmark

Joint author statement

If a thesis contains articles (i.e. published journal and conference articles, unpublished manuscripts, chapters etc.) made in collaboration with other researchers, a joint-author statement verifying the PhD student's contribution to each article should be made by all authors. However, if an article has more than three authors the statement may be signed by a representative sample, cf. article 12, section 4 and 5 of the Ministerial Order No. 1039 27 August 2013 about the PhD degree. We refer to the Vancouver protocol's definition of authorship.

A representative sample of authors is comprised of

- Corresponding author and/or principal/first author (defined by the PhD student), and if there are more authors:
- 1-2 authors (where appropriate, these should be the international/non-supervisor authors)

Title of the article	Effect of Hydrogen Bonding on Linear and Nonlinear Rheology of Entangled Polymer Melts
Author(s)	Aamir Shabbir, Hadi Goldansaz, Ole Hassager, Evelyne van Ruymbeke and Nicolas J. Alvarez
Journal/conference * if applicable	Macromolecules
Name of PhD student	Aamir Shabbir
Date of Birth	04.07.1988

Description of the PhD student's contribution to the abovementioned article

Carried out extensional rheological characterization, post processing of experimental data, and wrote part of first draft of this article including introduction and experimental methods details.

Signature of the PhD student 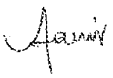 Date 02.09.2016

Signatures of co-authors

As a co-author I state that the description given above to the best of my knowledge corresponds to the process and I have no further comments.

Date (DD/MM/YY)	Name	Signature
02.09.2016	Hadi Goldansaz	
02.09.2016	Ole Hassager	
02.09.2016	Evelyne van Ruymbeke	
02.09.2016	Nicolas J. Alvarez	

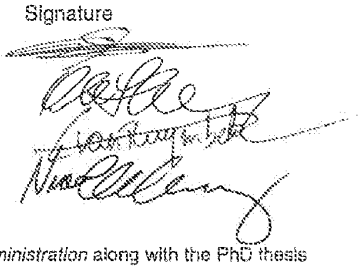

Joint author statements shall be delivered to the *PhD administration* along with the PhD thesis

PhD and Continuing Education
June 2016 | page 1/1

Technical University of Denmark

Joint author statement

If a thesis contains articles (i.e. published journal and conference articles, unpublished manuscripts, chapters etc.) made in collaboration with other researchers, a joint-author statement verifying the PhD student's contribution to each article should be made by all authors. However, if an article has more than three authors the statement may be signed by a representative sample, cf. article 12, section 4 and 5 of the Ministerial Order No. 1039 27 August 2013 about the PhD degree. We refer to the Vancouver protocol's definition of authorship.

A representative sample of authors is comprised of

- Corresponding author and/or principal/first author (defined by the PhD student), and if there are more authors:
- 1-2 authors (where appropriate, these should be the international/non-supervisor authors)

Title of the article	Linear Viscoelastic and Dielectric Relaxation Response of Unentangled UPy-Based Supramolecular Networks
Author(s)	Aamir Shabbir, Irakli Javakhishvili, Silvina Cerveny, Søren Hvilsted, Anne L. Skov, Ole Hassager and Nicolas J. Alvarez
Journal/conference * if applicable	Macromolecules
Name of PhD student	Aamir Shabbir
Date of Birth	04.07.1988

Description of the PhD student's contribution to the abovementioned article

Carried out rheological characterization, post processing of experimental data, and wrote first draft of this article.

Signature of the PhD student  Date 02.09.2016

Signatures of co-authors

As a co-author I state that the description given above to the best of my knowledge corresponds to the process and I have no further comments.

Date (DD/MM/YY)	Name	Signature
02.09.2016	Irakli Javakhishvili	
02.09.2016	Silvina Cerveny	
02.09.2016	Søren Hvilsted	
02.09.2016	Anne L. Skov	
02.09.2016	Ole Hassager	
02.09.2016	Nicolas J. Alvarez	

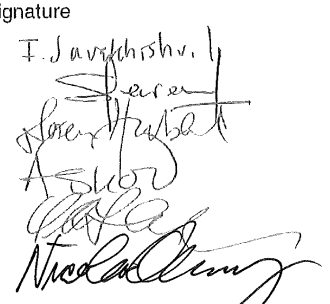

Joint author statements shall be delivered to the *PhD administration* along with the PhD thesis

PhD and Continuing Education
June 2016 | page 1/2

Technical University of Denmark

Joint author statement

If a thesis contains articles (i.e. published journal and conference articles, unpublished manuscripts, chapters etc.) made in collaboration with other researchers, a joint-author statement verifying the PhD student's contribution to each article should be made by all authors. However, if an article has more than three authors the statement may be signed by a representative sample, cf. article 12, section 4 and 5 of the Ministerial Order No. 1039 27 August 2013 about the PhD degree. We refer to the Vancouver protocol's definition of authorship.

A representative sample of authors is comprised of

- Corresponding author and/or principal/first author (defined by the PhD student), and if there are more authors:
- 1-2 authors (where appropriate, these should be the international/non-supervisor authors)

Title of the article	Non-linear shear and uniaxial extensional rheology of Polyether-ester-sulfonate copolymer ionomer melts.
Author(s)	Aamir Shabbir, Qian Huang, Guilhem P. Baeza, Quan Chen, Ralph. H. Colby, Dimitris Vlassopoulos, Nicolas J. Alvarez and Ole Hassager
Journal/conference * if applicable	Journal of Rheology
Name of PhD student	Aamir Shabbir
Date of Birth	04.07.1988

Description of the PhD student's contribution to the abovementioned article

Carried out extensional rheology measurements, did the analysis of experimental data, wrote the first draft of the paper.

Signature of the PhD student  Date 20.09.2016

Signatures of co-authors

As a co-author I state that the description given above to the best of my knowledge corresponds to the process and I have no further comments.

Date (DD/MM/YY)	Name	Signature
20.09.2016	Qian Huang	
20.09.2016	Guilhem P. Baeza	
20.09.2016	Quan Chen	
20.09.2016	Ralph. H. Colby	
20.09.2016	Dimitris Vlassopoulos	
20.09.2016	Nicolas J. Alvarez	

20.09.2016 Ole Hassager

Joint author statements shall be delivered to the *PhD administration* along with the PhD thesis

PhD and Continuing Education
June 2016 | page 1/1

Technical University of Denmark

Joint author statement

If a thesis contains articles (i.e. published journal and conference articles, unpublished manuscripts, chapters etc.) made in collaboration with other researchers, a joint-author statement verifying the PhD student's contribution to each article should be made by all authors. However, if an article has more than three authors the statement may be signed by a representative sample, cf. article 12, section 4 and 5 of the Ministerial Order No. 1039 27 August 2013 about the PhD degree. We refer to the Vancouver protocol's definition of authorship.

A representative sample of authors is comprised of

- Corresponding author and/or principal/first author (defined by the PhD student), and if there are more authors:
- 1-2 authors (where appropriate, these should be the international/non-supervisor authors)

Title of the article	Brittle Fracture in Associative Polymers: The Case of Ionomer Melts
Author(s)	Aamir Shabbir, Qian Huang, Quan Chen, Ralph H. Colby, Nicolas J. Alvarez and Ole Hassager
Journal/conference * If applicable	Soft Matter
Name of PhD student	Aamir Shabbir
Date of Birth	04.07.1988

Description of the PhD student's contribution to the abovementioned article

Carried out extenional rheological characterization, fracture experiments, post processing of experimental data, and wrote first draft of this article.

Signature of the PhD student Aamir Date 02.09.2016

Signatures of co-authors

As a co-author I state that the description given above to the best of my knowledge corresponds to the process and I have no further comments.

Date (DD/MM/YY)	Name	Signature
02.09.2016	Qian Huang	Qian Huang
02.09.2016	Quan Chen	
02.09.2016	Ralph H. Colby	
02.09.2016	Nicolas J. Alvarez	
02.09.2016	Ole Hassager	

Joint author statements shall be delivered to the *PhD administration* along with the PhD thesis

{2.7182818284}ϑφέρτυθιοπσδφγηξκλ